The University of Akron
IdeaExchange@UAkron

Honors Research Projects

The Dr. Gary B. and Pamela S. Williams Honors College

Spring 2015

Magnus Effect in Duct Flow

Jesse S. Batko
The University Of Akron, jsb84@zips.uakron.edu

Cameron W. Clarke
The University Of Akron, cwc13@zips.uakron.edu

Kenneth W. Smith Jr.
The University Of Akron, kws23@zips.uakron.edu

Please take a moment to share how this work helps you through this survey. Your feedback will be important as we plan further development of our repository.
Follow this and additional works at: http://ideaexchange.uakron.edu/honors_research_projects

Part of the Aerodynamics and Fluid Mechanics Commons, Aeronautical Vehicles Commons, Other Aerospace Engineering Commons, Other Engineering Science and Materials Commons, Other Mechanical Engineering Commons, and the Propulsion and Power Commons

Recommended Citation
Batko, Jesse S.; Clarke, Cameron W.; and Smith, Kenneth W. Jr., "Magnus Effect in Duct Flow" (2015). *Honors Research Projects*. 20.
http://ideaexchange.uakron.edu/honors_research_projects/20

This Honors Research Project is brought to you for free and open access by The Dr. Gary B. and Pamela S. Williams Honors College at IdeaExchange@UAkron, the institutional repository of The University of Akron in Akron, Ohio, USA. It has been accepted for inclusion in Honors Research Projects by an authorized administrator of IdeaExchange@UAkron. For more information, please contact mjon@uakron.edu, uapress@uakron.edu.

MAGNUS EFFECT IN DUCT FLOW

Senior/Honors Design Project

Abstract

This senior research project created to determine how Magnus Lift is impacted by duct flow. Simulations are a primary indicator on the effects of what will happen. A test was designed in detail, but was not conducted due to a lack of resources, funds, and time. It is imperative for the validity of the models and simulations that testing take place in the future.

Batko, Jesse (Mechanical Engineering),
Clarke, Cameron (Mechanical Engineering)
Smith, Kenneth (Aerospace Systems Engineering)

Executive Summary

The following research paper details the preliminary research carried out by this team. The project was originally conceived to determine if Magnus Lift could be utilized in an unconventional way to assist rockets during takeoff. Several conceptual designs were proposed, but the idea was scrapped when it became apparent that the team would not be able to generate the desired lift without inducing significant amounts of drag and additional weight on a rocket. Instead, the team focused on researching an interesting topic that hasn't been previously explored: Magnus lift on a cylinder within a duct.

An experimental procedure that could be carried out in a wind tunnel at the University of Akron was designed along with several models for a test fixture. In order to predict the results of the experiment, several preliminary CFD simulations were performed. Unfortunately, due to limited time and resources, the test fixture was not built and the experiment was not carried out. However, more detailed simulations were performed. Unfortunately, the results suggested that minimal lift is generated on a duct/cylinder system compared to a spinning cylinder in open air.

Several potential applications for utilizing the Magnus effect were suggested, such as assisting rockets during takeoff, or allowing trains to enter curves at higher speeds without derailing. Although Magnus effect in duct flow would likely provide negligible benefits, the potential uses for Magnus lift in open air are promising.

Contents

Executive Summary 1
Contents 2
Table of Figures 4
Table of Tables 5
1.0 Introduction 6
2.0 Background on Magnus Effect 6
3.0 Understanding Magnus Effect 7
3.1 Kutta-Joukowski Lift Theorem 8
4.0 Original Project Scope 9
4.1 Rocket Design Team 9
4.2 Designs 10
4.2.1 Design 1- Ventus Boosters 10
4.2.2 Design 2- Ventus Fins 11
4.2.3 Design 3- Ventus Nose Cone 12
4.2.4 Design 4-Tri-internal Ventus Boosters 13
4.3 CFD simulations 13
4.4 Analysis 16
4.5 Conclusion 17
5.0 Revised Project Scope 18
5.1 Purpose 18
5.2 Preliminary 2-D CFD Simulation Setup 18
5.3 Preliminary 2-D CFD Simulation Results 20
5.4 Preliminary 3-D CFD Simulation Setup 23
5.5 Preliminary 3-D CFD Simulation Results 25
5.6 Analysis 27
5.7 ANSYS Fluent Lift Force calculations 30
6.0 Wind Tunnel Testing 33
6.1 Test Fixture 33
6.1.1 Wind Tunnel 33
6.1.2 Design Constraints 34
6.1.3 Material Selection 34
6.1.4 Fixture Design 35

6.2 Test Setup 39
7.0 Final CFD 40
7.1 2-D 40
7.2 3-D 41
7.3 Analysis and Results of Lift Force 43
8.0 Potential Applications 46
8.1 Cars 46
8.2 Trains 46
8.3 Boats 49
8.4 Rockets 50
9.0 Conclusion 51
10.0 Future Research 51
11.0 Team Responsibilities 51
12.0 References 52
Appendix A: Using the Magnus Lift Equation 53
Appendix B: 2-D and 3-D CFD Results 55
B.1 Preliminary CFD 2D Trial 1 55
B.2 Preliminary CFD 3D (All Trial 2) 58
B.3 Final CFD 2D (All Trial 2) 61
B.4 Final CFD 3D 63
Appendix C: ANSYS Fluent Setup 70
Appendix D: Lift vs. Air Speed and Cylinder RPM 76
Appendix F: Derivation of Kutta-Joukowski Lift Theorem 77
Derivation 77
F.1 Uniform Flow 78
F.2 Source and Sink Flow 79
F.3 Doublet Flow 81
F.4 Vortex Flow 82
F.5 Summary 83
Lifting Flow over a Cylinder 84
Appendix G: Hand Notes and Calculations 87

Table of Figures

Figure 1: Classic Magnus Effect Experiment 6
Figure 3: Magnus Lift 7
Figure 4: Visualization of Magnus Lift Due to Viscous Effects 8
Figure 5: Net lift generated by opposing cylinders 9
Figure 6: Design 1 featuring ventus boosters between fins 10
Figure 7: Design 2 featuring ventus boosters over fins 11
Figure 8: Design 3 featuring ventus boosters in the nosecone 12
Figure 9: Design 4 featuring internal ventus boosters 13
Figure 10: Pressure Map for Design 4 14
Figure 11: Design 4 velocity magnitudes 15
Figure 12: Design 4 Pathlines 15
Figure 20: Velocity magnitudes (vertical orientation) 16
Figure 14: Analysis of Design 4 Pathlines 17
Figure 15: Initial dimensions used for CFD simulations 19
Figure 16: Various ceiling/floor positions for initial CFD studies 19
Figure 17: Mesh for 2D simulation 19
Figure 25: Viscous model setup 20
Figure 19: Position 1 Case 1 Pressure and Velocity Gradients 21
Figure 20: Position 1 Case 2 Pressure and Velocity Gradients 21
Figure 21: Position 4 Case 1 Pressure and Velocity Gradients 22
Figure 22: Position 4 Case 2 Pressure and Velocity Gradients 22
Figure 23: First 3D design for testing 23
Figure 24: Initial 3D mesh 23
Figure 25: Complex meshing around screws 24
Figure 26: 3D mesh without screws 24
Figure 27: Side view of 3D mesh 25
Figure 28: New 3D meshing technique 25
Figure 29: Position 1 3D Pressure and Velocity Contours 26
Figure 30: Position 4 3D Pressure and Velocity Contours 27
Figure 31: Position 1 2D Velocity Gradients. Case 1 (left) and Case 2 (Right). 28
Figure 32: Position 4 Velocity Gradients. Case 1 (left) and Case 2 (right). 28
Figure 33: Long duct contours of pressure (top left), velocity (top right) and turbulence (bottom). 29
Figure 34: 2D and 3D simulations for Position 4, Case 2 30
Figure 35: Force vs duct height 31
Figure 36: Lift force vs duct height 31
Figure 37: The University of Akron's Aerolab Wind Tunnel 33
Figure 38: Working section of the Aerolab wind tunnel. Note the "sting" located in the center of the box 33
Figure 39: First Design - Sting and Cylinder Attachment 35
Figure 40: First Design cylinder assembly and duct (left) with proposed battery and motor placement (right) 36
Figure 41: Second Design cylinder/sting fixture. Views detailing interior motor attachment and placement (top, middle) and a cross sectional view showing bearing placement (bottom) 37
Figure 42: New Design - Full Test Fixture 38
Figure 43: 1/8" gap between rotating cylinder and duct wall 38
Figure 44: 2-D CFD results for position 1 of final design 40
Figure 45: 2-D CFD results for position 4 of final design 41
Figure 46: New mesh technique to include 1/8" gap between the cylinder and the duct walls 41
Figure 47: 3-D CFD simulation results for position 1 of final design 42

Figure 48: 3-D CFD results for position 4 of final design 42
Figure 49: Compares viscous forces vs wall positon for both cylinder and duct walls 44
Figure 50: Comparing X force for both the cylinder and duct walls 44
Figure 51: comparing lift forces of both cylinder and duct wall 45
Figure 52: shows the net force of the cylinder and duct system 45
Figure 53: Possible use for Magnus lift on a motor vehicle 46
Figure 54: Example of train with Magnus stabilizers. Retracted during normal operation (left) and extended and spinning during a turn for stability (right) 47
Figure 55: Basic passenger train car dimensions and forces around a turn 48
Figure 56: Examples of Flettner ships 49
Figure 57: Uniform Flow 78
Figure 58: Source and Sink Flow 80
Figure 59: Forming a Solid Boundary Using Sources and Sinks 81
Figure 60: Uniform Flow+Doublet Flow=Flow Over A Cylinder 82
Figure 61: Vortex Flow 83
Figure 62: Non-lifting Flow Over a Cylinder+Vortex Flow=Magnus Lift 84
Figure 63: Vortex Strength and Stagnation Point 85

Table of Tables

Table 1: Cases for 2-D study 18
Table 2: Lift and drag on the cylinder at all positions 30
Table 3: Change in lift on the cylinder from position to position. 31
Table 4: Shows the forces acting on the cylinder 43
Table 5: Shows the forces acting on the duct walls 43
Table 6: Summary of Velocity Equations for Various Types of Flow 83

1.0 Introduction

Baseball has long been a national pastime that many Americans have cherished. To this day millions of people pack ballparks to be entertained and cheer for their hometown team. Everyone one loves homeruns and high scoring games, however it is usually a pitcher's duel that is one of the most intriguing matchups.

Pitchers use a variety of pitches from fast ball to change-up, however there is not a more devastating pitch than the curveball. With a curveball the ball appears to be heading right toward the batter but then breaks into the strike zone. This pitch seems to defy all physical laws, but in reality it utilizes a very intuitive effect known as Magnus effect.

2.0 Background on Magnus Effect

The history of Magnus effect is filled with many great thinkers who contributed key observations and scientific experiments that described Magnus effect between the 17th and 20th century. It was first observed by Sir Isaac Newton during the 17th century. In a letter addressed to Oldenburg, Sir Isaac Newton described the path a tennis ball took, resembled a curved line when hit with an oblique racket (1). He effectively observed a tennis ball that was "sliced", which is a technique in tennis where the racket puts spin on the ball causing the ball to curve in mid-air.

The next big name in discovering Magnus effect was a Professor of Physics at the University of Berlin by the name of Gustav Magnus. He was credited with developing one of the first scientific experiments that was set up to observe this strange effect 2). His science experiment can be seen in Figure 1 below.

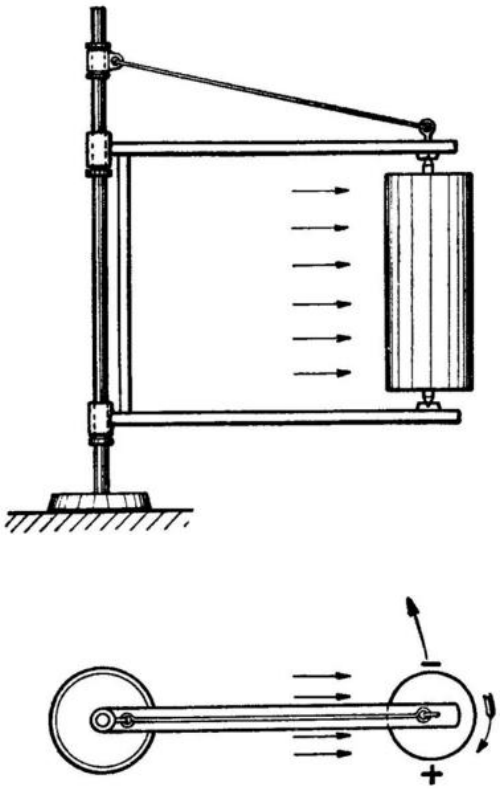

Figure 1: Classic Magnus Effect Experiment

This experiment consisted of a rotating cylinder between two bearings on a rotating arm with air directed at the cylinder. Gustav Magnus observed that the spinning cylinder would move on the rotating arm when it was struck with air (2). It is to note that no force calculations were done at this point and at that point this effect came to be known as Magnus Effect (2).

In 1912, Lafay conducted research on the subject and reported that spinning cylinders could produce significantly greater lift than planes with the same surface area (3). In addition, Lafay conducted additional research showing that spinning cylinders could also produce a force in opposite direction predicted by Magnus, though this was only for specific conditions.

Anton Flettner became one of the first people to find a practical use for the Magnus effect when he developed the first Flettner-rotor ship in the early 20th century (4). This ship utilized spinning cylinders with endplates as a method of propulsion, rather than sails. This sort of ship used much less power than screw propulsion ships, and was more effective than sails. However, the flettner-rotors were not as fast or reliable as screw-propulsion, and so they generally weren't explored further (4). However, the idea that Magnus lift can be used in practical applications is exciting.

3.0 Understanding Magnus Effect

The Magnus effect describes the effect of a shear force experienced by a rotating body in a circular flow. If we consider a rotating body in a flow, it is subjected to a transverse force. This acts perpendicular to the direction of flow and also perpendicular to the axis of rotation. For this reason, the force is also referred to as shear force.

For example, for the clockwise rotation of a spinning cylinder in a uniform flow, as shown in Figure 3 (5), the particles are accelerated at the top of the ball and slowed at the bottom. The velocity distribution around the ball is thus inhomogeneous. Since we are considering incompressible conditions, the Bernoulli equation, which can be seen below, is valid.

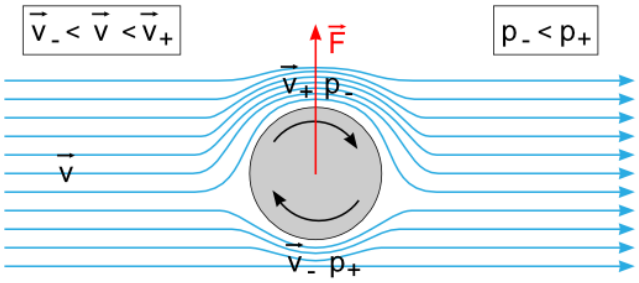

Figure 2: Magnus Lift

$$P + \frac{1}{2}\rho v^2 + \rho g z = Constant$$

Bernoulli's equation states that the total pressure is a constant value along a streamline. As we concluded earlier, the velocity at the top of the spinning is moving faster than that of the bottom. This phenomenon is caused by the airflow sticking to the surface of the cylinder and traveling with the rotation of the cylinder because of viscous effects. The top of the cylinder is working concurrently with the uniform flow creating faster velocities and the bottom part of the cylinder is opposing the direction of uniform flow resulting in slower velocities. This can be seen depicted in Figure 3. Though they are not along the same streamline, it can be concluded that the total pressures are the same since this is uniform flow. Thus, with the velocity at the top being greater than that of the velocity at the bottom, it can be concluded that the pressure at the top of the cylinder must be lower.

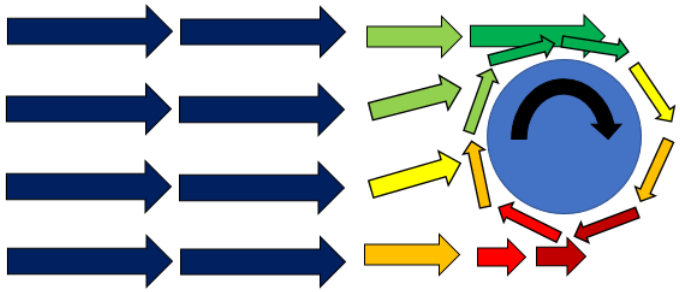

Figure 3: Visualization of Magnus Lift Due to Viscous Effects

This is very important discovery, since it is precisely the difference in static pressures that generates lift. Think of it as a stability problem. When there is a pressure gradient high pressure wants to move to lower pressure till homogeneity persists. This is the most stable condition. Pressure gradients cause flow through pipes and with no pressure gradient there is no flow. Similarly, this high pressure at the bottom of the cylinder wants to equalize, thus it generates a force toward the top of the cylinder.

The simple relationship $F = \Delta P A$, where ΔP is the pressure difference between the top and bottom and A is the cross-sectional area of the ball or cylinder, demonstrates how a force can be generated from a pressure differential. It is this principal that explains lift of an airfoil.

3.1 Kutta-Joukowski Lift Theorem

A relatively simple equations exists for determining the lift force generated by air flowing over a spinning cylinder. This equation is known as the Kutta-Joukowski lift theorem, named for the two aerodynamicists who developed it (6). The equation is simply:

$$L = \rho * V * G$$

Where *L* is the lift, ρ is the air density, *V* is the velocity of the air flow, and *G* is the vortex strength. The vortex strength is determined easily by:

$$G = 2 * \pi * r * V_r$$

Here, *r* is the radius of the cylinder and V_r is the tangential velocity of the rotating cylinder. This vortex strength is a measure of the circulation, or local spin, or the air around the cylinder (7).

This equation is used to estimate the lifting force on a spinning cylinder and was used to generate the table in Appendix D, as well as determining forces discussed in Section 8.2. An in depth derivation of the Kutta-Joukowski lift theorem can be seen in Appendix F. The derivation is taken from The Fundamentals of Aerodynamics by John D. Anderson (15).

4.0 Original Project Scope

The original project scope that the team set out to investigate was to design a system that utilized the Magnus effect to help produce lift for a rocket during flight. Since the velocity of wind hitting the cylinder has a governing impact on Magnus effect, it was worth investigating how it could assist a rocket during launch. Winds generated by a rocket during launch approach velocities of Mach three. If these winds can be utilized and proper rotational velocity of the cylinder is achieved, large lift could be generated. This will have a large impact on the price of the rocket because if sufficient lift force is generated, the size of the engines and the amount of fuel needed to launch objects into low earth orbit (LEO) would be minimized. This in turn will make the rocket lighter and thus, less expensive vehicle to use. Currently, the price to launch 1 kg of supplies to LEO is $28,000 and the price of one rocket launch varies from $60 million (SpaceX) to $190 million (NASA).

Even though designing a system utilizing Magnus lift can be used on a rocket to take advantage of high wind speeds, it also offers a set of challenges to overcome. Like any system, the usual challenges exist, such as cost of materials and if an internal or external system would be more beneficial. Some of the more unique challenges presented from this system design are redirecting the airflow to make the life force vertical and overcoming the drag force induced by this redirecting of air.

The reason for redirecting the air is because in order to have a vertical lift, the wind has to be hitting the cylinder at a horizontal direction to create a force that is perpendicular to the flow. A horizontal direction would be too difficult to do since it will generate too much drag so a more conservative route to redirect the wind at a 45 degree angle was tried. This method of redirecting the wind would generate a lift force with both an x and y component. The y component is the main focus to generate a vertical lift. It was determined that if more than one cylinder was used that were spinning in opposite directions, it would cancel out the x components while combining the y components as seen in Figure 4.

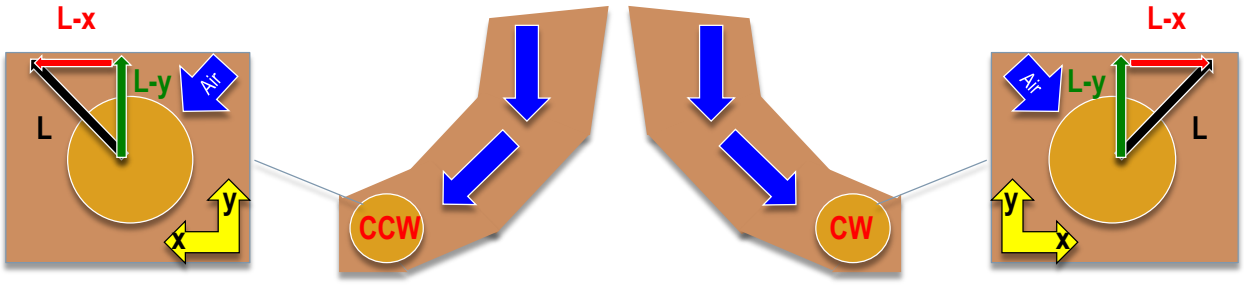

Figure 4: Net lift generated by opposing cylinders

4.1 Rocket Design Team

The idea to use Magnus effect to assist rocket launch came during a rocket design meeting at the University of Akron. The team was exploring different ideas to help generate extra lift for the rocket. These ideas included using larger engines, more combustible fuel, and to design a custom graphite nozzle. The problem that we ran into was using larger engines which would add more weight to the rocket which required more fuel for the engines which once again, would increase the weight of the rocket. It seemed it was a never ending paradox. This led to less conventional and more unique ways to try and generate lift for the rocket. The idea to use Magnus effect became the front runner when it was found out that it could produce significant lift and has had success when used on boats and aircrafts. It was then agreed upon by

the team that designs could be used on the competition rocket to test the theory of Magnus effect and rockets.

4.2 Designs

While exploring different types of designs, both internal and external systems were investigated. In total, four designs were made. Each design were called Ventus boosters because Ventus is Latin for wind and the goal was to use wind to generate lift much like a booster engine is used on a rocket today.

4.2.1 Design 1- Ventus Boosters

The first design had three boosters between the fin assembly as shown in Figure 5.

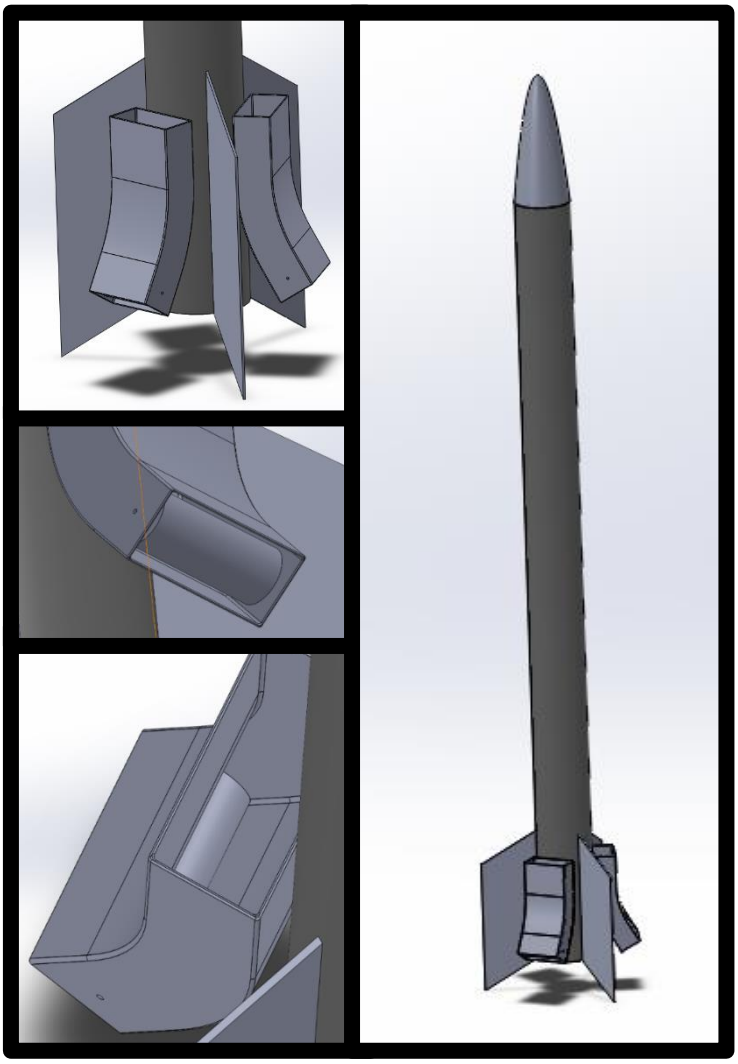

Figure 5: Design 1 featuring ventus boosters between fins

This required that an external duct system had to channel air to the spinning cylinder that were located at the end of the duct system. Design one was rejected because the duct system added a lot of surface

area which added more drag. There also was not any space to place the motors or power source for the rotation of the cylinder. Another concern is that the booster would negatively affect stability.

4.2.2 Design 2- Ventus Fins

Design 2 put the Ventus boosters and combined them with the fin assembly as shown in Figure 6:

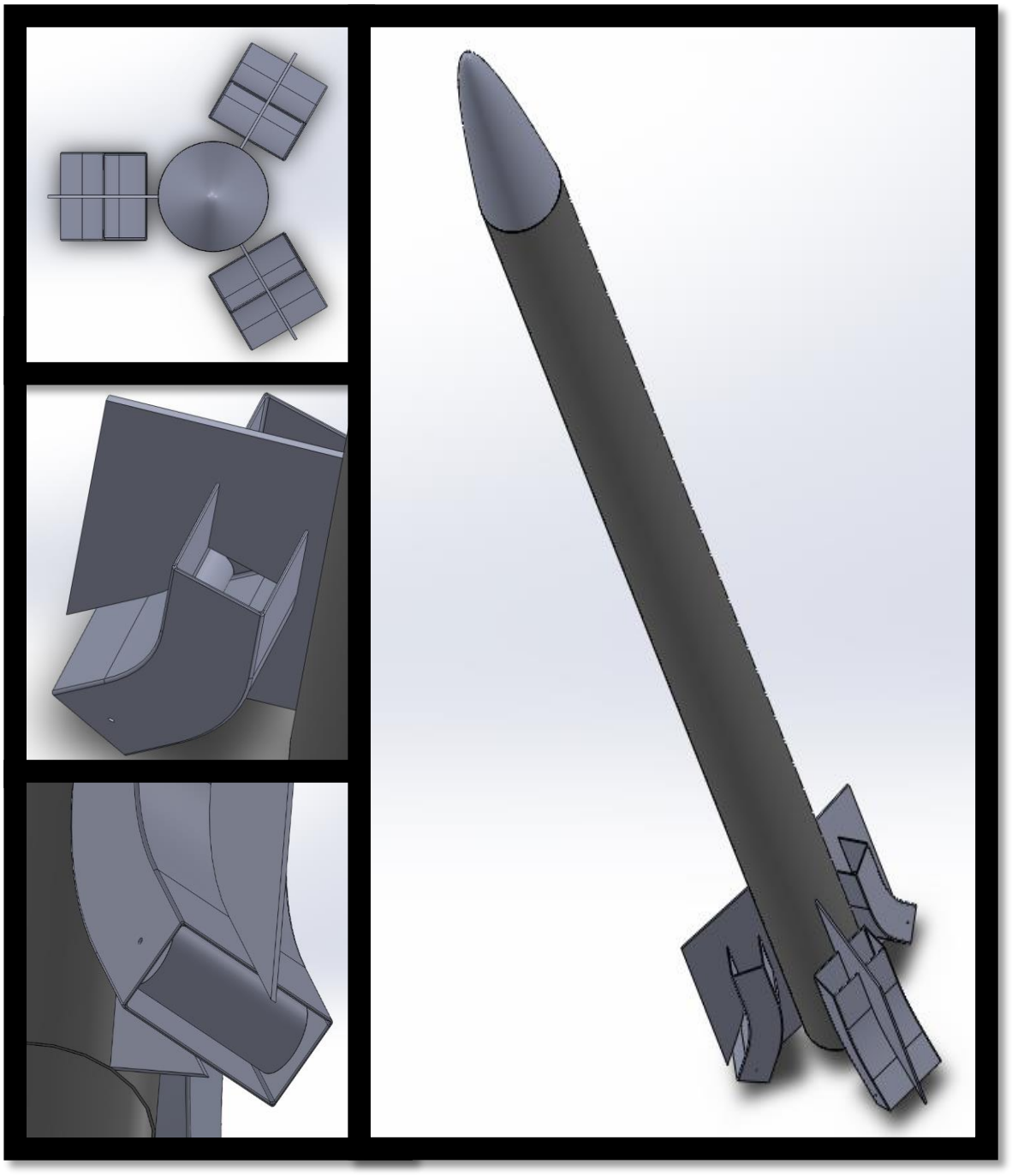

Figure 6: Design 2 featuring ventus boosters over fins

This design was also rejected due to the fact that the increase in surface area, which is shown in the upper left, greatly increased drag. The design was also rejected because there was a fear that speed of the rocket would create a shockwave that would be at the tip of the nose cone which would prevent air from reaching the duct system at the tail of the rocket. It was determined that an internal system would be more desirable.

4.2.3 Design 3- Ventus Nose Cone

Design 3 was the first internal system explored where the duct system and cylinders were placed in the nose cone, as seen in Figure 7.

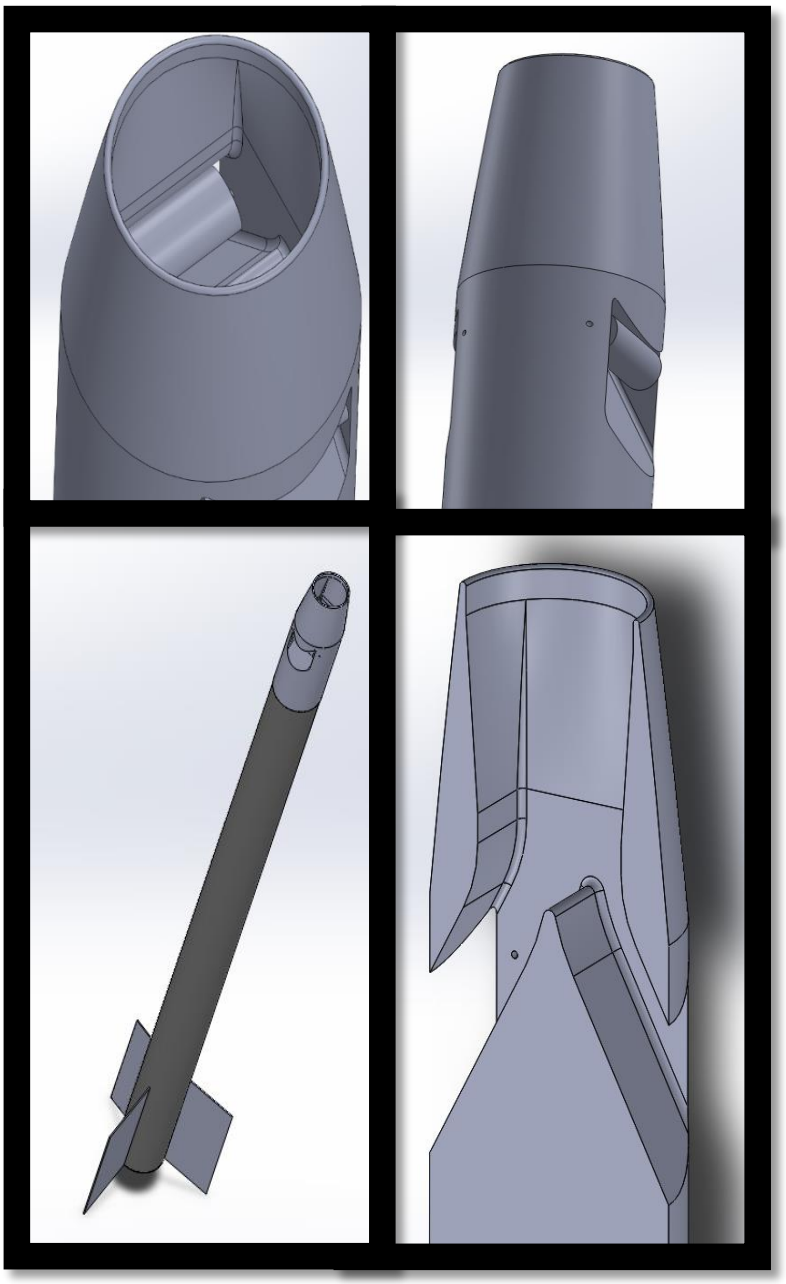

Figure 7: Design 3 featuring ventus boosters in the nosecone

The nose cone seemed like the best place but it provided very little room for any of the hardware plus there was a chance that placing everything in the top of the rocket would make it top heavy and possibly unstable.

4.2.4 Design 4-Tri-internal Ventus Boosters

This was the second internal design that placed three ventus booster inlets where the diameter of a rocket changes.

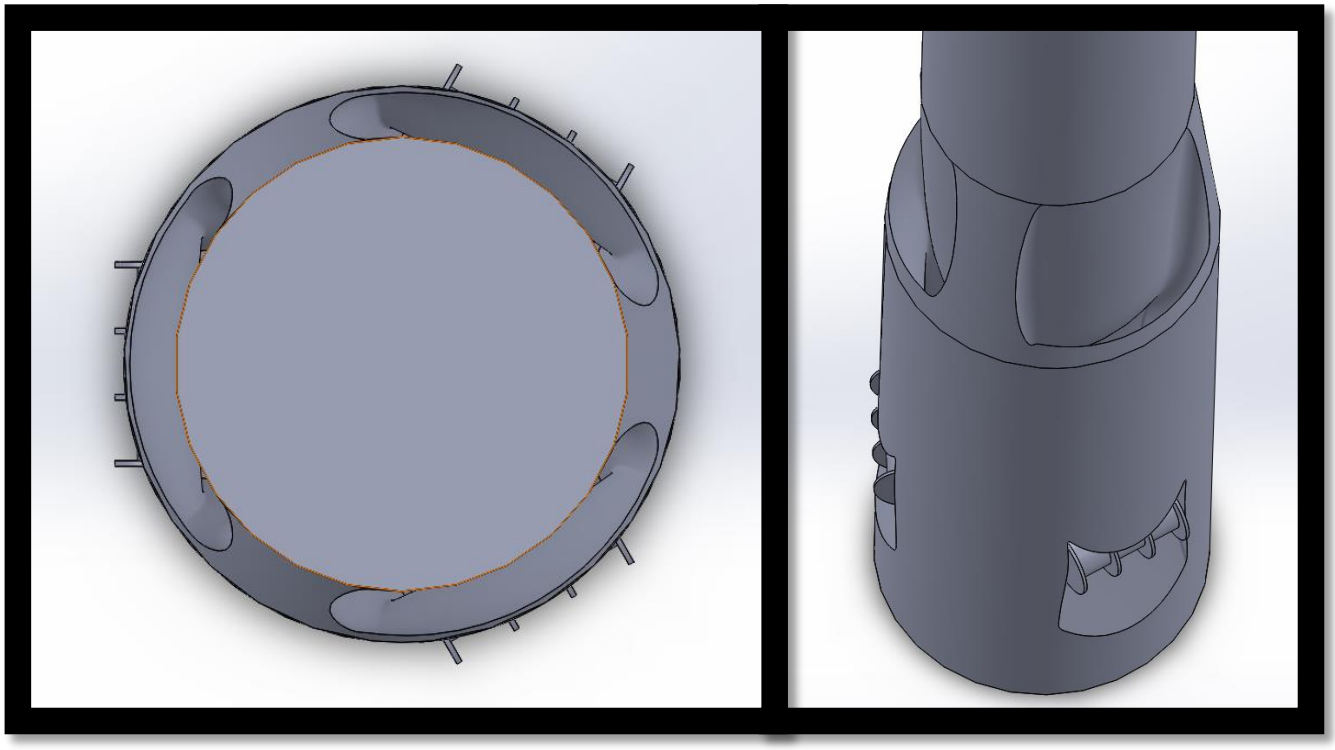

Figure 8: Design 4 featuring internal ventus boosters

As seen in Figure 8, the fourth design allowed for the largest cylinders of the four designs to be used and also allowed for the most space to redirect the air needed to create a more vertical lift force. This design was selected to move forward with and run two-dimensional CFD simulations on.

4.3 CFD simulations

When performing two-dimensional simulations, pressure and velocity were studied. A section cut was made of the model shown above. The path for which the fluid could take is marked in blue while the rocket solid is indicated in white and is at the bottom of the picture. The rocket direction is indicated by the red arrow. The speed of the flow was set to 200 m/s with the rotational velocity set to 1000 radians per second in the clockwise direction.

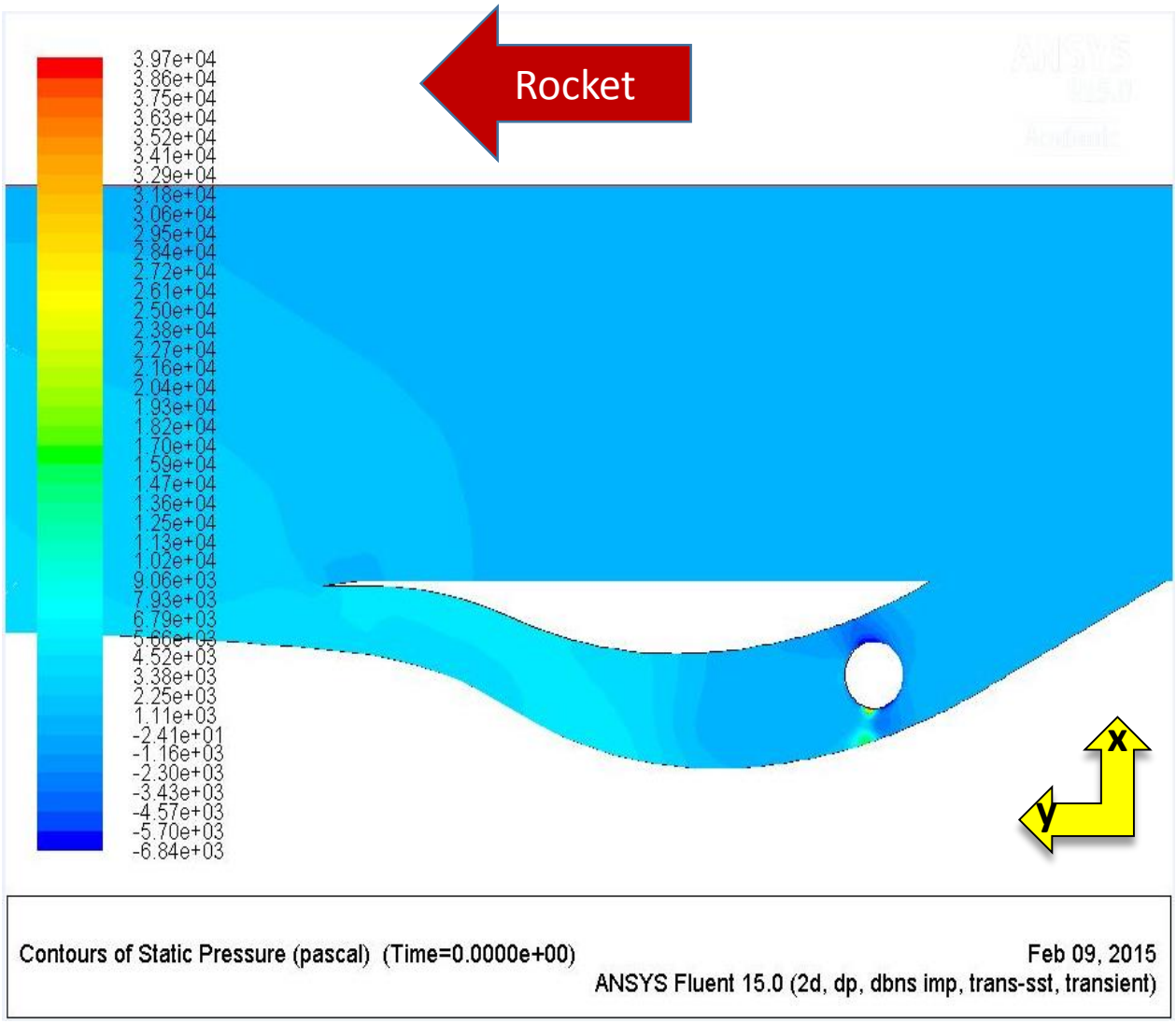

Figure 9: Pressure Map for Design 4

Figure 9 shows the lowest pressure slightly above and to the left of the spinning cylinder. Velocity vectors were then looked at to see in better detail where the flow was traveling the fastest followed by the particle pathways to see the paths that the air takes. These can be seen in Figure 10 and Figure 11, respectively.

The analysis of all three figures is done in the following section, section 4.4.

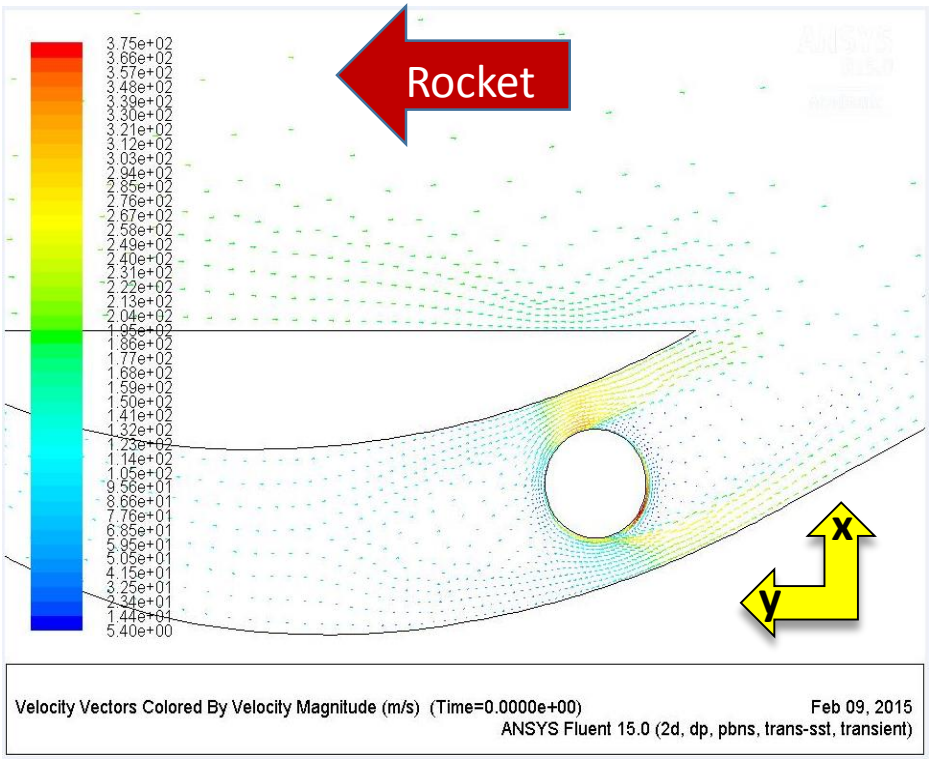

Figure 10: Design 4 velocity magnitudes

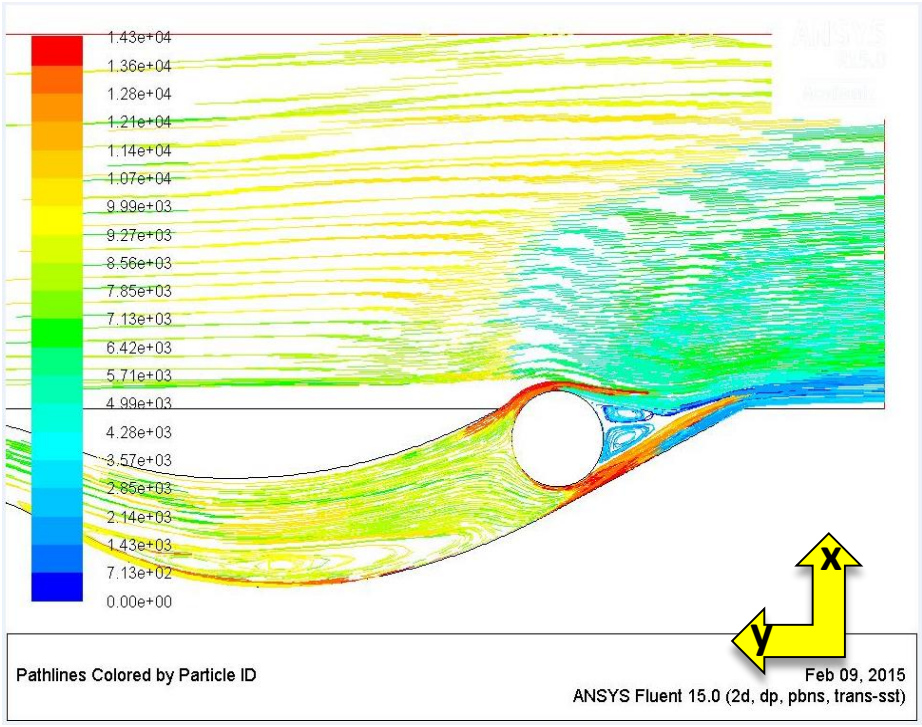

Figure 11: Design 4 Pathlines

4.4 Analysis

Zooming in around the cylinder and rotating the picture to the correct direction, a more thorough analysis can be done. It can be seen that the magnitude of the lifting force shown by the black arrow did not achieve the desired angle of 45 degrees or greater. This resulted in a smaller vertical lift (shown by the green arrow) and a larger horizontal lift (shown by the red arrow).

Even though the large horizontal lift could help out with stabilization, the small vertical lift was not great enough to overcome the drag forces that were a resultant of the duct system and cylinder.

Upon closer investigation, a small patch of high velocity air flow can be seen on the backside of the spinning cylinder. This was an interesting anomaly that appeared and it's suspected that the walls of the duct had something to do with it. It was also strange that the air was hitting at a higher point on the cylinder than expected. It was determined that a closer look at the pathways of the particle were needed.

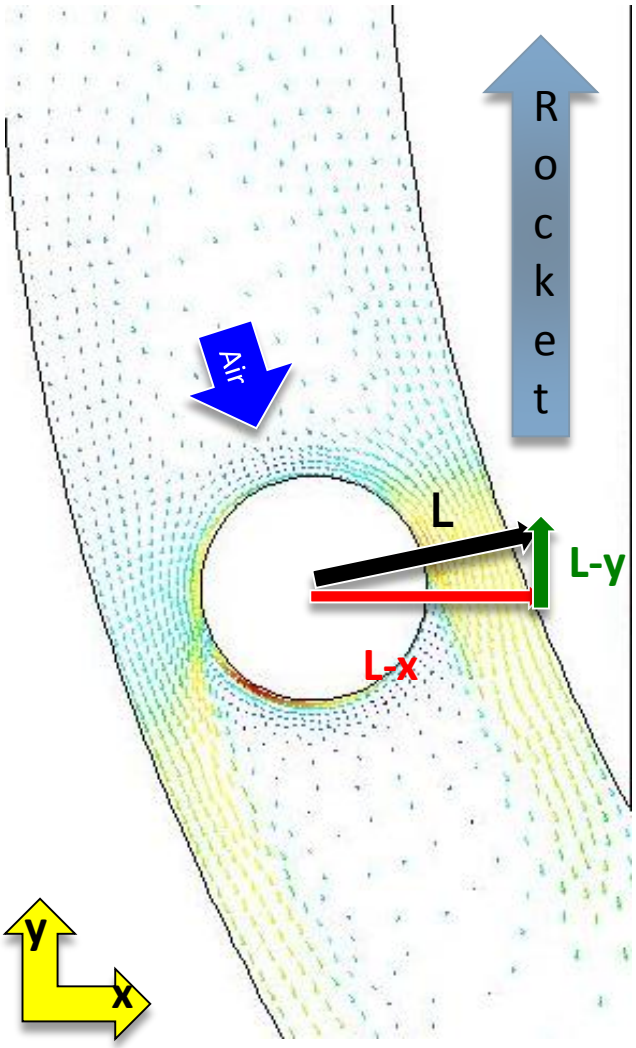

Figure 12: Velocity magnitudes (vertical orientation)

Upon further investigation, it shows that the air was denied access to taking full advantage of the duct. This can be seen in Figure 13. As shown in view A, which shows a zoomed in view of the bottom area of the duct, a vortex of air became trapped in the pocket of the duct which blocked the air from accessing the full curve. This made the point where the air hit the cylinder higher than expected and explains why the vertical component of the lift force was so small. View B shows where the air actually hits the cylinder.

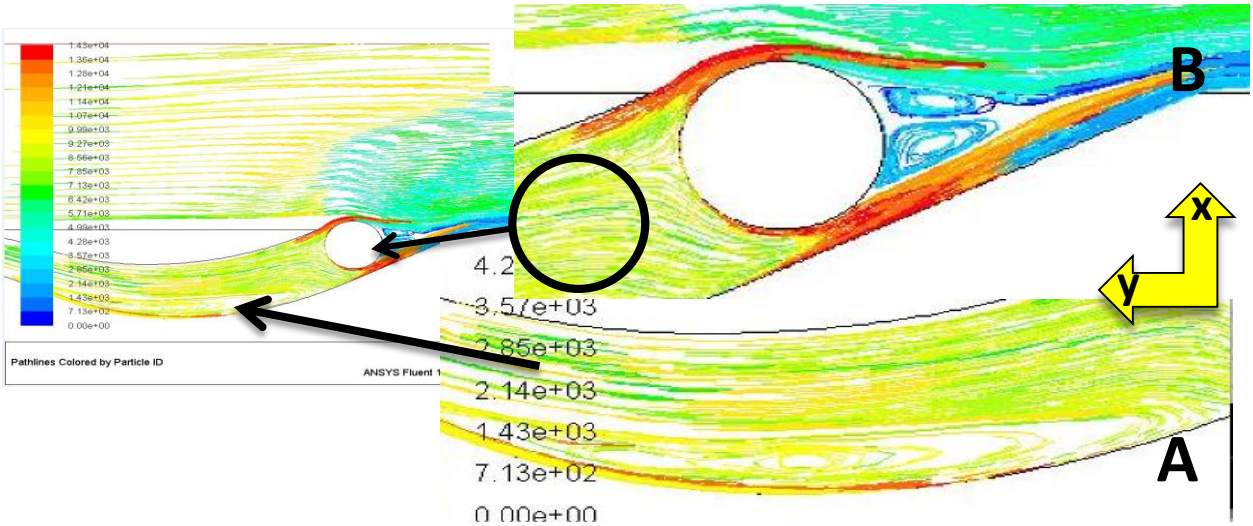

Figure 13: Analysis of Design 4 Pathlines

4.5 Conclusion

At this point it was concluded that there was no feasible way to get enough of a lift force to overcome the drag. Also, since the objective was to get a cylinder to spin two times faster than what the air was hitting it at, it would be impossible with today's technology to find a motor that can spin at speeds approaching Mach 6 if the rocket was traveling at speeds of Mach 3. It was determined that continuing with this project would prove to be fruitless so another project was needed. It was agreed upon that Magnus effect was to be kept at the center of study and since an anomaly was seen when a cylinder was spinning in a duct, that investigating how duct flow affects Magnus effect should become the new focal point of the project.

5.0 Revised Project Scope

Keeping the study of Magnus effect at the focus, a new project was devised. This new project was to study the affect duct flow had on Magnus effect and what happens if the walls (the floor and ceiling) of the duct enclosed on the spinning cylinder.

The revised project scope was to design a system that can be tested with both CFD and wind tunnel testing. The system would include a duct that is able to collapse the ceiling and floor around a spinning cylinder assembly. This design must allow for the cylinder to spin at relatively high RPMs and therefore must include a motor and drive system.

5.1 Purpose

The purpose of this new project was to see if duct flow had any bearing on the Magnus effect on a spinning cylinder. We wanted to see the properties of Magnus effect in duct flow with varying internal dimensions. Possible applications that could benefit from using Magnus effect in ducts can be seen in Section 8.

It was desired to have four different positons for both the floor and ceiling to run CFD simulations on. We sought to capture the effects enclosed walls would have on the velocity and pressure which in turn, affect Magnus. Does Magnus effect work in a duct flow? Does enclosing the walls increase, decrease or have no effect on Magnus effect? This project aimed at trying to find out the answers to those questions.

5.2 Preliminary 2-D CFD Simulation Setup

Simulations were ran with a duct in four different positions and at two different cases where a different wind speed and rotational velocity were chosen for each case. The case speeds are seen Table 1:

Table 1: Cases for 2-D study

	Inlet Airspeed	RPM
Case 1	52 mph (23.27 m/s)	5000 RPM (23.27 m/s)[-523.6 rads/sec]
Case 2	26 mph (11.64 m/s)	5000 RPM (23.27 m/s)[-523.6 rads/sec]

It should be noted that case 2 is where the rotational velocity is two times greater than the inlet airspeed so that the 2-to-1 ratio is reached and the greatest lift-to-drag is achieved. Case 1 has a velocity ratio of 1-to-1.

The dimensions of the test fixture that were simulated using ANSYS Fluent can be seen in Figure 14:

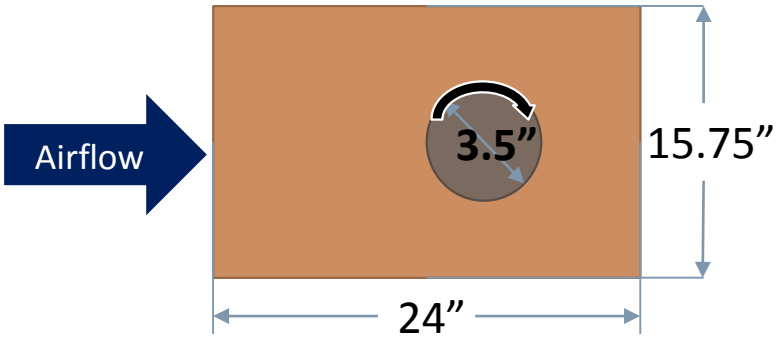

Figure 14: Initial dimensions used for CFD simulations

Simulations were ran with the duct floor and ceiling at four different positions and each position shortened the total height of the duct by 2.75 inches as shown in Figure 15:

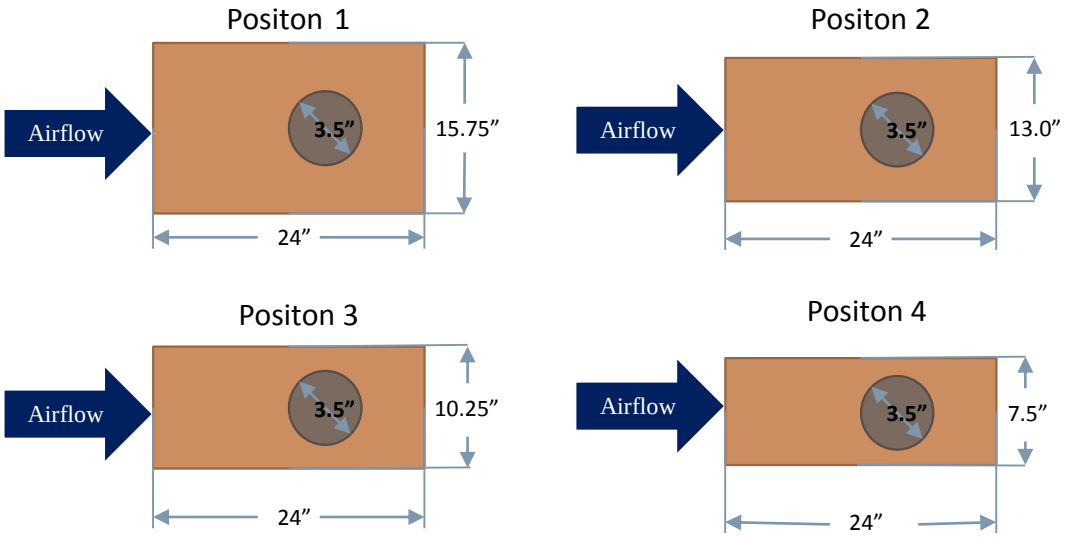

Figure 15: Various ceiling/floor positions for initial CFD studies

Starting with ANSYS Fluent, a model of the system shown above was drawn up. Next, the system was given a mesh as seen in Figure 16:

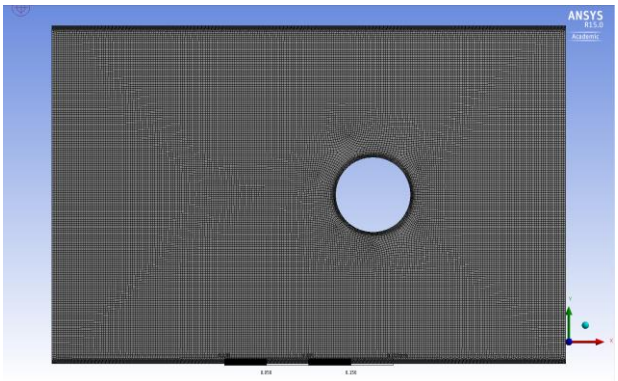

Figure 16: Mesh for 2D simulation

The picture above and the explanation below is for position 1 where the walls are the farthest away from the cylinder. Focus was put along the edge of the cylinder so the pressure and velocity can be seen in as much detail as possible. The edge of the cylinder was selected to be a moving wall with a rotational velocity of -523.6 rads/sec. The negative indicated a clockwise rotation.

Next, came the setup of the model. The window of the options is seen in Figure 25:

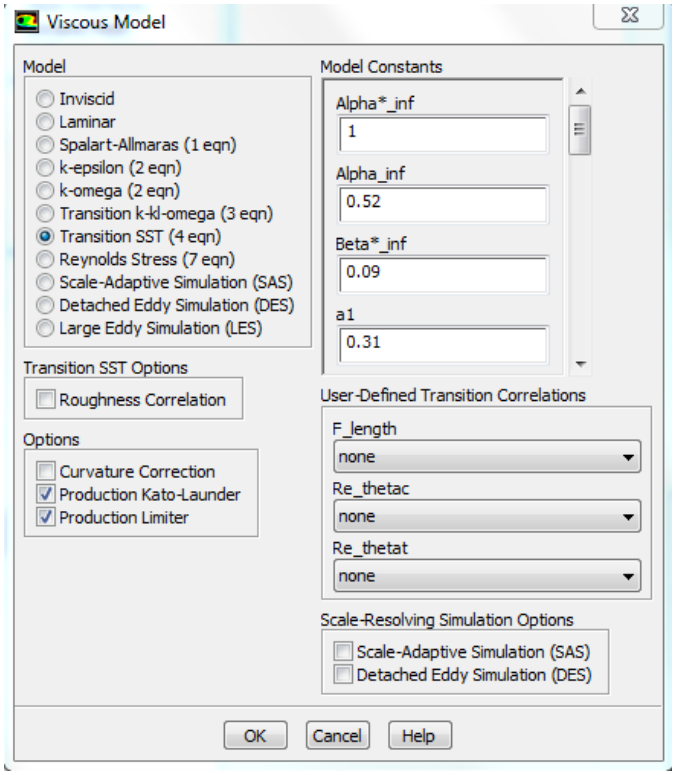

Figure 17: Viscous model setup

In order to understand which model was most appropriate, it had to be determined if the flow was laminar or turbulent. For this, the Reynolds number had to be found.

$$Re = \frac{v \cdot D_H}{\nu}$$

Where ν is the kinematic viscosity of air, v is the velocity of the air and D_H is the hydraulic diameter which is needed to convert the square duct into a circular duct. The equation for the hydraulic diameter is:

$$D_H = \frac{4 \cdot A}{P}$$

Where A is the cross-sectional area and P is the perimeter of the square duct. Plugging in the numbers gave a Reynolds number of 150,000 so the flow was turbulent. Next, the turbulent model was selected which was the Transition SST. This model was selected because Transition SST is a more advanced turbulence model that combines the advantages of k-omega and k-epsilon in predicting aerodynamic flows and particularly good at predicting boundary layers under strong adverse pressure gradients (8). This model is also a well-known model suited for channel flow and rotating cylinder (8). 2500 to 3000 iterations were ran for each position. Each 2-D test at each position converged. In terms of the solver used, the density-based solver was used because it is more accurate at high speed flows (9). The rest of the set up for the CFD simulation can be found in Appendix C.

5.3 Preliminary 2-D CFD Simulation Results

Only pressure and velocity results for position 1 and position 4 of each case will be shown and compared. This can be seen in Figure 18-Figure 21 below. The rest of the results can be found in Appendix B.

Position 1	Inlet Airspeed	RPM	Velocity Ratio
Case 1	52 mph (23.27 m/s)	5000 RPM (23.27 m/s)[-523.6 rads/sec]	1 to 1

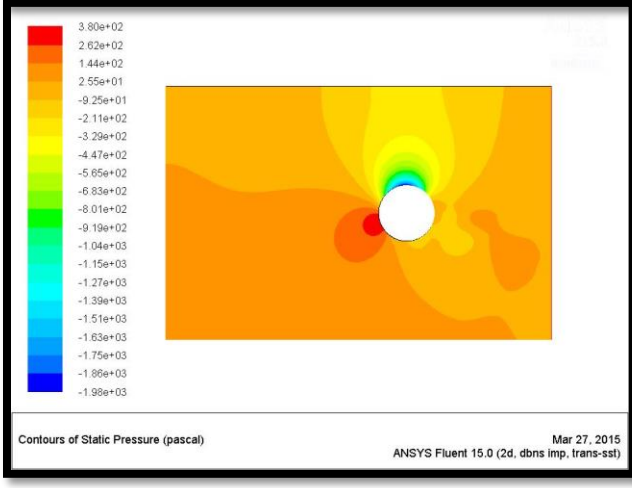

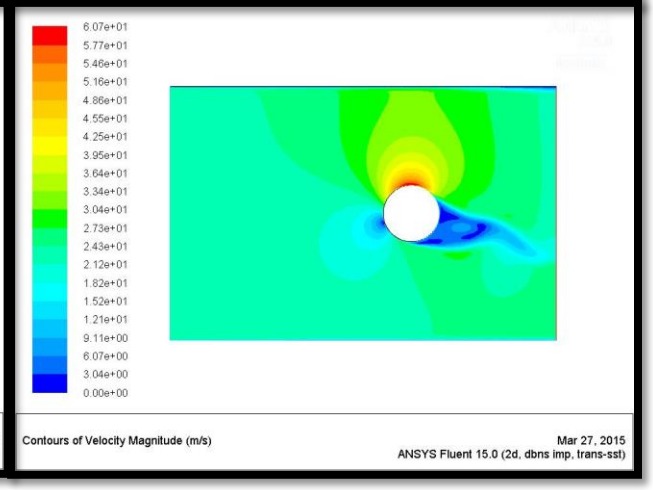

Figure 18: Position 1 Case 1 Pressure and Velocity Gradients

Position 1	Inlet Airspeed	RPM	Velocity Ratio
Case 2	26 mph (11.64 m/s)	5000 RPM (23.27 m/s)[-523.6 rads/sec]	2 to 1

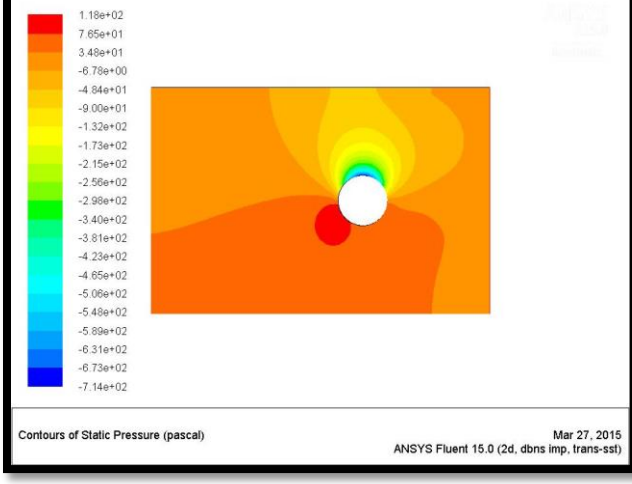

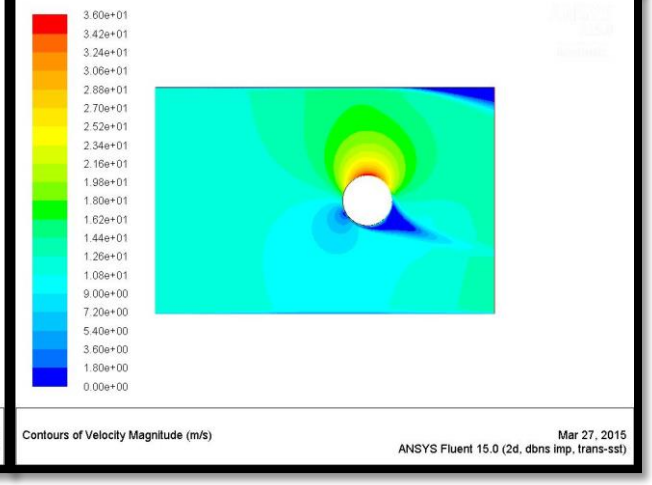

Figure 19: Position 1 Case 2 Pressure and Velocity Gradients

Position 4	Inlet Airspeed	RPM	Velocity Ratio
Case 1	52 mph (23.27 m/s)	5000 RPM (23.27 m/s)[-523.6 rads/sec]	1 to 1

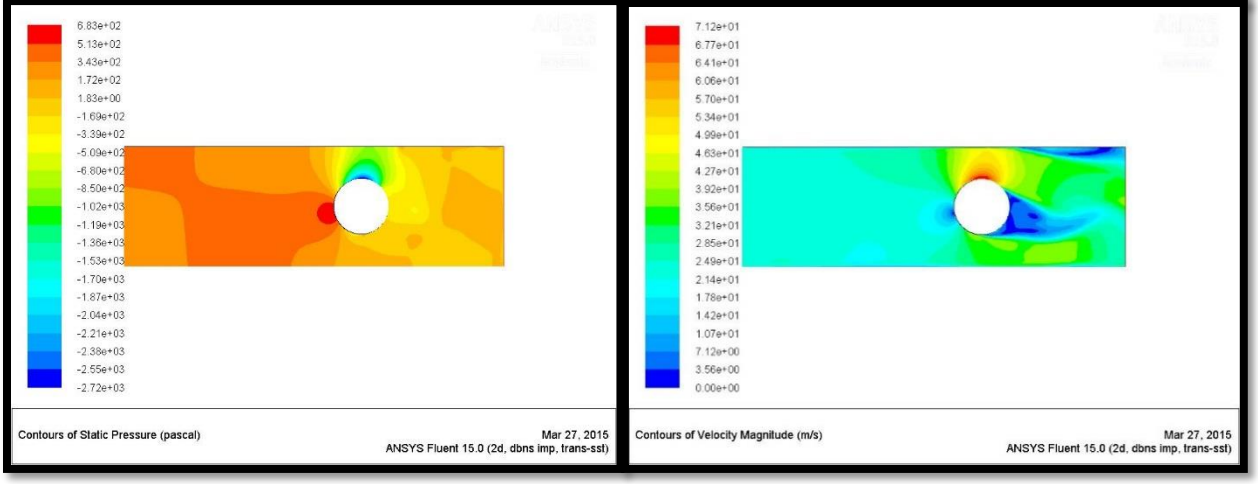

Figure 20: Position 4 Case 1 Pressure and Velocity Gradients

Position 4	Inlet Airspeed	RPM	Velocity Ratio
Case 2	26 mph (11.64 m/s)	5000 RPM (23.27 m/s)[-523.6 rads/sec]	2 to 1

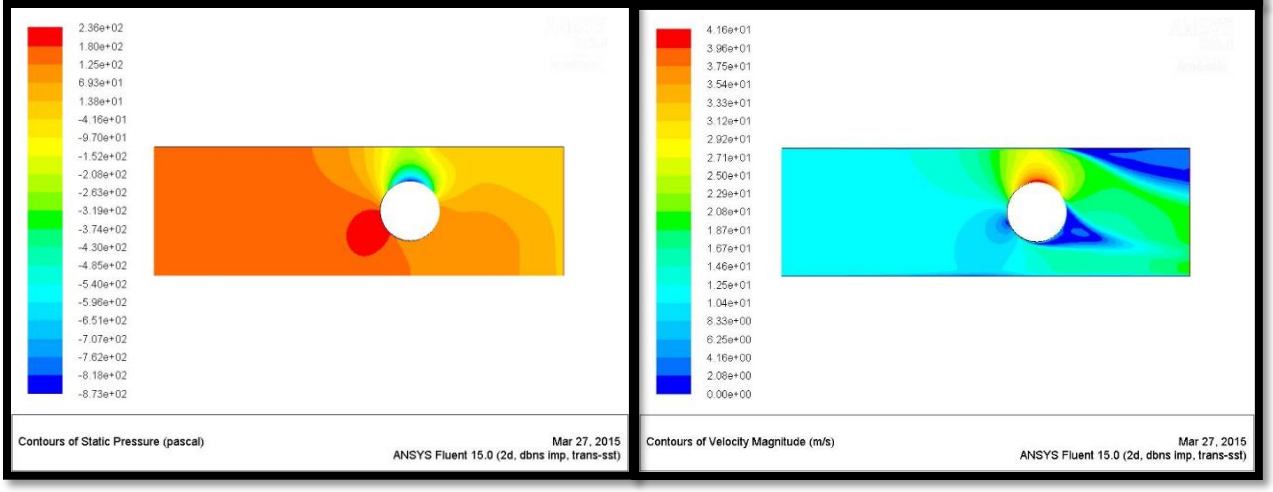

Figure 21: Position 4 Case 2 Pressure and Velocity Gradients

The results of the 2-D simulation looked promising because for each case low pressure was seen above the rotating cylinder and a high pressure below indicating that there was lift. A cylinder and duct assembly were designed in SolidWorks so 3-D simulations could be done. The dimensions of the first design match the same ones that were done with the 2-D simulations except we decided to make the duct 15.75 inches square. The first design is seen in Figure 22:

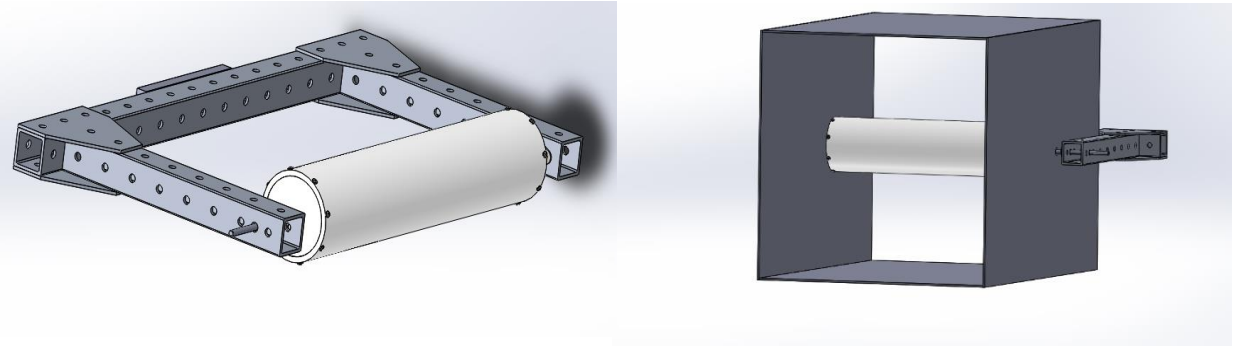

Figure 22: First 3D design for testing

5.4 Preliminary 3-D CFD Simulation Setup

The same set up as the 2-D simulations were used for the 3-D simulations in terms of the model used, change of internal dimensions and velocity of both the air and cylinder. Only case two speeds were used to show the desired 2-to-1 speed ratio of cylinder to air inlet speed.

There were come difficulties with the meshing part. At first, the model was directly imported from SolidWorks to ANSYS Fluent and is shown in Figure 23:

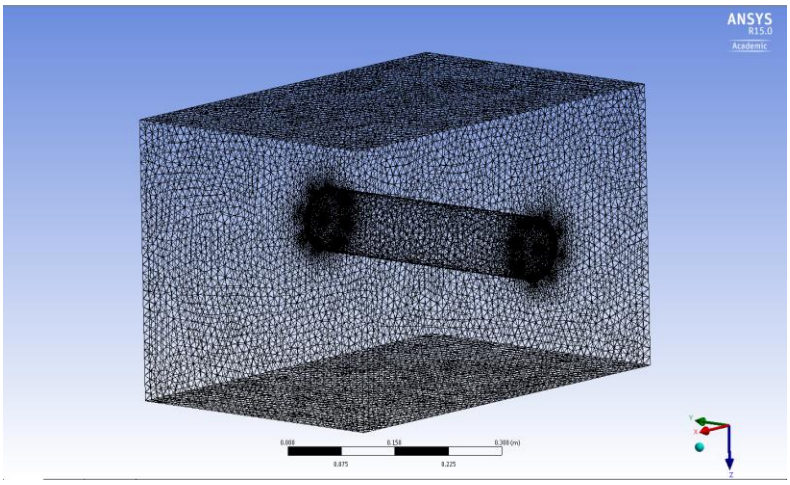

Figure 23: Initial 3D mesh

Taking a closer look at the meshed model reveals that the computer added complex meshing to where the screws were which used up a lot of the computing power. This can be seen in Figure 24.

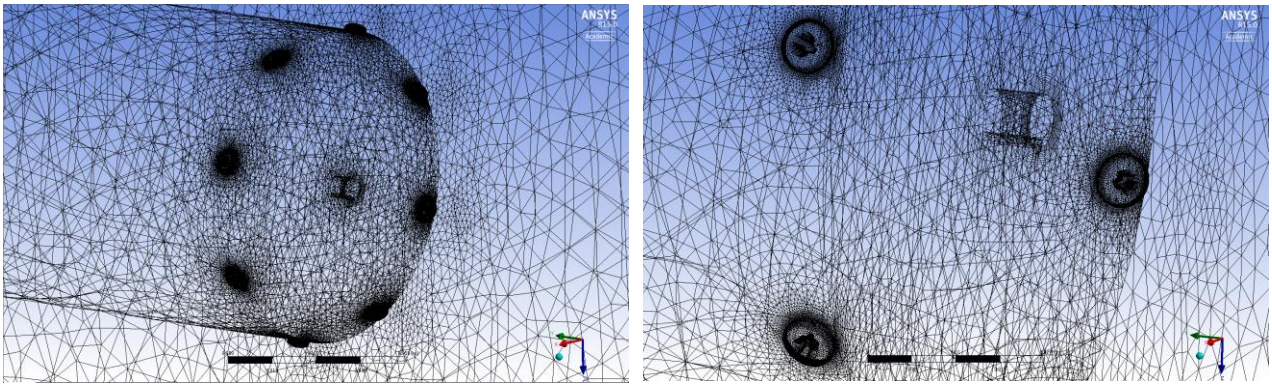

Figure 24: Complex meshing around screws

This made the computer run extremely slow and caused the software to crash. A simpler version had to be made so there were no screws. This is illustrated in Figure 25.

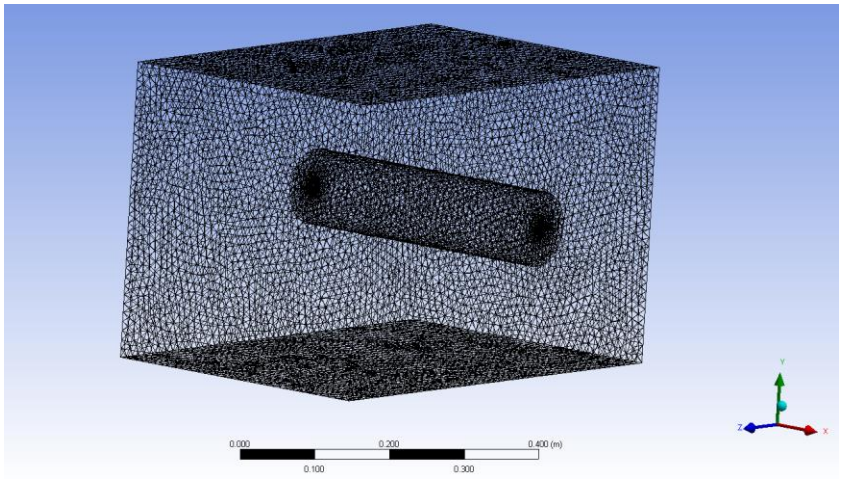

Figure 25: 3D mesh without screws

The new mesh was a lot simpler but still represented the design model very well. This allowed the computer to successfully compute CFD simulations.

Like the 2-D model, the 3-D model mesh focused on the cylinder face itself so the pressure and velocity could be shown in great detail. A side-view of the mesh is seen in Figure 26.

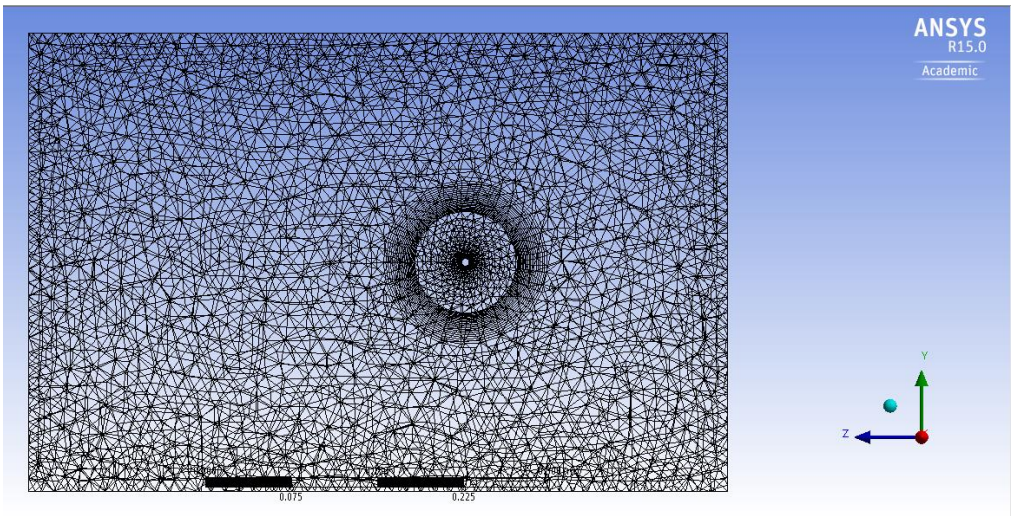

Figure 26: Side view of 3D mesh

Still, the simulations being ran were still not converging and anything over 500 iterations risked diverging. A new mesh technique had to be used. This new mesh is shown in Figure 27

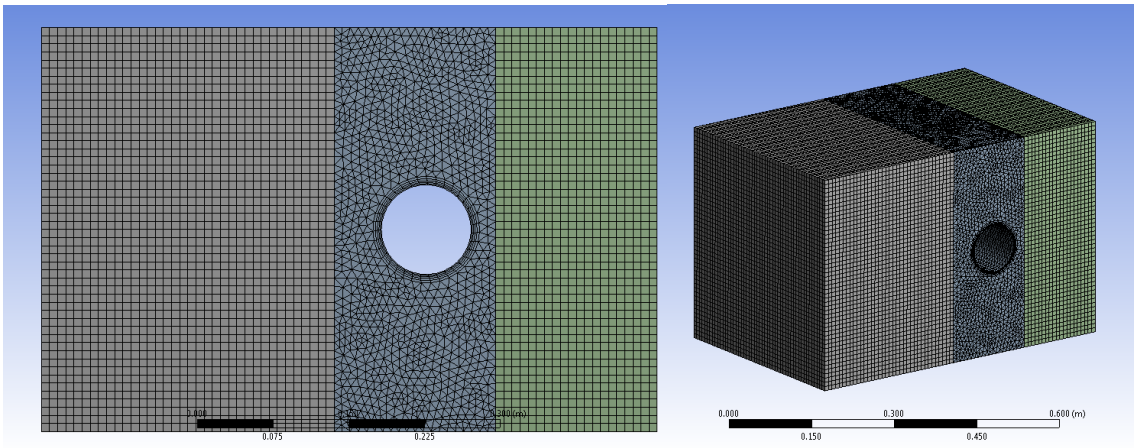

Figure 27: New 3D meshing technique

This technique split up the duct into three sections, the inlet, cylinder and the outlet sections. The inlet and outlet sections were fairly basic but the cylinder section was denser with more elements so the Magnus effect can be seen in more detail in this section. ANSYS Fluent was able to compute these meshed models better than the previous meshed models, and all simulations converged.

5.5 Preliminary 3-D CFD Simulation Results

Since the 2-D results were promising, 3-D simulations were ran. Due to the length of time it took to run 3-D simulations, only the four positons from case 2 were ran and the results of the simulations can be seen in Figure 28 and Figure 29 below. Only pressure and velocity results of positions one and four will be compared. The remainder of the results for all the positons can be viewed in Appendix B.

Position 1	Inlet Airspeed	RPM	Velocity Ratio
Case 2	26 mph (11.64 m/s)	5000 RPM (23.27 m/s)[-523.6 rads/sec]	2 to 1

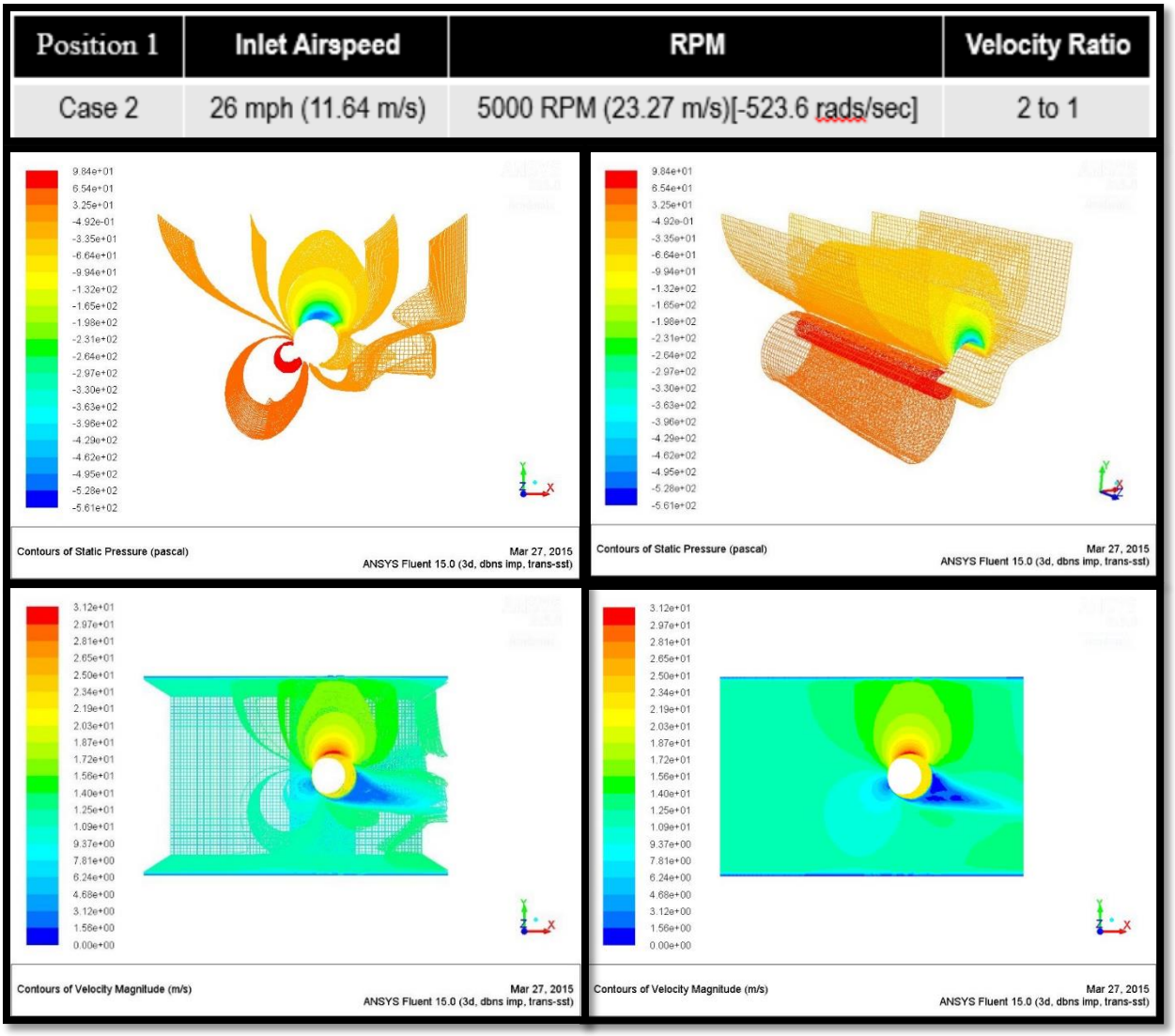

Figure 28: Position 1 3D Pressure and Velocity Contours

Position 4	Inlet Airspeed	RPM	Velocity Ratio
Case 2	26 mph (11.64 m/s)	5000 RPM (23.27 m/s)[-523.6 rads/sec]	2 to 1

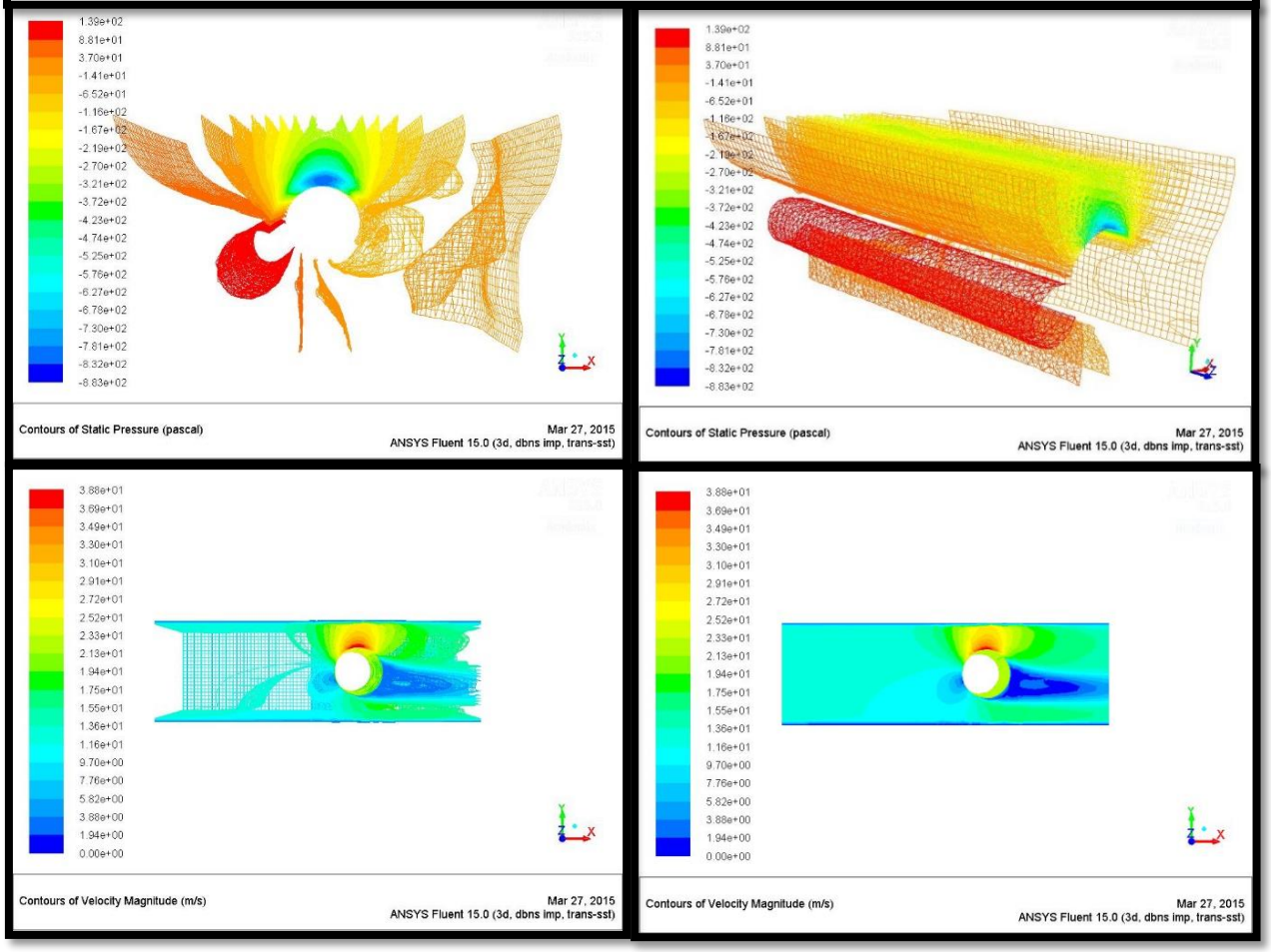

Figure 29: Position 4 3D Pressure and Velocity Contours

5.6 Analysis

Looking at the 2-D cases, there were some differences in the pressures and velocity charts between the two cases. Case 2 looked to be more stable than case 1. This is probably because the inlet air velocity for case 2 was half of what the velocity was for case 1. Another reason is the velocity ratio between the inlet velocity and rotational velocity was at the desired 2-to-1 ratio. The desired ratio case (case 2) was better able to hand the air flow and had a more stable pressure distribution than case 1.

Comparing the velocities of both 2-D cases shows some differences as well. Velocity contours for both cases at position 1 can be seen in Figure 30.

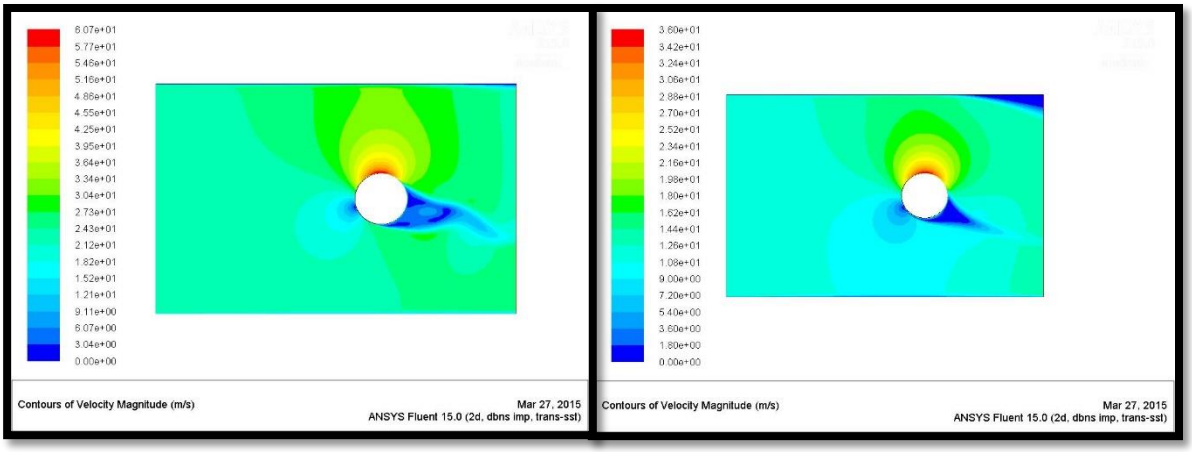

Figure 30: Position 1 2D Velocity Gradients. Case 1 (left) and Case 2 (Right).

Case 1 is on the left and case 2 is on the right. It can be seen that in case 2, there is a slow spot forming in the top right corner while there is none forming in case 1. Looking at position 4 for both cases reveals that the slow spot is now developing in case 1 and has become more pronounced in case 2. This can be seen in Figure 31.

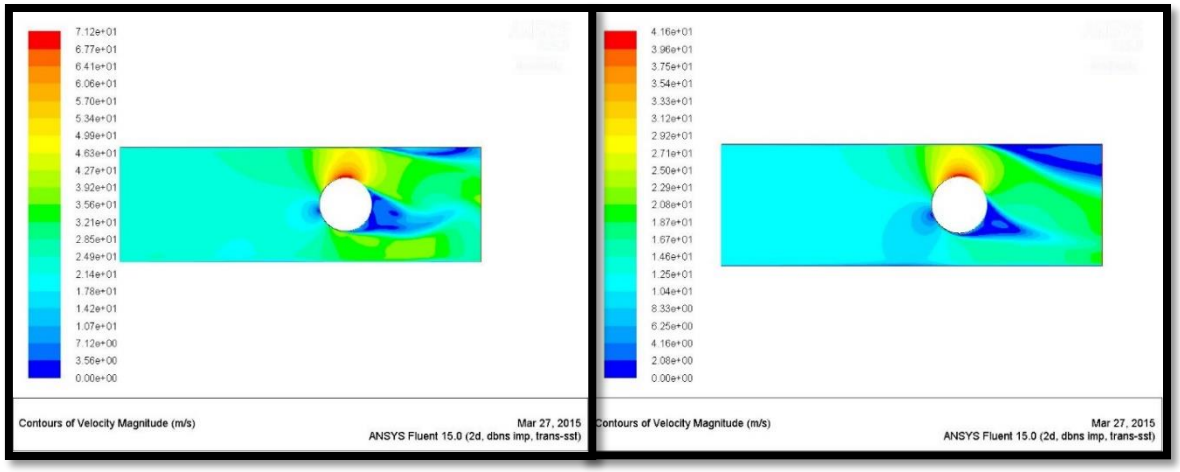

Figure 31: Position 4 Velocity Gradients. Case 1 (left) and Case 2 (right).

Seeing that there is an interesting boundary layer developing behind the rotating cylinder, the downstream duct for case 2, at position 4, was extended. The pressure, velocity and turbulence contour graphs can be seen in Figure 32.

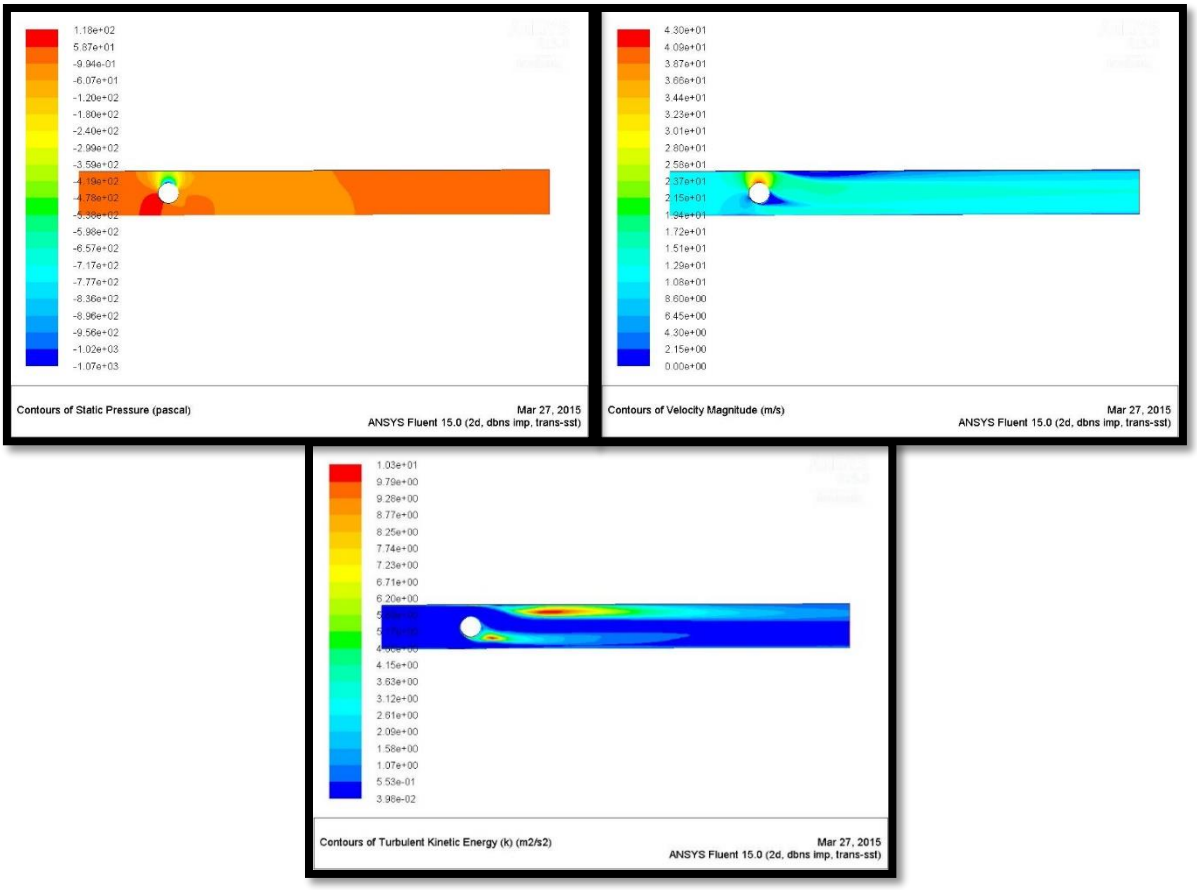

Figure 32: Long duct contours of pressure (top left), velocity (top right) and turbulence (bottom).

Increasing the length of the duct did affect the pressure readings along with the velocity readings. This is to be expected since the extended length of the duct would affect how the pressure is distributed. Extending the length did however, serve its purpose and revealed the boundary layer. Looking at the turbulence contour graph shows that there is a high turbulent kinetic energy behind the cylinder and on the upper wall. This acts like a channel itself causing a majority of the air to travel above the cylinder and back to the middle of the duct while creating a 'wall' below the cylinder causing a slower flow of air and thus, a higher pressure region.

Comparing the 2-D simulations with the 3-D simulations shows some difference as well. For starters, the boundary layer that develops at the top of the 2-D case does not show in the 3-D case, as seen in Figure 33.

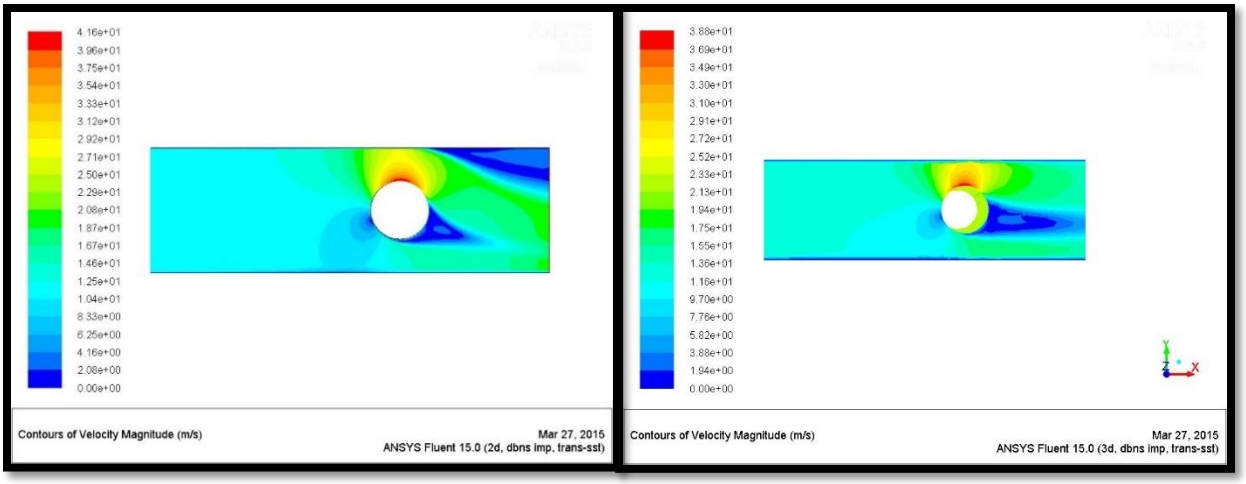

Figure 33: 2D and 3D simulations for Position 4, Case 2

The picture on the left is the 2-D case while the picture on the right is the 3-D case. Both are case two, position four. It is not sure why the boundary layer is not seen but one theory could be that the mesh for the 3-D case was not dense or fine enough to capture the boundary level.

5.7 ANSYS Fluent Lift Force calculations

Comparing the lift force between the 4 positions and the 5th extra position shows an increase of lift force in both the y direction and x direction. The x direction increases because the stagnation point at the front of the cylinder increases with the increase of airflow as the duct inner dimensions decrease. Looking at the Y force, it shows between position 1 and position 2, there is very small change which implies that position 1 is open air conditions. As seen in Table 2, the percent increase in lift from position 1 to position 2 is minimal.

Table 2: Lift and drag on the cylinder at all positions

POSITION	X FORCE (N)	Y FORCE (N)	VISCOUS (N)	TOTAL Y FORCE (N)
1	1.324077	13.403676	-.0042833	13.39939
2	1.324882	13.412348	-.0043406	13.40800
3	1.003606	15.280142	-.0053745	15.27476
4	2.640816	18.430393	-.0100023	18.42039
5 (EXTRA)	4.255512	22.591839	-.0141061	22.57773

We can conclude that the boundary effects implemented from the wall at position 1 are not significant enough to play a major role in the impact of Magnus lift on the cylinder. Table 3 below shows the percentage change of the lift force as the internal dimensions of the duct decrease.

Table 3: Change in lift on the cylinder from position to position.

POSITION	Δ% X FORCE	Δ% Y FORCE	Δ% VISCOUS	Δ% TOTAL Y FORCE	Δ% DUCT HEIGHT
1	0	0	0	0	0
2	0.06079707	0.06469867	1.3377536	0.06425666	-17.4603
3	-24.2033507	13.9996371	25.4756846	13.9959356	-34.9206
4	99.4458026	37.5025254	133.518549	37.4718551	-52.381
5 (EXTRA)	221.394602	68.5495755	229.327855	68.4981928	-61.9048

It may seem that the percentage increase of the X force and viscous forces far outweigh the percentage increase of the Y force but the actual Y forces changes are far greater than the x forces and the viscous forces, as seen in Figure 34.

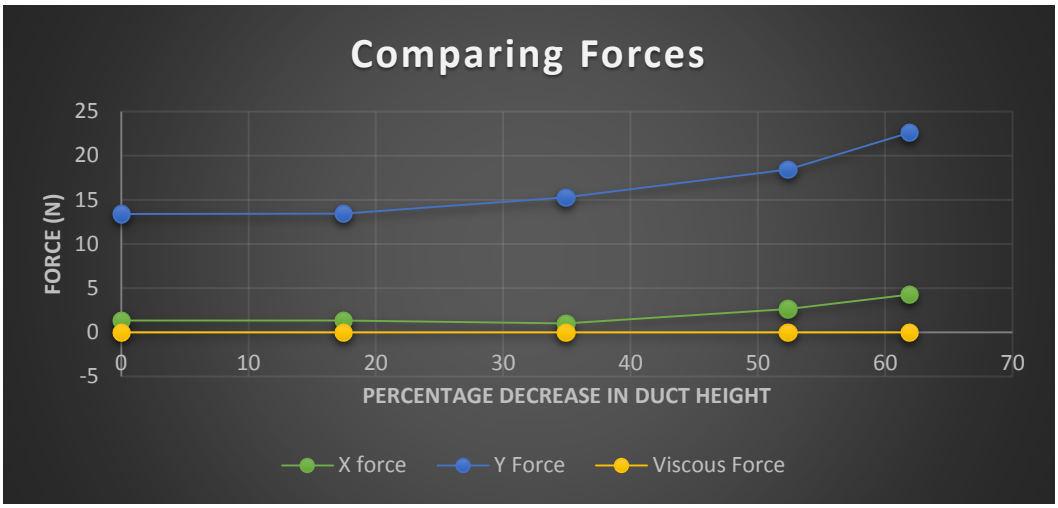

Figure 34: Force vs duct height

Graphing the percentage change of the duct height and the Y force shows how the change in duct height effects the Y force, as seen in Figure 35.

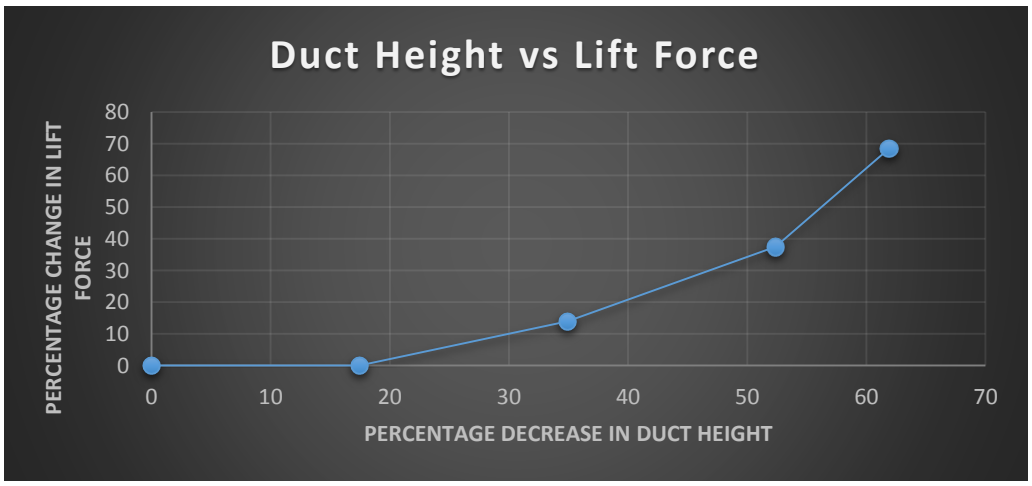

Figure 35: Lift force vs duct height

Seeing promise with the preliminary simulations, we moved on to optimizing the cylinder and duct design and optimizing the ANSYS Fluent simulations. It was determined to look at the effect the walls would have on the experiment. A decrease in pressure above the cylinder and an increase in pressure below could produce a downward force on the walls which could hinder the lifting force of the spinning cylinder.

6.0 Wind Tunnel Testing

6.1 Test Fixture

6.1.1 Wind Tunnel

In order to understand how enclosed spaces such as ducts affect Magnus Lift, real world testing is desired along with simulations. To do this, an Aerolab wind tunnel belonging to the University of Akron was chosen to provide consistent conditions for testing. In order to get the data desired from testing, a fixture is required that can spin a cylinder at high speeds and change duct sizes while still operating within constraints required by the Aerolab wind tunnel. The Aerolab wind tunnel that will be used in testing can be seen in Figure 36.

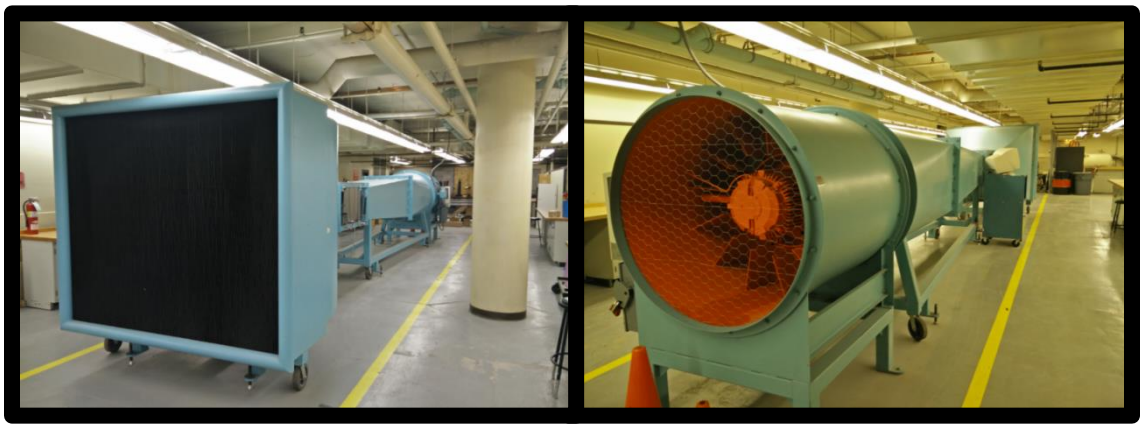

Figure 36: The University of Akron's Aerolab Wind Tunnel

The working portion of the Aerolabs wind tunnel is a 20" tall by 28" wide by 48" long section in the center of the tunnel. Near the center of this box is a fixture known as the "sting." The sting is designed so that airfoils can be mounted directly in the center of the tunnel for analysis. It can determine both lift and drag on any object attached to it. There is 26" of usable space before the sting. This section of the tunnel can be seen in Figure 37. The sting is capable of measuring up to 25lbs of force in any direction. In addition, the tunnel is capable of producing air speeds in excess of 100mph.

Figure 37: Working section of the Aerolab wind tunnel. Note the "sting" located in the center of the box

6.1.2 Design Constraints

As discussed in the previous section, any fixture designed must work within the constraints required by the Aerolabs wind tunnel. In addition, the design is limited by the funds available to the students. A list of constraints can be broken down as follows:

1. **Size**: The test fixture must fit within the 20”x28”x26” section of wind tunnel directly upstream of the sting. This will that a spinning cylinder can be enclosed in a uniform duct without having to accommodate the sting. The fixture must also be designed slightly smaller than the allowed space so that it can be easily loaded and unloaded from the wind tunnel.

2. **Weight**: The sting can measure up to 25lbs of force. This means that anything mounted to it must weigh less than 25lbs if positive lift is expected, otherwise any measured data may be skewed. For example, if the fixture weighed 30lbs, the sting would only read a force of -25lbs. If 5lbs of lift was generated, the sting would still only read -25lbs. However, if the fixture weighs 15lbs, the sting would read -10lbs of force. This means the sting can then detect 35lbs of lift before exceeding its limits again.

3. **Motor Speed**: The Aerolab wind tunnel can produce air speeds over 100mph. However, air speeds that can reasonably be tested are limited by how fast the chosen motor can spin the cylinder. Previous research indicates that a desirable rotational speed for the cylinder is when the cylinder’s tangential velocity is twice as fast as the air flowing around it. This would ensure air speeding up over the top of the cylinder, while slowing down below it. Unfortunately, extremely high rpms are required to obtain this speed ratio for small cylinders. For example, for an airspeed of 100mph, a cylinder with a 4” diameter would have to rotate at a speed of 8400 revolutions per minute in two have the desired speed ratio. Obviously, it is difficult to find a small motor capable of doing this.

4. **Cost**: Perhaps one of the most limiting constraints is the available funds. At the University of Akron, students can expect around $250 for their Mechanical Engineering senior project. If they are in the Honors College, they can expect a matching $250. This means the ideal budget for the entire test fixture should be less than $500.

6.1.3 Material Selection

Based on the constraints listed in the previous section, materials should be selected with two factors in mind: weight and cost. Materials should be as lightweight as possible so the fixture will weigh under 25lbs. However, they should still be strong enough to support the weight. In addition, the materials need to be budget friendly so the test fixture doesn’t exceed $500.

Aluminum is a strong, lightweight material often used in aerospace applications. In addition, it is very lightweight; about one third of the weight of steel. As an added bonus, aluminum is a readily available and fairly cheap. With these points in mind, aluminum is a good choice for the structure of the fixture.

The spinning cylinder itself is another case. It also needs to be lightweight and cheap, but it is harder to find readily available aluminum tubing that would be easy to machine. However, PVC piping is very cheap, it's common, it's easy to work with, and it is still strong enough for this application. As such PVC is a good choice as a material for the spinning cylinder.

Endcaps for the spinning cylinder and connecting pieces need to be, again, easily machined, lightweight, and cheap. ABS plastic is a widely used, cost effective, rigid material, and will be used for the design.

6.1.4 Fixture Design

In addition to the several design constraints, there are several objectives that the test fixture should satisfy. First, the fixture should consist of two separate parts: one mounted to the sting, and one mounted to the wind tunnel itself. The part mounted in the wind tunnel will be a duct that a spinning cylinder can sit inside of. This duct should be able to change in size. Ideally, the top and bottom portions of the duct will be able to move up and down. That way it will be easier to determine the effects of enclosing spinning cylinders in tighter spaces. The sting attachment will hold the spinning cylinder. The sting attachment will feed through the "duct" so that the spinning cylinder will be as close to the duct walls as possible. Finally, due to limited manufacturing abilities, the entire test fixture should be easy to build. This means screw together construction is vastly preferable to welding.

The test fixture design has gone through several revisions. The first design that was explored included a very sturdy, lightweight sting attachment and a heavy duct fixture. The sting attachment was to be built from rugged aluminum square framing. This part also held the spinning cylinder and attached bearings on a solid aluminum shaft. This can be seen in Figure 38. The cylinder (schedule 40 PVC with a 3.5" OD) would be attached to the shaft via ABS plastic endplates and a keyway.

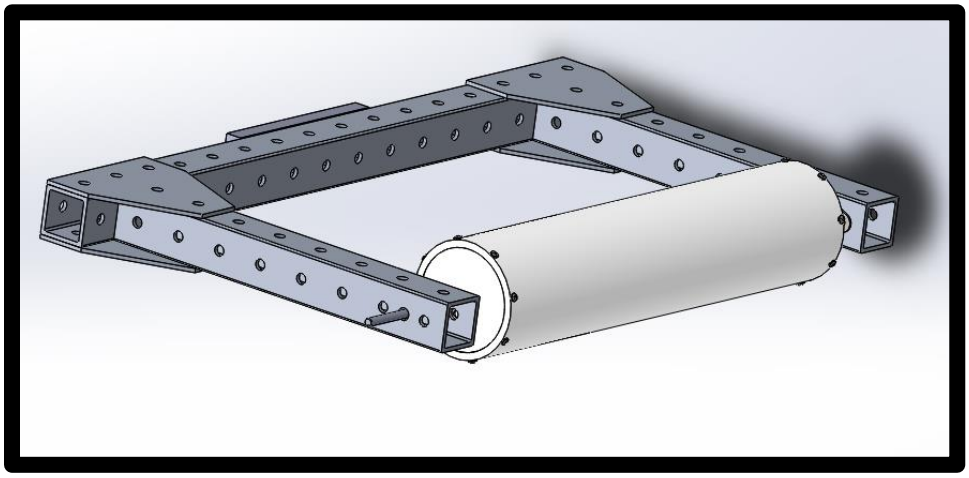

Figure 38: First Design - Sting and Cylinder Attachment

The sting attachment would be mounted so the cylinder would be inside the duct fixture. The motor and accompanying batteries would be installed beneath the duct fixture, and would be attached to the cylinder shaft via a chain and sprocket or belt drive system, as seen in Figure 39.

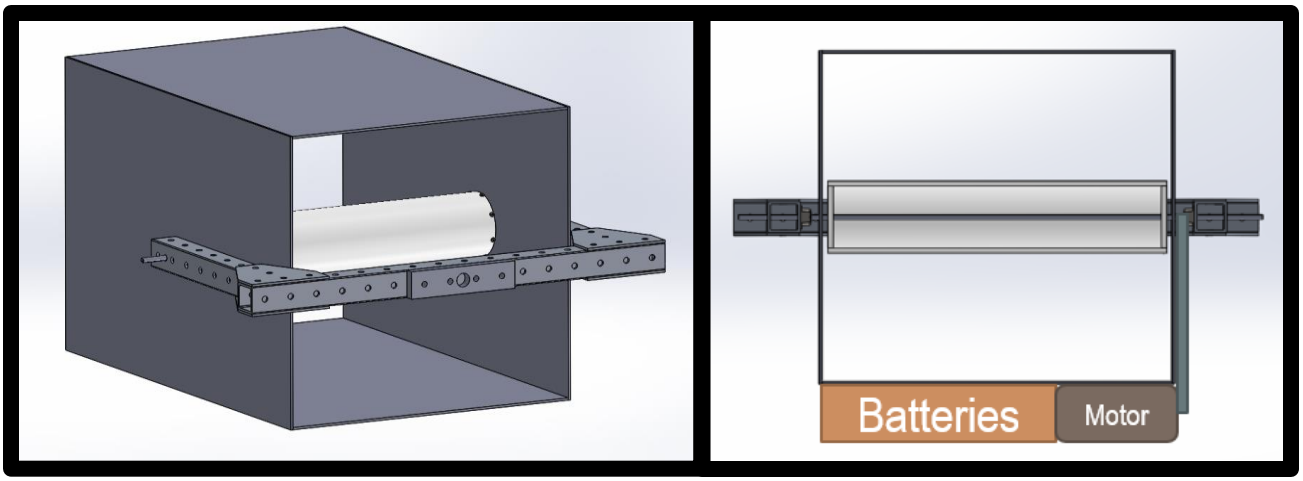

Figure 39: First Design cylinder assembly and duct (left) with proposed battery and motor placement (right)

The first design was rejected before completion for a multitude of reasons. First, mounting the motor and batteries below the duct reduced the total space that could be used for air flow, thus limiting the scope of the experiment. This limitation gets worse depending on the size of the motor or batteries. Next, the external motor mounting could lead to erroneous data. The tensioning of the belt or chain as well as the weight of the gearing system influence the force that the sting would be reading. Finally, the structure of the sting/cylinder attachment was unnecessarily bulky. This would likely cause excessive drag on the sting, making it difficult to judge what magnitude of drag is acting on the cylinder itself.

A new design was conceived that would mostly solve the previously mentioned issues. This design used aluminum hand rail as the structural support. As before, the cylinder is made with PVC pipe (4" OD this time), with ABS endplates. However, this design has a motor mounted inside the cylinder that is attached via a machined ABS plastic coupler. This motor is an Ampflow E30-150; a 1HP motor capable of speeds up to 5600RPM. Unlike the first design, the new fixture has a stationary shaft that does not rotate. The cylinder rotates about the shaft on a series of 3 bearings inlayed in the endcaps and coupler. Detailed views of this assembly can be seen in Figure 40.

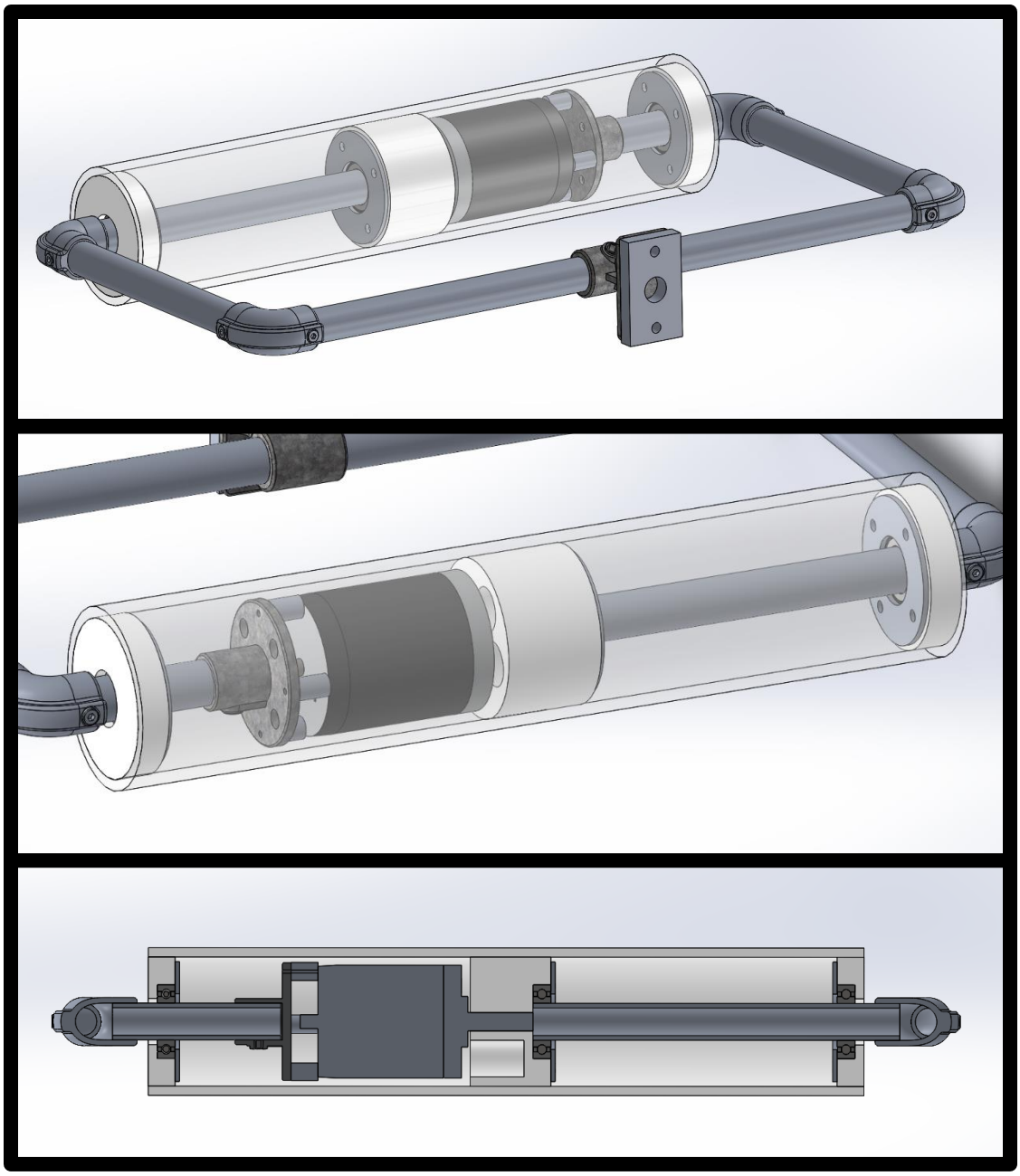

Figure 40: Second Design cylinder/sting fixture. Views detailing interior motor attachment and placement (top, middle) and a cross sectional view showing bearing placement (bottom)

This design is more aerodynamic than the first design since the hand rail is smoother and takes up less space than the structural supports of the first design. It also solve motor placement and drivetrain issues. This design also allows for a wider cylinder as well as a slightly larger diameter, since the hand rail is so much slimmer than the structural framing. However, due to the internal motor mount, this sting assembly is heavier. Without screws, it weighs roughly 12lbs (calculated with SolidWorks mass properties), while the previous design weighted only 6lbs. 12lbs, however, is still within the design parameters. As with the first design, the cylinder is mounted in a separate duct fixture, as seen in Figure 41.

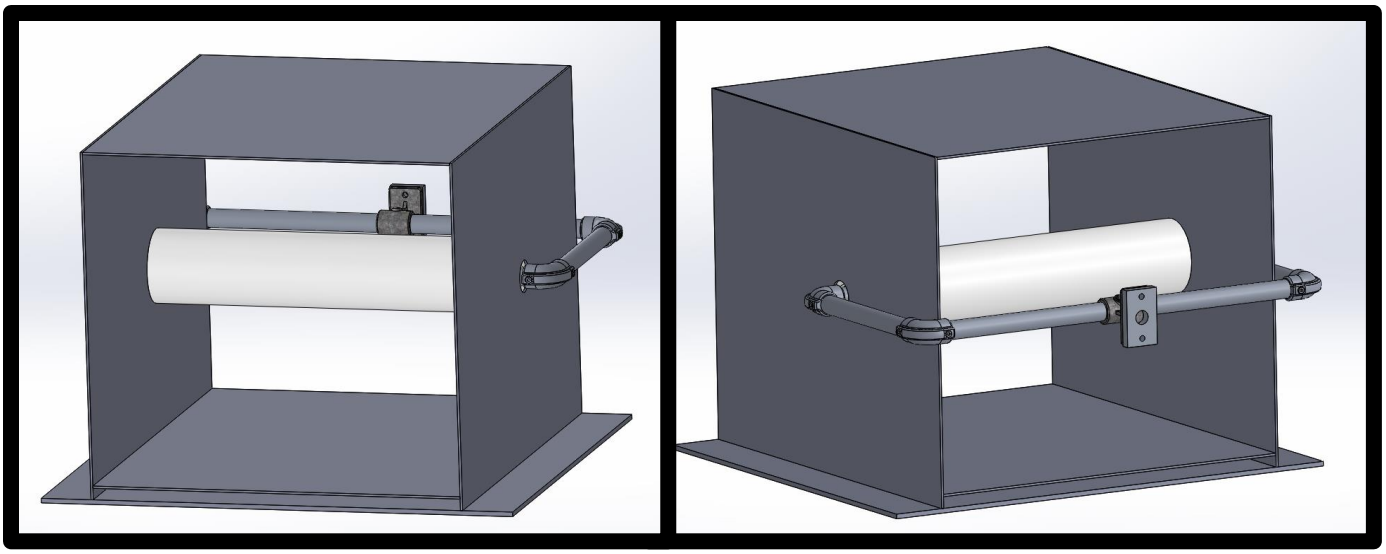

Figure 41: New Design - Full Test Fixture

Because of the integrated bearing design, the cylinder can be mounted very close to the duct walls. The current design has a 1/8” gap between cylinder and duct walls. Keeping this gap thin (as seen in Figure 42) will help prevent the generation of vortices near the duct wall that may interfere with test results.

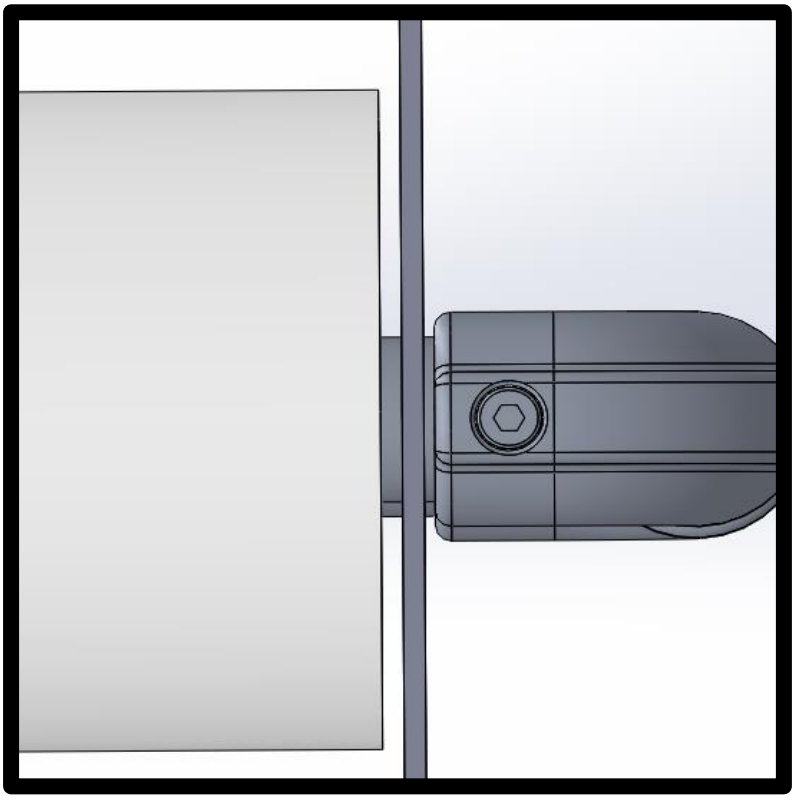

Figure 42: 1/8" gap between rotating cylinder and duct wall

6.2 Test Setup

The following is a desired test procedure to be carried out upon the completion of the test fixture and CFD testing.

1. Place test fixture in the Aerolab wind tunnel. Ensure the cylinder fixture is securely attached to the sting.

2. Run the power wire down the sting and out of the wind tunnel via a side port.

3. Place the “duct” part of the fixture in Position 1, allowing an 18 inch vertical duct height.

4. Turn on the wind tunnel. Power up until a constant air velocity of 30mph (~13.3 m/s) is achieved.

5. Begin recording lift and drag on the cylinder.

6. Turn on the integrated cylinder motor and slowly ramp up the speed until 5000rpm is achieved.

7. Hold 5000rpm for 10 seconds and slowly reduce motor speed until it comes to a rest.

8. Turn off the motor and stop recording.

9. The motor is likely very hot due to poor airflow inside the fixture. Allow ample time to cool before continuing the next trial.

10. Set the fixture to Position 2. Repeat steps 4-9.

11. Repeat steps 4-9 for Position 3 and 4.

12. Repeat procedure for additional trials to ensure consistent data.

7.0 Final CFD

The following shows the 2-D and 3-D CFD results for position 1 and 4 for the final design shown above. Similar to the test ran for the preliminary design, the duct will decrease in total height but instead, it will decrease by four inches instead of 2.75 inches for the preliminary tests. All other pictures of the other positions can be found in the Appendix B.

7.1 2-D

Figure 43 shown below gives similar results as the preliminary CFD results. The only difference is, in order to keep the 2 to 1 velocity ratio, the inlet airspeed had to be increased since the increase of the cylinder diameter increased its' tangential speed.

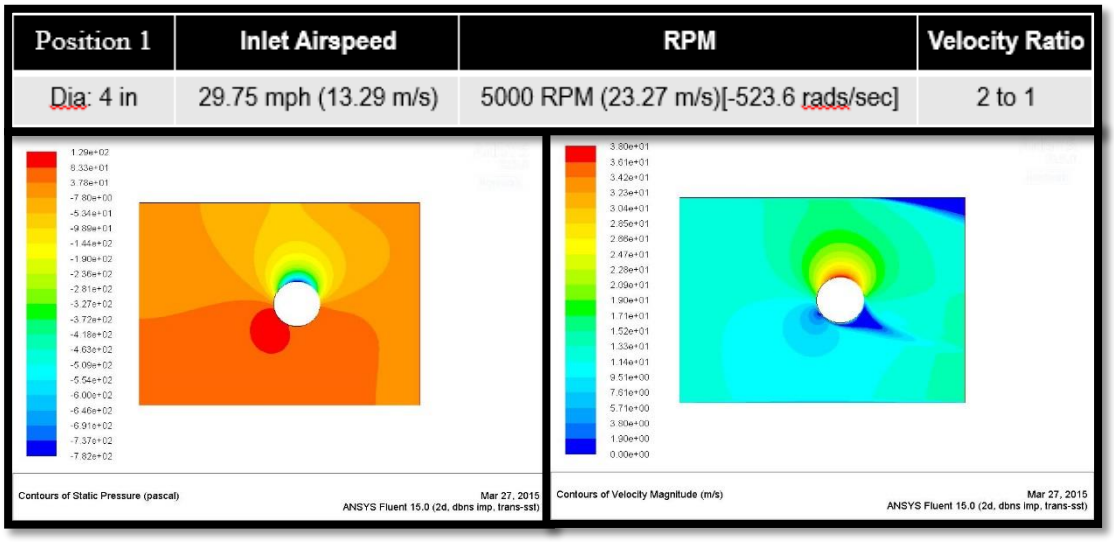

Figure 43: 2-D CFD results for position 1 of final design

Figure 44 shows similar results as the preliminary CFD results but the velocity shown above has a larger separation of boundary layer than position 4 of the preliminary CFD results.

Position 4	Inlet Airspeed	RPM	Velocity Ratio
Dia: 4 in	29.75 mph (13.29 m/s)	5000 RPM (23.27 m/s)[-523.6 rads/sec]	2 to 1

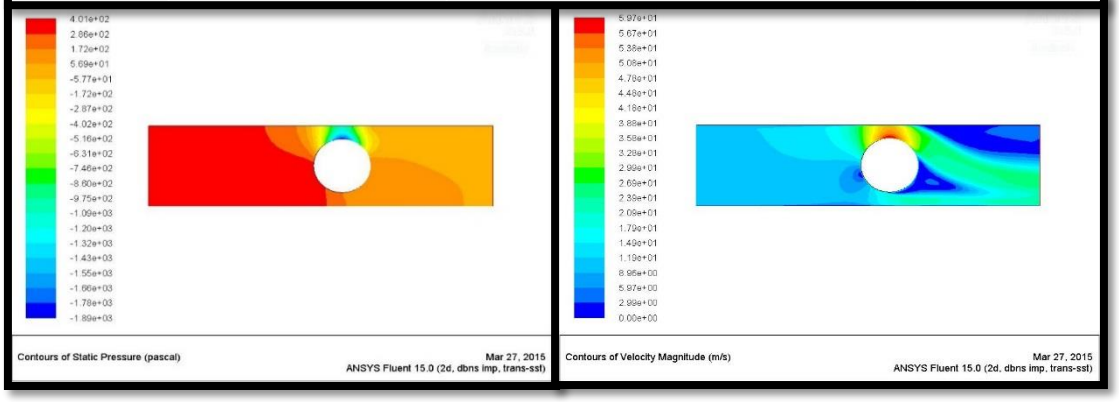

Figure 44: 2-D CFD results for position 4 of final design

7.2 3-D

The new mesh was set up the same way as the preliminary mesh however, it was desired to see what effect the 1/8” inch boundary would have on the pressure and velocity gradients. This mesh set up is seen in Figure 45. Figure 46 below showed that even the 1/8” had an effect on the pressure gradient. There seems to be some shedding which allows high pressure to overcome the low pressure above causing a “hump” above the spinning cylinder.

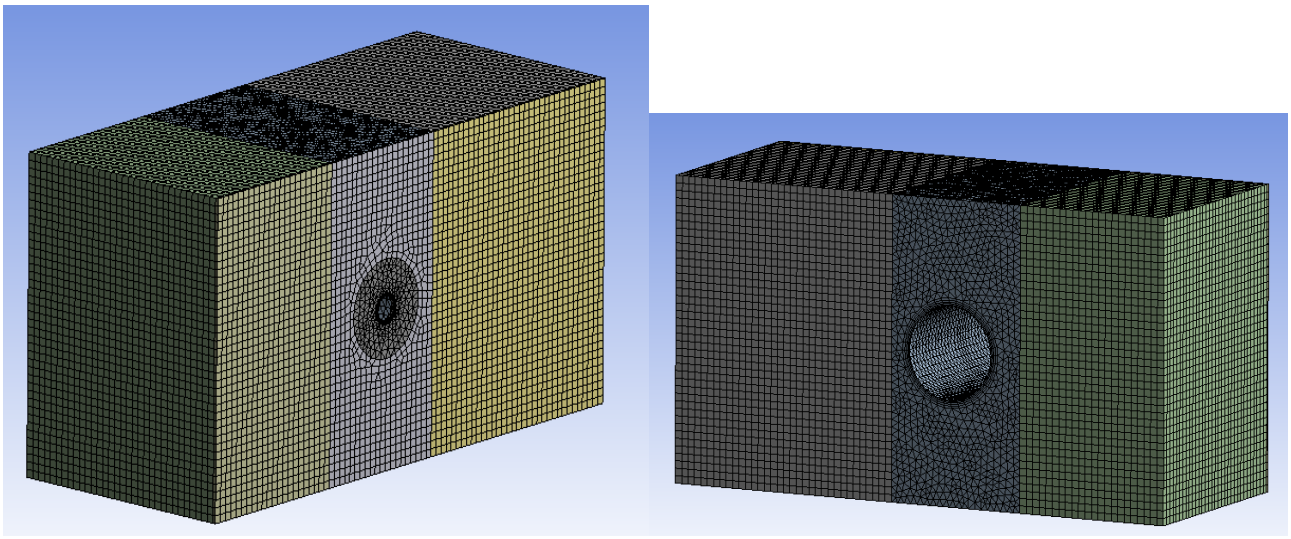

Figure 45: New mesh technique to include 1/8" gap between the cylinder and the duct walls

Position 1	Inlet Airspeed	RPM	Velocity Ratio
3D	29.75 mph (13.29 m/s)	5000 RPM (23.27 m/s)[-523.6 rads/sec]	2 to 1

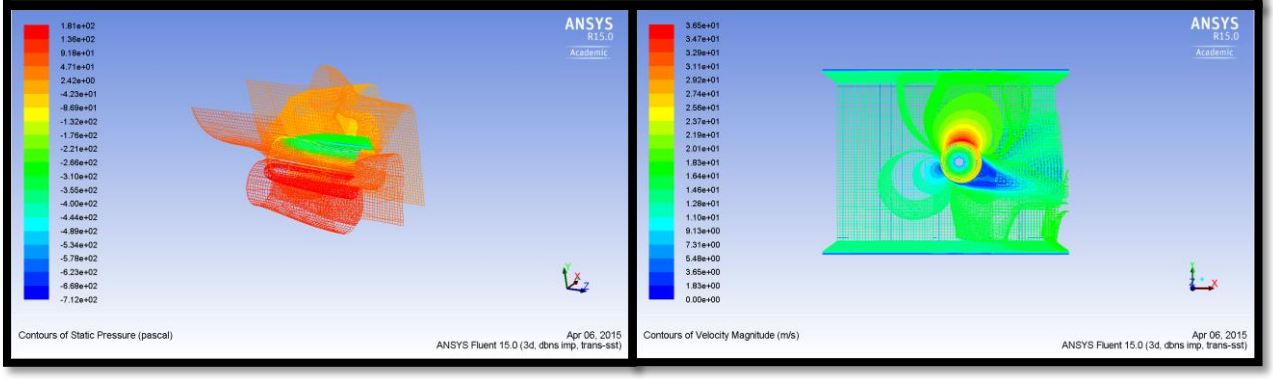

Figure 46: 3-D CFD simulation results for position 1 of final design

Figure 47 shown below shows similar results as the preliminary 3-D CFD results except the low pressure "hump" seen above the cylinder.

Position 4	Inlet Airspeed	RPM	Velocity Ratio
3D	29.75 mph (13.29 m/s)	5000 RPM (23.27 m/s)[-523.6 rads/sec]	2 to 1

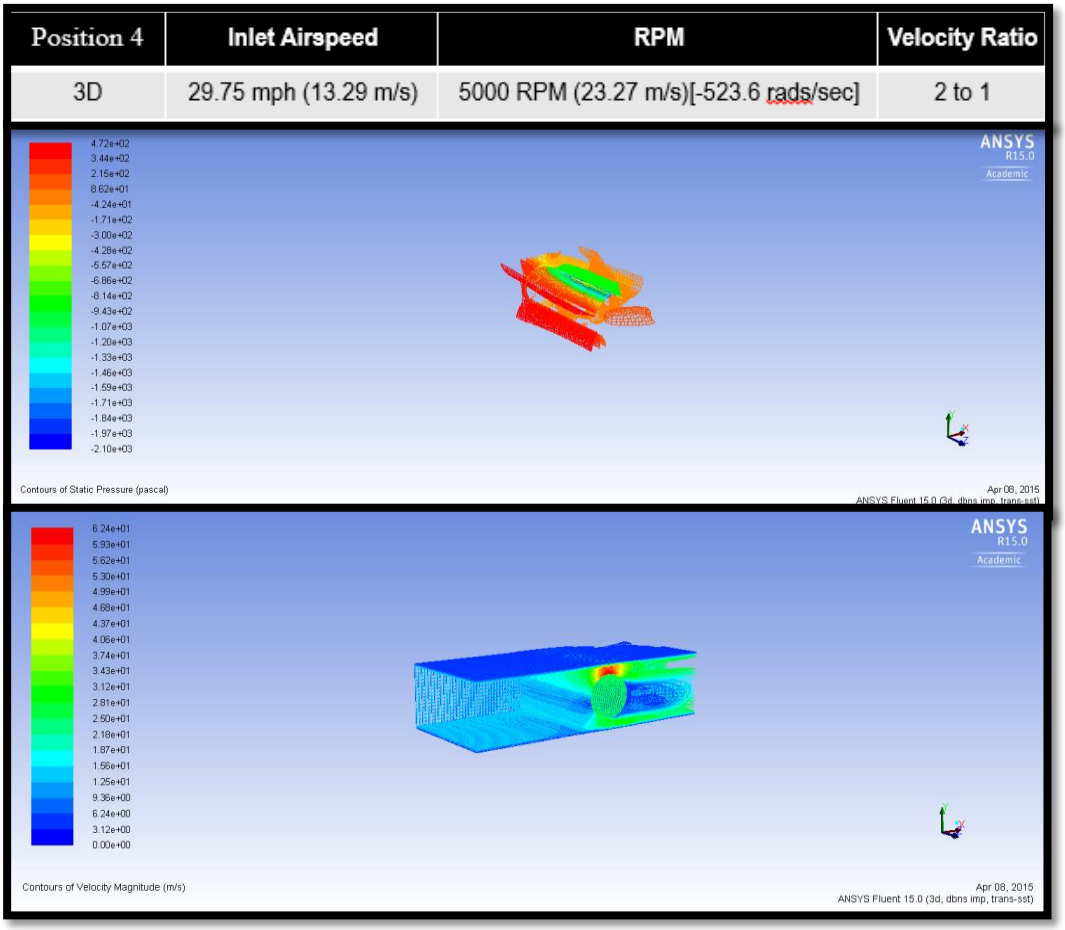

Figure 47: 3-D CFD results for position 4 of final design

7.3 Analysis and Results of Lift Force

The forces of both the cylinder and the duct walls were investigated. The Y forces, X forces and the viscous forces were compared and graphed below. Table 4 and Table 5 below shows the forces acting on the cylinder and the duct walls.

Table 4: Shows the forces acting on the cylinder

CYLINDER			
POSITION	**X Force (N)**	**Y Force (n)**	**Viscous (N)**
1	7.1236454	21.64304	-0.02367428
2	6.6069488	22.28368	-0.02832292
3	7.7551732	26.86234	-0.02585854
4	16.2938766	47.85444	-0.03402344

Table 5: Shows the forces acting on the duct walls

DUCT WALLS			
POSITION	**X Force (N)**	**Y Force (n)**	**Viscous (N)**
1	0.002436801	-17.457514	0.04495931
2	0.0052044	-17.953669	0.05175896
3	0.0033016	-27.309754	0.03583354
4	0.007747	-47.112336	0.03065732

These forces were graphed for both the duct walls and the cylinder for comparison and can be seen in Figure 48, Figure 49, Figure 50, and Figure 51.

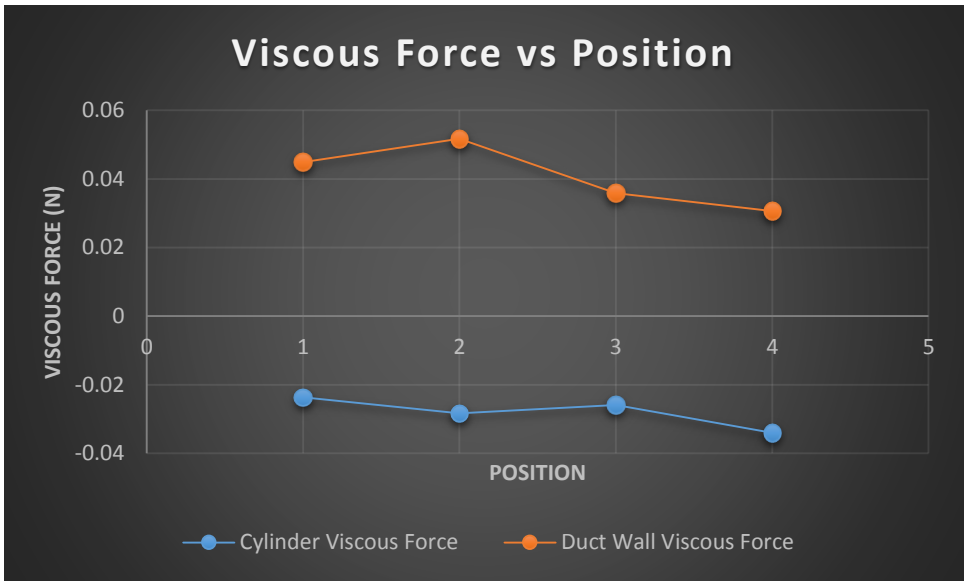

Figure 48: Compares viscous forces vs wall positon for both cylinder and duct walls

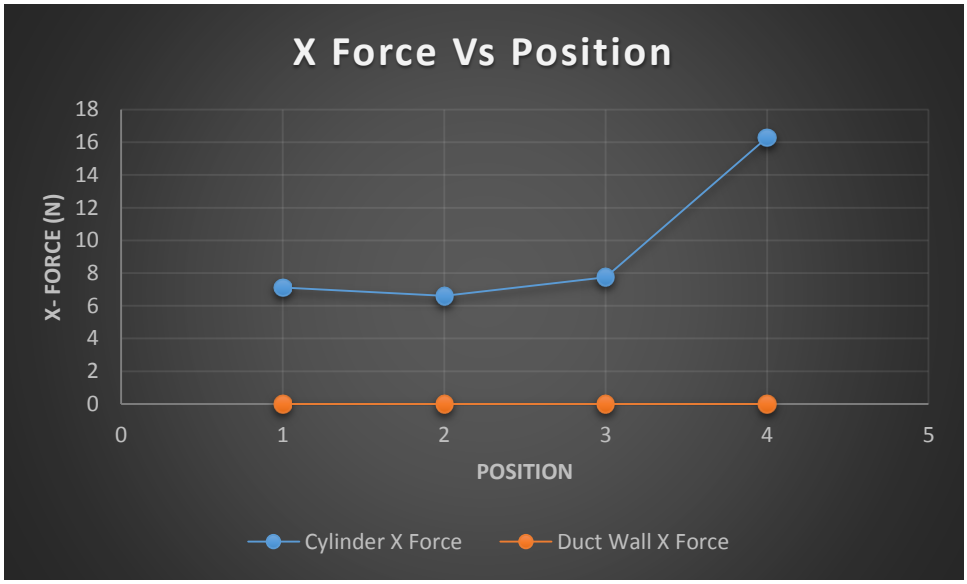

Figure 49: Comparing X force for both the cylinder and duct walls

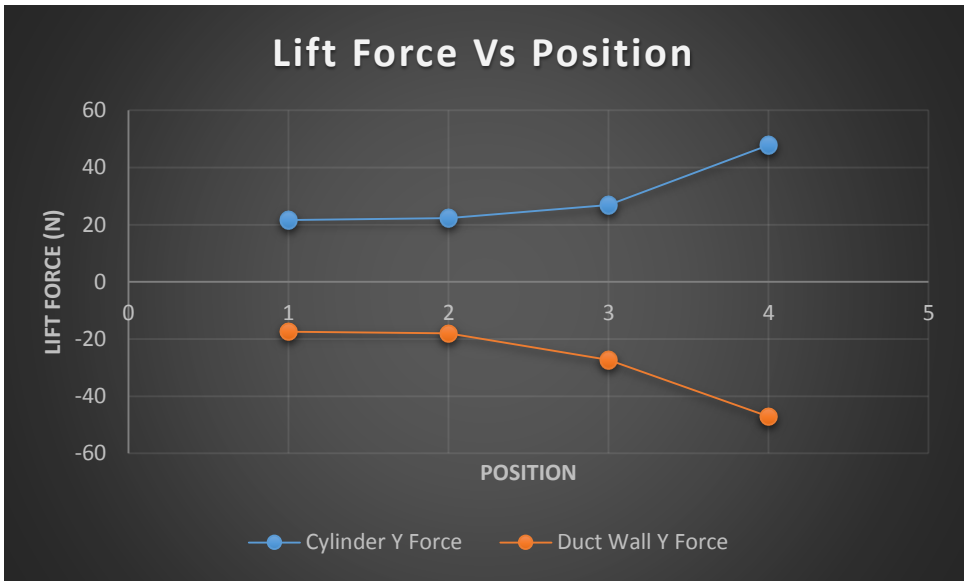

Figure 50: comparing lift forces of both cylinder and duct wall

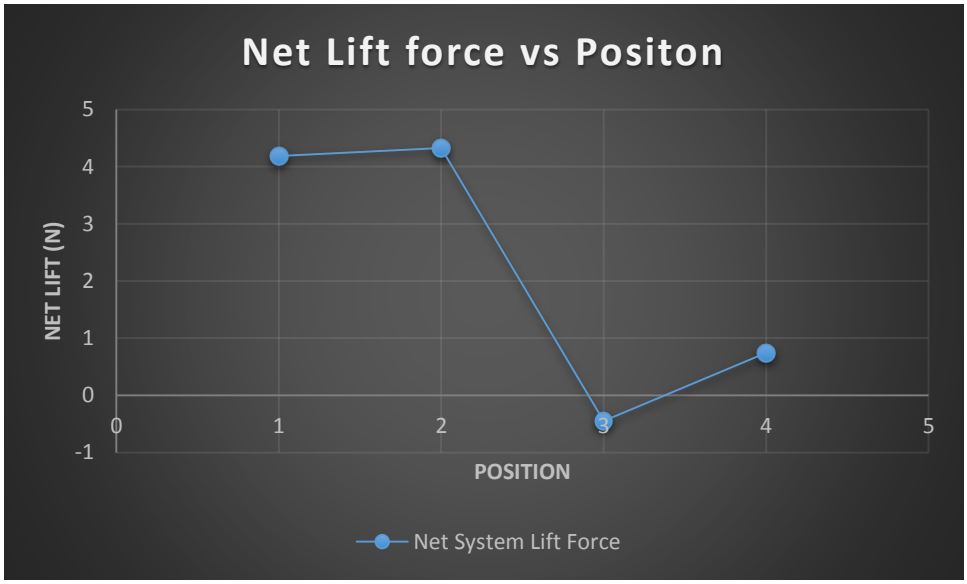

Figure 51: shows the net force of the cylinder and duct system

As seen in Figure 50 and Figure 51 above, the forces made by the cylinder were basically canceled out by the forces produced by the duct walls. This shows that Magnus effect does not work at all in duct flow.

8.0 Potential Applications

8.1 Cars

Originally we saw an increased lift on a cylinder in duct flow. However, we determined needed to look at the system as a whole since the lift on the system would affect the whole body. It was seen that the magnified lift was negated by a pressure force acting on the walls in the opposite direction. It was then concluded that the idea for using lift to either increase the rolling resistance of a vehicle on a snowy day, or decrease the coefficient of rolling resistance for better gas mileage on nice days, was not plausible.

However, Figure 52 shows an illustration of a possible contraption that could have been used to achieve the variable rolling resistance of tires using the force generated of Magnus Effect in duct flow.

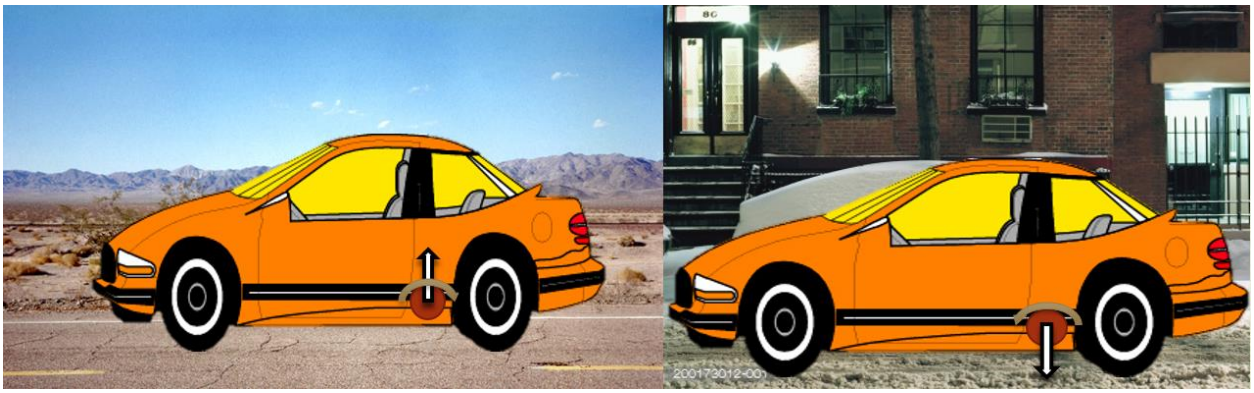

Figure 52: Possible use for Magnus lift on a motor vehicle

8.2 Trains

Trains are meant to be a safe, fast and cheap way to travel. Between the years of 2001 and 2010, there have been 8092 train accidents that involved derailment (10). Some of these train accidents are with cargo trains carrying various raw materials like crude oil or merchandise while other accidents occur with passenger trains. There are many factors that cause these accidents but the two biggest factors are from trains traveling too fast around a bend or fatigue by the operator (11).

It was decided that a system using spinning cylinders and Magnus could help prevent train derailments which could save lives and prevent raw materials such as crude oil from spilling into the environment. This possibility is explored in more detail below.

An original application for this project was to add ducts to train cars with spinning cylinders inside. These ducts could open and close when needed. However, Magnus effect in duct flow has proven not to be useful. Regardless, the idea of using Magnus lift to prevent train derailment is a novel idea that was explored anyway. Figure 53 depicts an example of a system that could be used on freight and passenger trains.

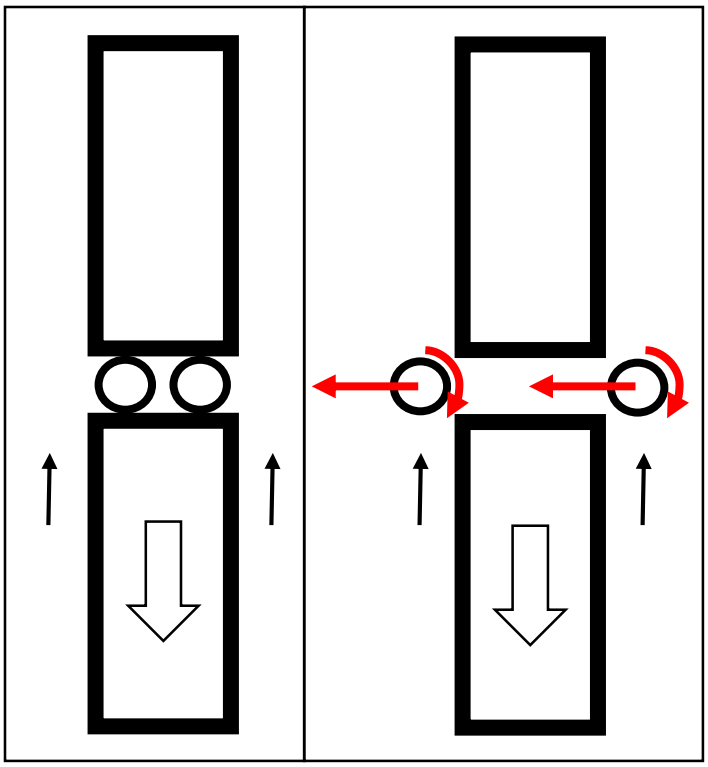

Figure 53: Example of train with Magnus stabilizers. Retracted during normal operation (left) and extended and spinning during a turn for stability (right)

As seen in Figure 53, two cylinders would be stored between train cars during normal operation. These would be stored between the cars in order to keep the train as aerodynamic as possible. However, during tight cornering maneuvers, the cylinders would extend and spin at high rates, using the relative air velocity to generate a lifting force. This lifting force could help prevent the train from tipping around curves.

A real world example of how these spinning cylinders could help is an examination of the December 2013 passenger train derailment that killed 4 people (12). During this incident, the passenger train entered a curve with a 30mph speed limit at 82mph. While not much technical information is available, some quick assumptions can help determine why the train tipped over. Figure 54 shows a basic free body diagram of a passenger car train going around a curve. Fg refers to the force acting on the car due to gravity, while Fc denotes force due to centripetal acceleration. Center of gravity is assumed to be around 2.3m from the bottom of the car, and 1.6m from the side. The red dot refers to the tipping point of the train. If the moment generated by Fc is greater than the moment generated by Fg, the train will tip.

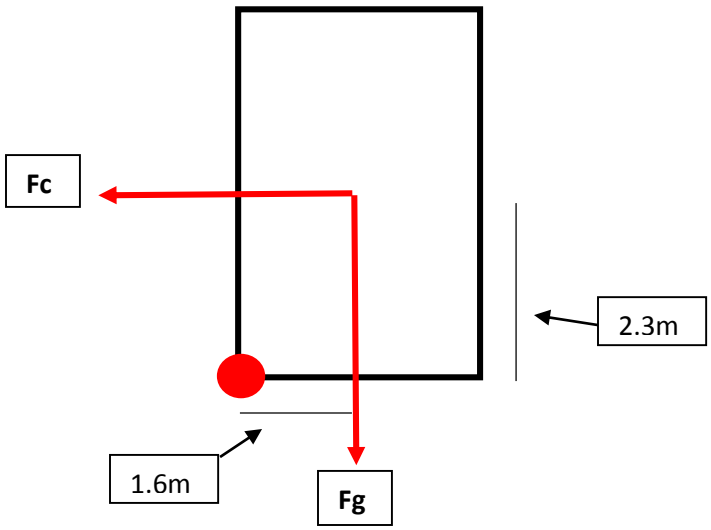

Figure 54: Basic passenger train car dimensions and forces around a turn

In order to determine what forces were acting on the train during derailment, we need the radius of curvature of the bend it derailed on. The following equation is used to determine the maximum speed a train is allowed to enter a curve (13).

$$Vmax = \sqrt{\frac{E * g * r}{G}}$$

In this equation, E is the track superelevation, which is how much higher the outside rail is than the inner rail (slope). G is the track gauge, which is standardized at 4ft 8.5in. g is the acceleration due to gravity and r is the curve radius (13). The track superelevation is generally around 6in (13).

Plugging in 30mph for Vmax and solving for r, we find that the radius of curvature was about 566ft, or 172 meters. Next, we can solve for the centripetal acceleration of the car. This is simply

$$a_c = \frac{V^2}{r}$$

Where V is the tangential velocity and r is the radius of curvature. Considering that the train entered the curve at 82mph (36.7m/s), we can calculate the centripetal acceleration to be about 7.83 m/s^2.

Next we can calculate the moments generated by both forces. We will call Tc the moment generated by centripetal forces and Tg the moment caused by the weight of the train and gravity.

$$Tc = m * a_c * 2.3m$$

$$Tg = m * a_g * 1.6m$$

The mass of the train car, *m*, is about 65700kg. Using 9.8m/s^2 for the acceleration due to gravity, we calculate a moment of nearly 1180000 N-m for Tc, and slightly over 1030000 N-m for Tg. This leaves a 150000 N-m difference. Since Tc is much larger than Tg, it is easy to understand how the train tipped.

However, by adding spinning cylinders as proposed in Figure 53, a lifting force can be used to counter the centripetal acceleration.

Appendix D shows a table that uses the Kutta-Joukowski theorem to predict lift at different speeds. For a cylinder that is 2ft in diameter, 10ft long, and spinning at 4200 rpm, a theoretical lift of 7900lbs is generated when traveling at 82mph. With two cylinders working together, 15800lbs or 70281 Newtons would be generated. This would generate a moment of around 161500 N-m that opposes the centripetal acceleration. While this isn't an extremely high lift or moment, it could theoretically have been just enough to prevent the train from tipping.

Obviously, this sort of method for preventing trains from tipping would be extremely expensive. An elaborate system would have to be installed on every train car. Very powerful motors would have to be used in order to spin the cylinders at the high speeds required. In this case, the benefit of the spinning cylinders seems very small compared to the possible cost. However, it is an interesting idea that could be explored in the future, as better technology becomes available.

8.3 Boats

Some boats already utilize the benefits of Magnus Effect. A rotor ship, or Flettner ship, is a ship designed to use the Magnus effect for propulsion. To take advantage of this effect, it uses rotorsails which are powered by an engine. German engineer Anton Flettner was the first to build a ship which attempted to tap this force for propulsion.

Examples of these Flettner ships can be seen in Figure 55. These ships are actually still used today thanks in large part by their fuel economy. The German wind-turbine manufacturer Enercon launched and christened its new rotor-ship E-Ship 1 on 2 August 2008. The ship was used to transport turbines and other equipment to locations around the world. The maiden delivery of turbines for Castledockrell Windfarm arrived in Dublin Port on 11th Aug 2010. On 29 July 2013, Enercon provided a press release claiming a potential for "operational fuel savings of up to 25% compared to same-sized conventional freight vessels (14).

Figure 55: Examples of Flettner ships

8.4 Rockets

The biggest issues with rockets is the perpendicular airflow does not result in any beneficial lift force. Thus there is a redirection of airflow that has to be possible. Some jet aircraft have successfully redirected air for thrust, but not to this degree.

So another plausible way of looking at using spinning cylinders on rockets, is to use their ability to cause a force perpendicular to airflow, is to use it for stability purposes. By using a spinning cylinder, a force causing the rocket to rotate about its center of gravity axis could be made. This spinning could make the rocket more stable than it was previously. This is why bullets and some missiles are spun.

However, drag is added and aerodynamics forces are changing on the fins of a rocket. Rockets are going straight up (generally) and are designed as such, but now when there are dynamic forces acting perpendicular to the fins instead of parallel, subsequent drag would increase. However, this could be another developmental area.

9.0 Conclusion

Originally we saw an increased lift on a cylinder in duct flow. It was then concluded that we needed to look at the system as a whole since the lift on the system would affect the whole body. It was seen that the magnified lift was negated by a pressure force cause by the walls in the opposite direction.

Though the outcome may seem bleak as of now, we still believe there is a certain plausibility and application to Magnus Effect in duct Flow.

10.0 Future Research

Much time was spent conducting and analyzing simulations. Many experts have said that turbulence modeling and simulation is very unreliable. We believe that test should be conducted to verify the results found in this paper. It would be recommended to have two sets of data, one where just the lift on the cylinder is calculated, and the other where the lift of the system is calculated and compare.

Results would be beneficial since it is impossible to simulate real life effects in a model. Perhaps with our model there were conditions that were not accounted for and the outcome of the experiment would be more optimistic than our results.

Additionally, just as a side thought, we also believe it would be beneficial to see how integral the surface roughness is to Magnus effect. Would a baseball and a tennis ball, being geometrically similar, cause the same amount of force, or would one produce more lift than the other?

11.0 Team Responsibilities

	Research	2-D Simulations	3-D Simulations	Analysis	Solidworks/ Experiment Design	Report Writing
Jesse Batko	✓	✓	✓	✓		✓
Cameron Clarke	✓		✓	✓	✓	✓
Kenneth Smith	✓					✓

12.0 References

[1] Thomson, J. J. "The Dynamics of a Golf Ball." Popular Science Monthly and World's Advance. Vol. 78. N.p.: McCure, Phillips, 1911. 190-91. Print.

[2] Seifert, Jost. "A Review of the Magnus Effect in Aeronautics." Progress in Aerospace Sciences 55 (2012): 17-45. Web. 1 Mar. 2015.

[3] Lafay A. Contribution expe´ rimentale a l'ae ´ rodynamique du cylindre et a´ l'e´tude du phe´nomene de Magnus. Revue de Me ´ chanique 1912;30:417–42.

[4] Seifert, Jost. "A Review of the Magnus Effect in Aeronautics." Progress in Aerospace Sciences 55 (2012): 17-45. Web.

[5] Celli, Vittorio. "Circulation and the Magnus Effect." Circulation and the Magnus Effect. The University of Virginia, n.d. Web.

[6] Benson, Tom. "Lift of a Rotating Cylinder." Lift of a Rotating Cylinder. NASA, 12 June 2014. Web. 21 Apr. 2015. <http://www.grc.nasa.gov/WWW/k-12/airplane/cyl.html>.

[7] "Vorticity, Circulation and Potential Vorticity." Vorticity, Circulation and Potential Vorticity. 3.1 Definitions (n.d.): n. pag. Columbia University. Columbia University. Web. <http://www.columbia.edu/~irs2113/3_Circulation_Vorticity_PV.pdf>.

[8] Argyropoulos, C.d., and N.c. Markatos. "Recent Advances on the Numerical Modelling of Turbulent Flows." *Applied Mathematical Modelling* 39.2 (2015): 693-732. Web. 26 Mar. 2015.

[9] Gallardo, Javier G. "FLUENT- Compressible Flow in a Nozzle." FLUENT. Ed. Sebastien Lachance-Barrett. Cornell University, 08 Feb. 2014. Web. 20 Apr. 2015. <https://confluence.cornell.edu/display/SIMULATION/FLUENT+-+Compressible+Flow+in+a+Nozzle-+Step+4+*New>.

[10] Liu, Xiang, M. Rapik Saat, and Christopher P. L. Barkan. "Analysis of Causes of Major Train Derailment and Their Effect on Accident Rates." Transportation Research Record: Journal of the Transportation Research Board 2289.-1 (2012): 154-63. Web. 20 Apr. 2015.

[11] Lowy, Joan. "Here's Why so Many Oil Trains Have Derailed This Year." Business Insider. Business Insider, Inc, 10 Mar. 2015. Web. 20 Apr. 2015. <http://www.businessinsider.com/heres-why-so-many-oil-trains-have-derailed-this-year-2015-3>.

[12]Hampson, Kevin McCoy Rick, and John Bacon. "Commuter Train Derailment Kills 4 in NYC." USA Today. Gannett, 02 Dec. 2013. Web. 20 Apr. 2015.

[13]Speed Limit on Railway Curves (Use of SuperElevation on Railways) (n.d.): n. pag. Open Rails. GNL. Web. <openrails.org>.

[14]"State-of-the-art Cargo Ship to Dock with Haul of Wind Turbines." Silicon Republic. IDA Ireland, 08 Oct. 2010. Web.

[15] Anderson, John D. Fundamentals of Aerodynamics. 5th ed. Boston: McGraw-Hill, 2001. Print.

Appendix A: Using the Magnus Lift Equation

$$L' = \rho_\infty V_\infty \Gamma$$

This is the lift per unit span as derived before. All one would need to do to find lift would be multiply by its span. We will represent this value with the letter "D."

$$L = \rho_\infty V_\infty \Gamma \mathrm{D}$$

Let us take an example:

Given a random scenario as shown below, how much lift would we generate?

SCENARIO

NAME (UNITS) [VARIABLE]	Value
UNIFORM AIR VELOCITY TOWARD CYLINDER (M/S) $[V_\infty]$	50
SPIN OF THE CYLINDER (REVS/S) [S]	800
AVERAGE DENSITY OF AIR (KG/M³) $[\rho_\infty]$	1.225
RADIUS OF CYLINDER (M) $[r]$	0.5
LENGTH OF CYLINDER (M) [D]	3

All these values could be easily controlled in an experimental setting.

Looking at the equation we already have three unknowns that are known, incoming air velocity, air density and span length, but vortex strength requires more manipulation.

First we must obtain the rotational velocity, or spin in m/s instead of revolutions/second.

$$V_r = 2\pi r S = 2\pi(0.5\ m)\left(800\frac{revs}{s}\right) = 2{,}153.274\frac{m}{s}$$

Vr again is the rotational speed of the cylinder, a visualization can be seen below.

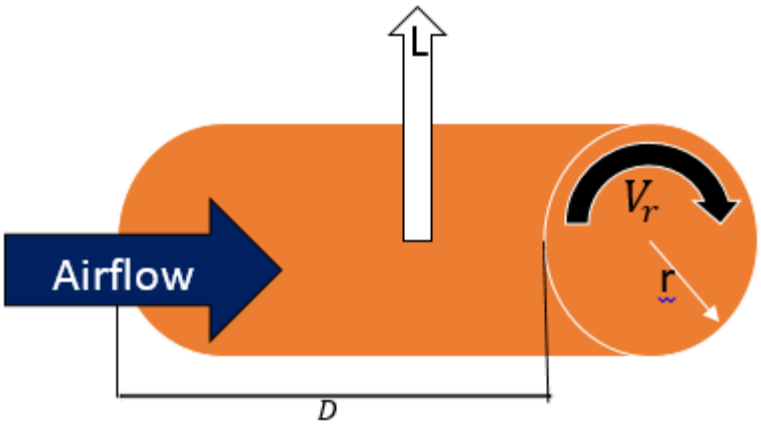

Using Vr, we can now find the vortex strength

$$\Gamma = 2\pi r V_r = 2\pi(0.5\ m)\left(2{,}153.274\frac{m}{s}\right) = 7{,}895.684\frac{m^2}{s}$$

Now we can finally find the lift generated on the cylinder:

$$L = \rho_\infty V_\infty \Gamma \mathrm{D} = \left(1.225\frac{\mathrm{kg}}{\mathrm{m}^3}\right)\left(50\frac{m}{s}\right)\left(7{,}895.684\frac{m^2}{s}\right)(3\ m)$$

$$L = 1.45083 * 10^6\ \frac{kg * m}{s^2} = 1.45083 * 10^6\ N$$

Appendix B: 2-D and 3-D CFD Results

B.1 Preliminary CFD 2D Trial 1

Positon 1

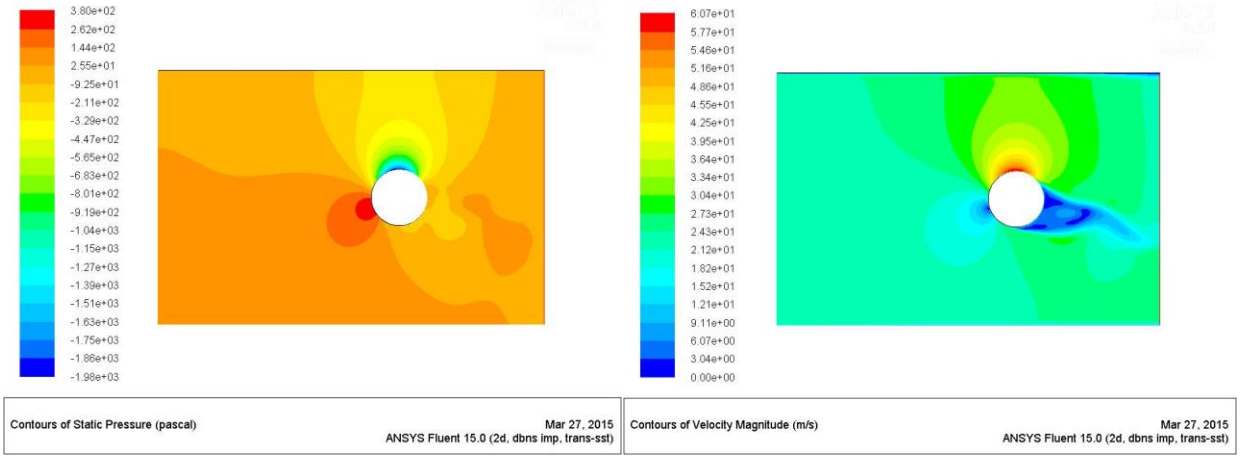

Positon 2

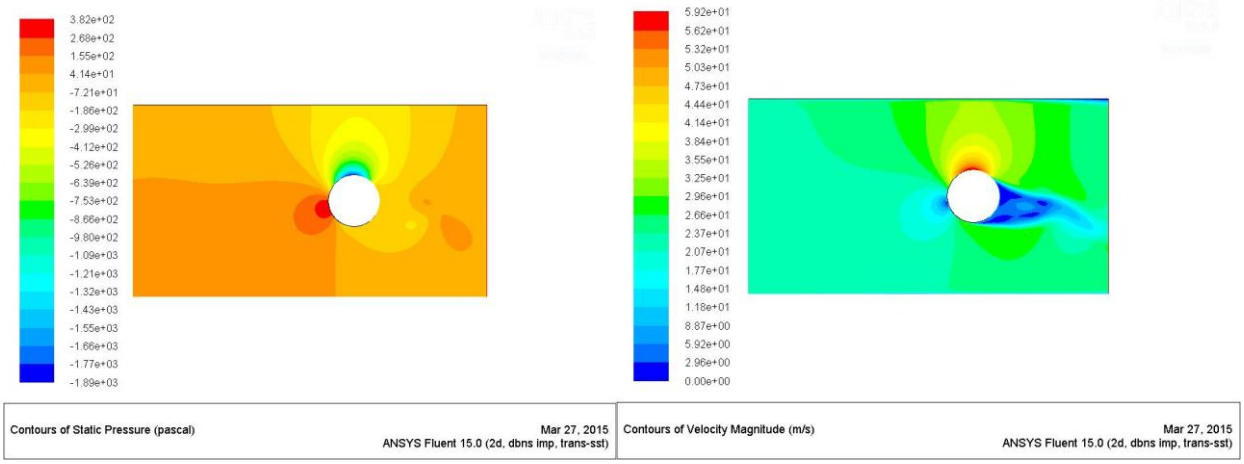

Position 3

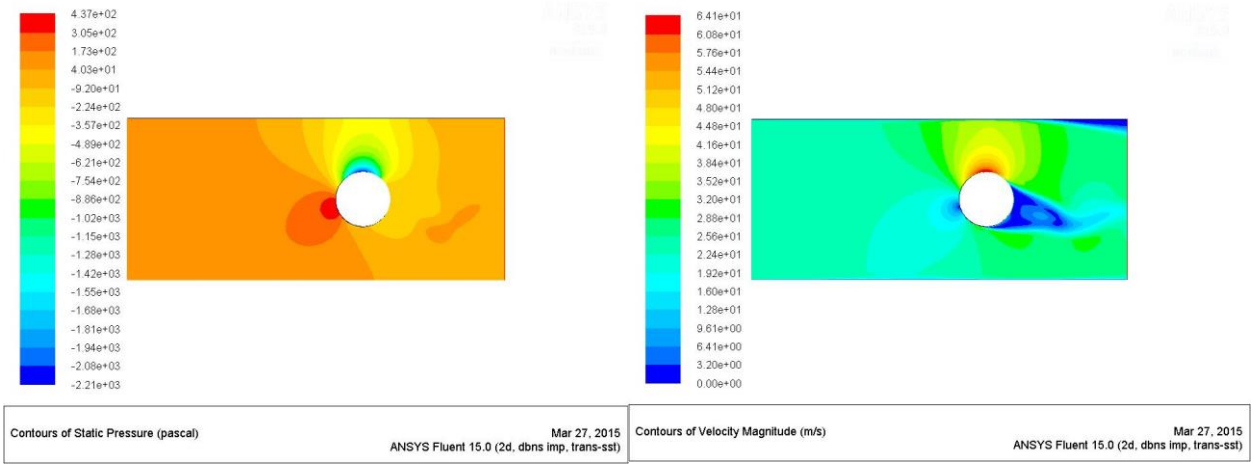

Position 4

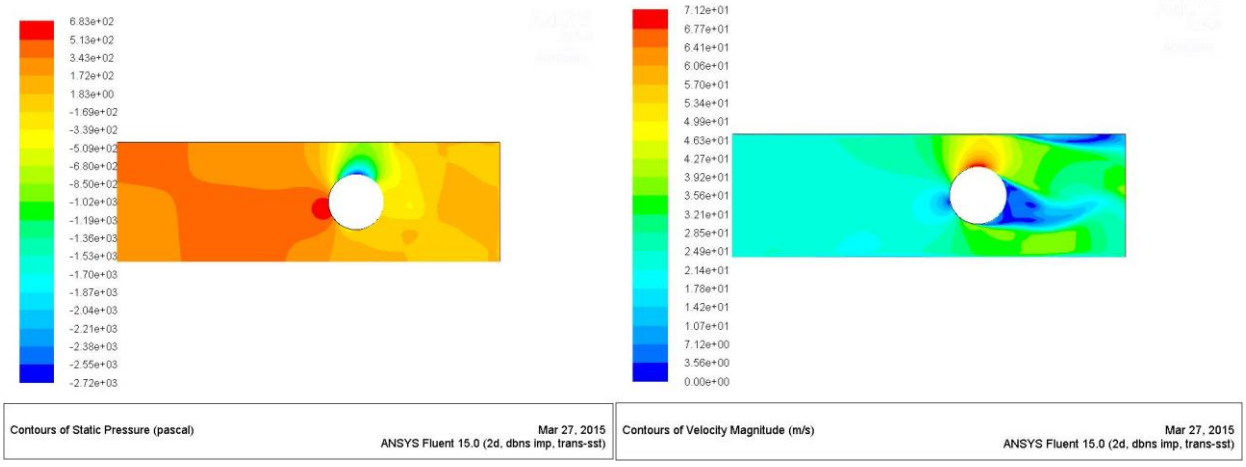

Trial 2

Position 1

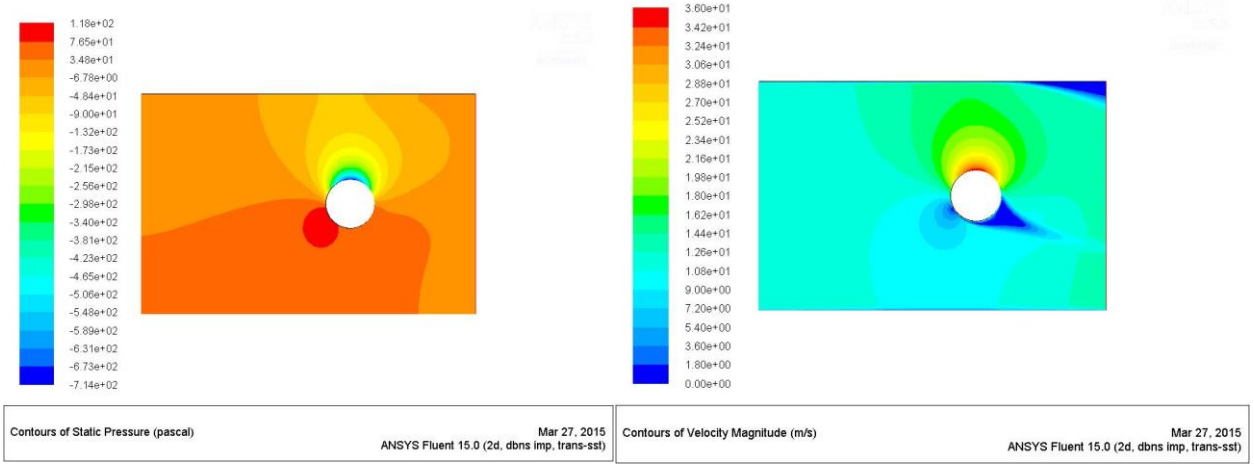

Position 2

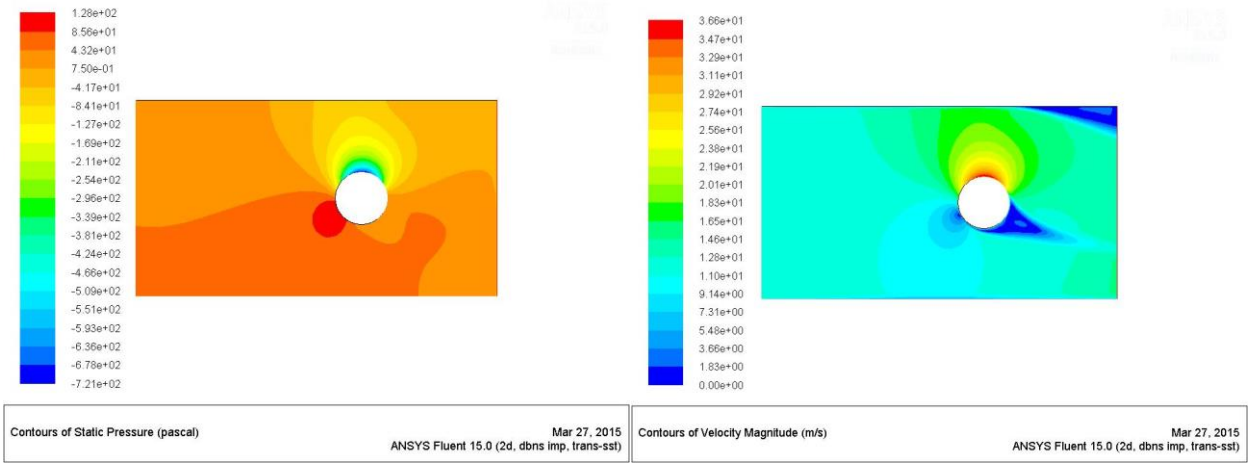

Positon 3

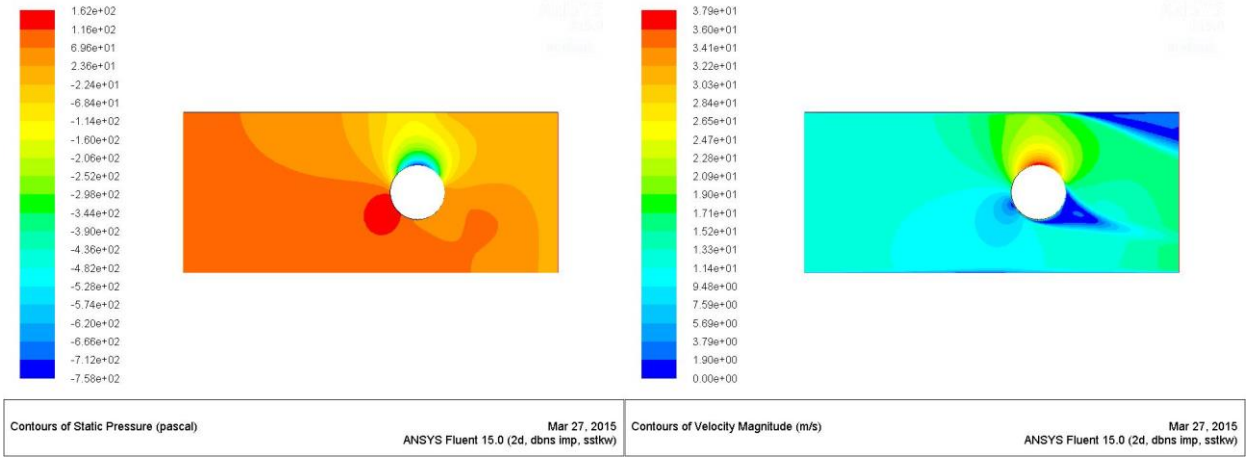

Position 4

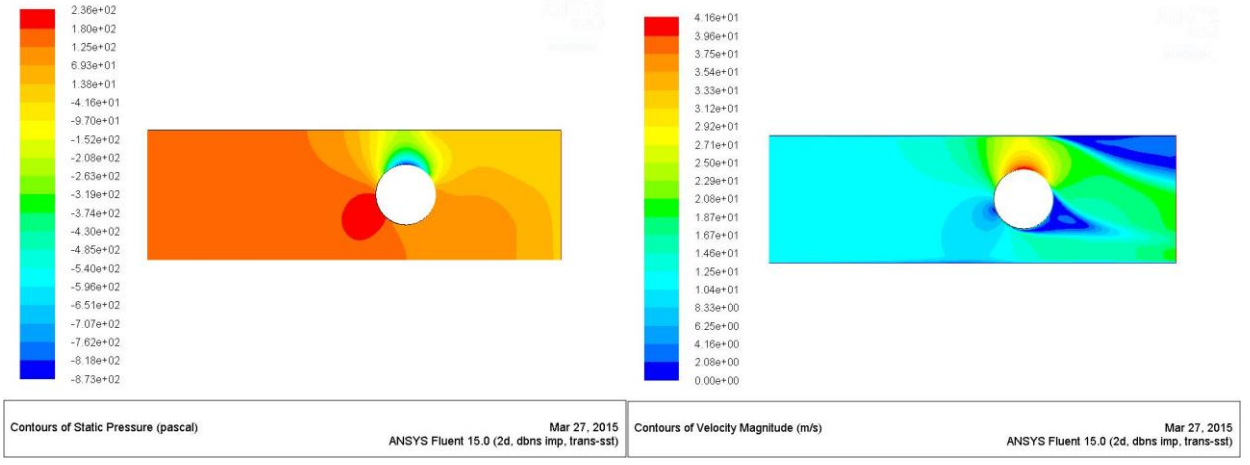

B.2 Preliminary CFD 3D (All Trial 2)

Position 1

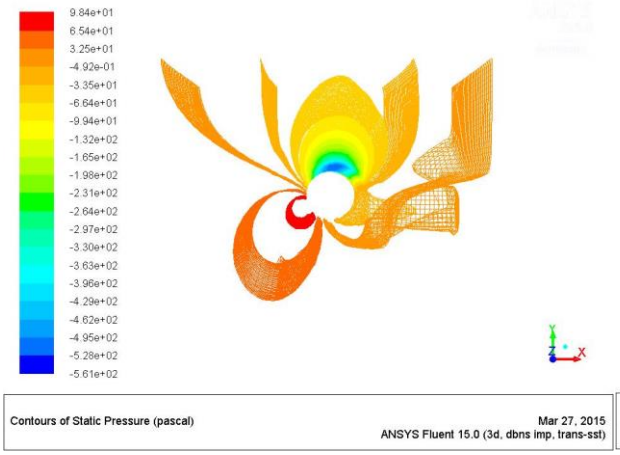

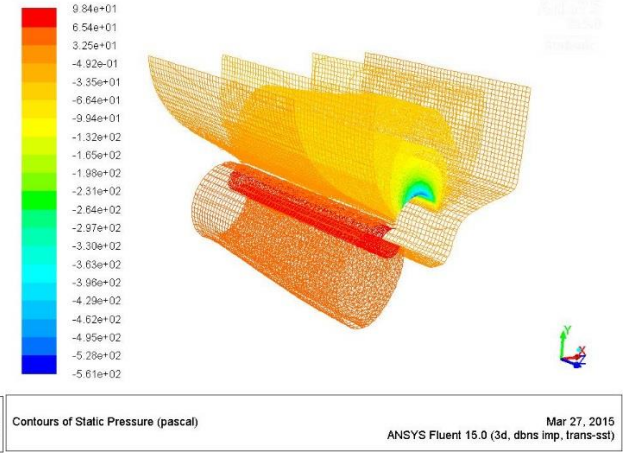

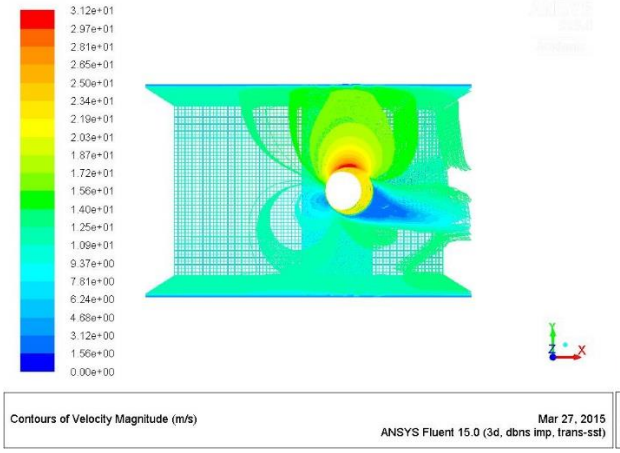

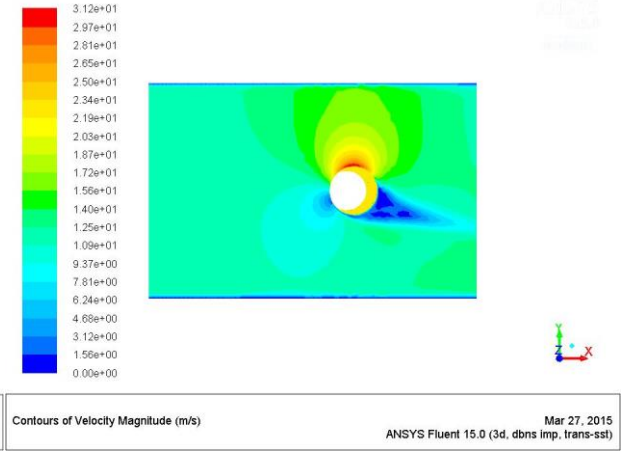

Position 2

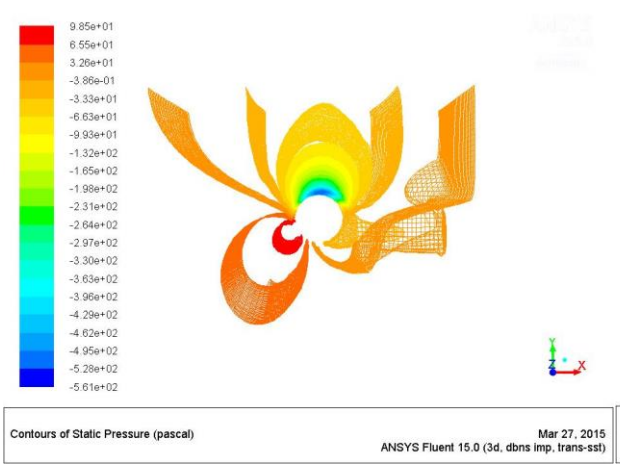

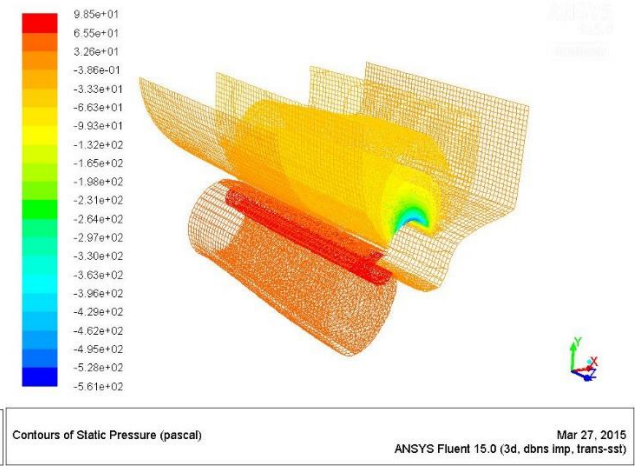

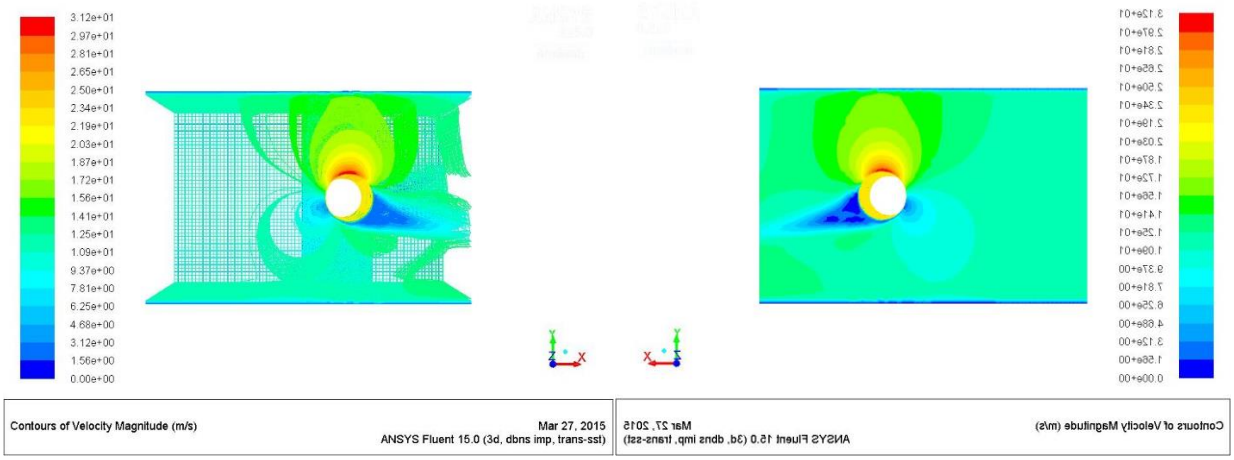

Position 3

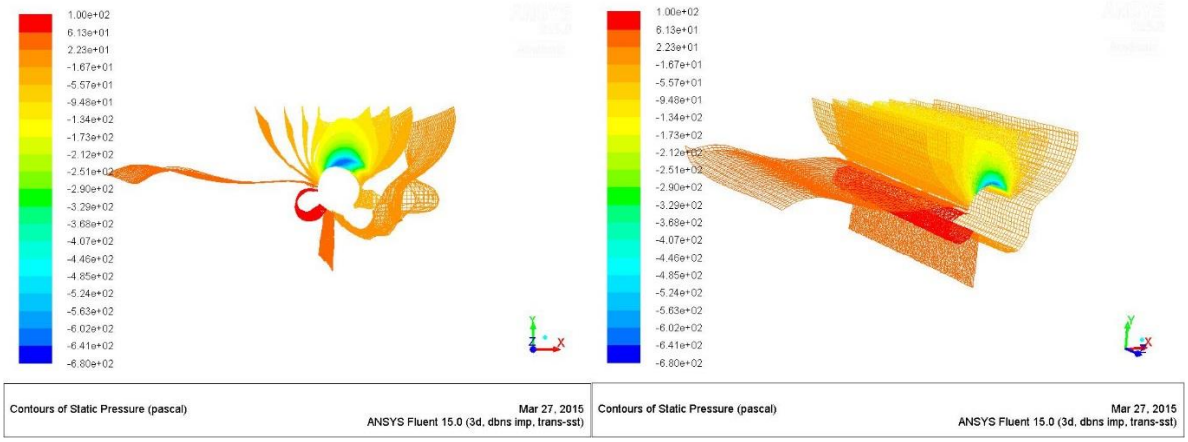

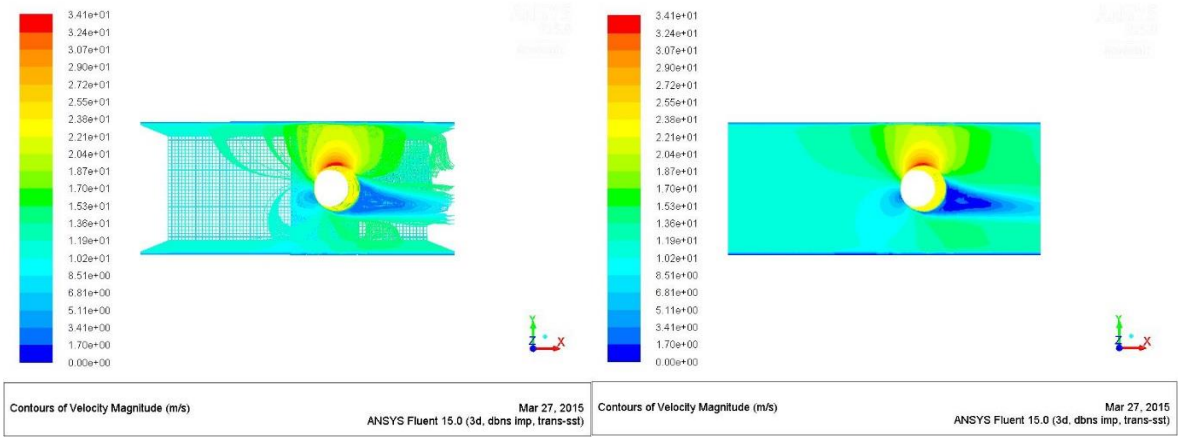

Position 4

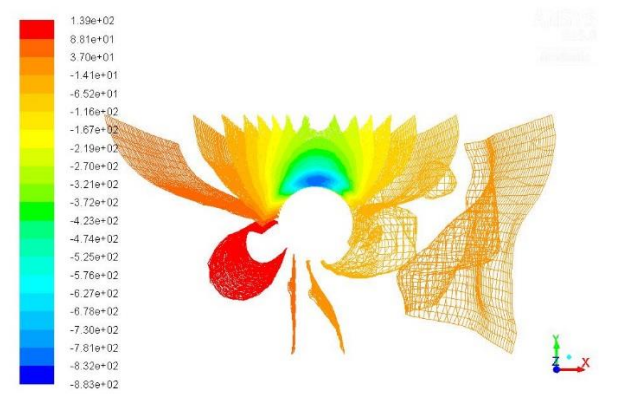

Contours of Static Pressure (pascal)

Mar 27, 2015
ANSYS Fluent 15.0 (3d, dbns imp, trans-sst)

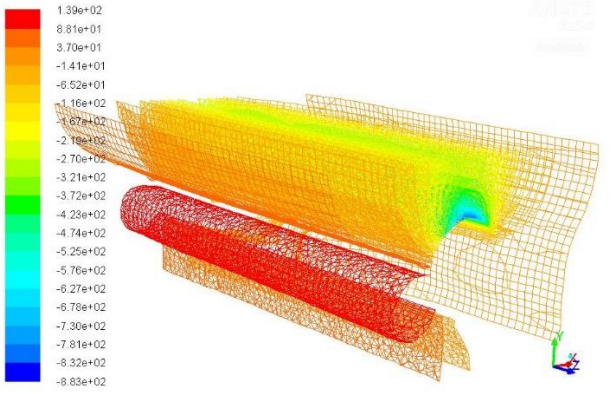

Contours of Static Pressure (pascal)

Mar 27, 2015
ANSYS Fluent 15.0 (3d, dbns imp, trans-sst)

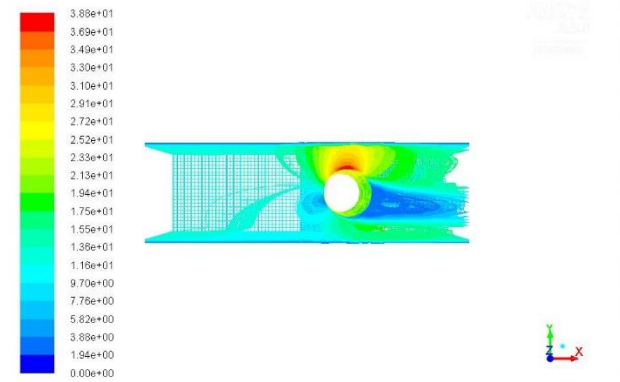

Contours of Velocity Magnitude (m/s)

Mar 27, 2015
ANSYS Fluent 15.0 (3d, dbns imp, trans-sst)

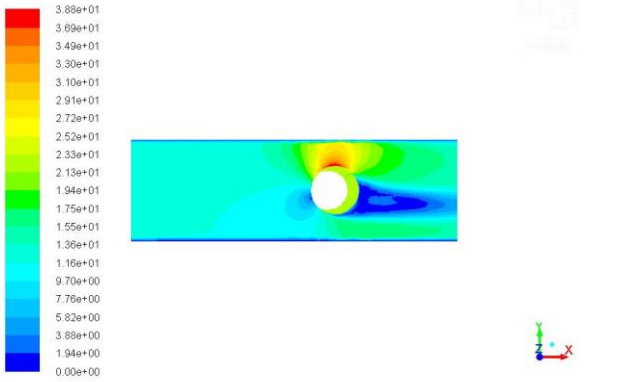

Contours of Velocity Magnitude (m/s)

Mar 27, 2015
ANSYS Fluent 15.0 (3d, dbns imp, trans-sst)

Position 5

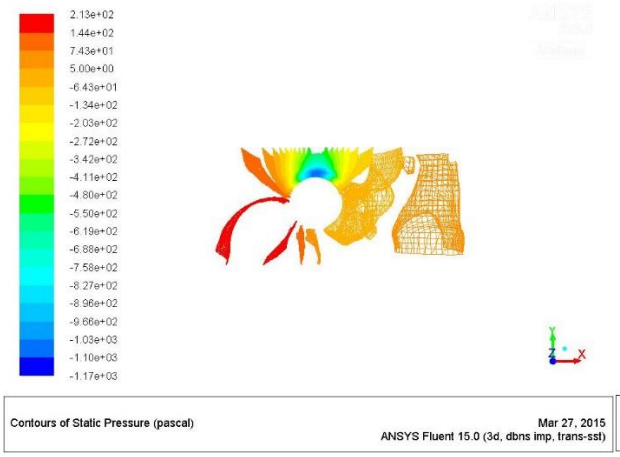

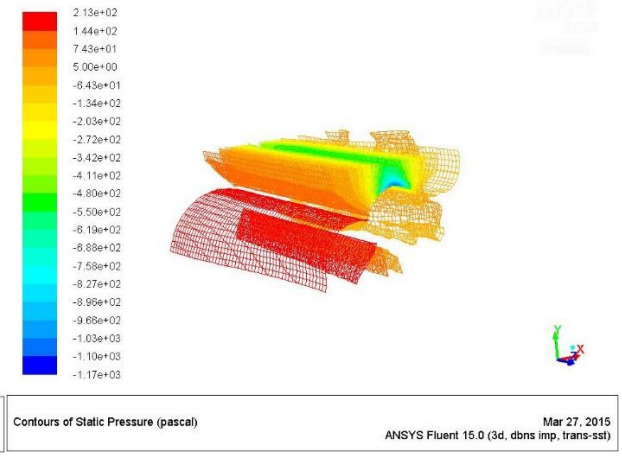

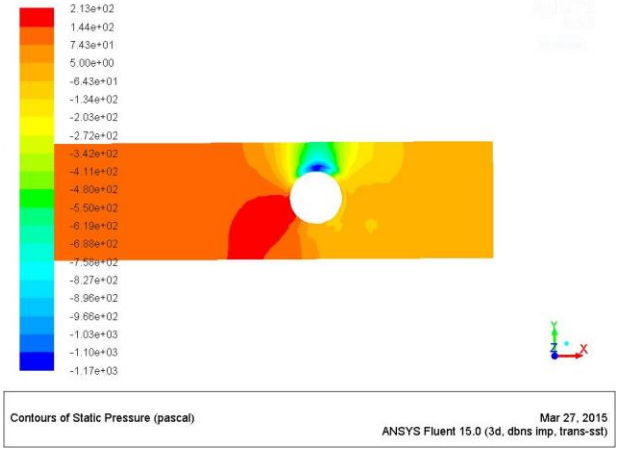

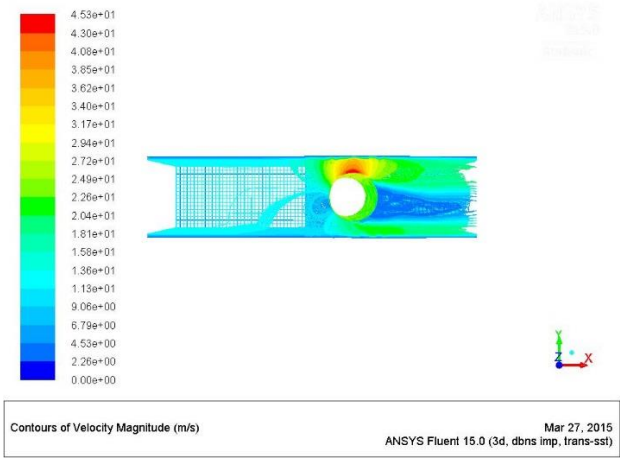

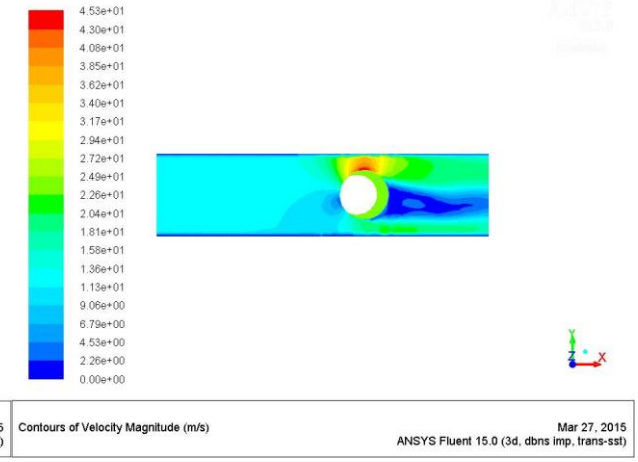

B.3 Final CFD 2D (All Trial 2)

Position 1

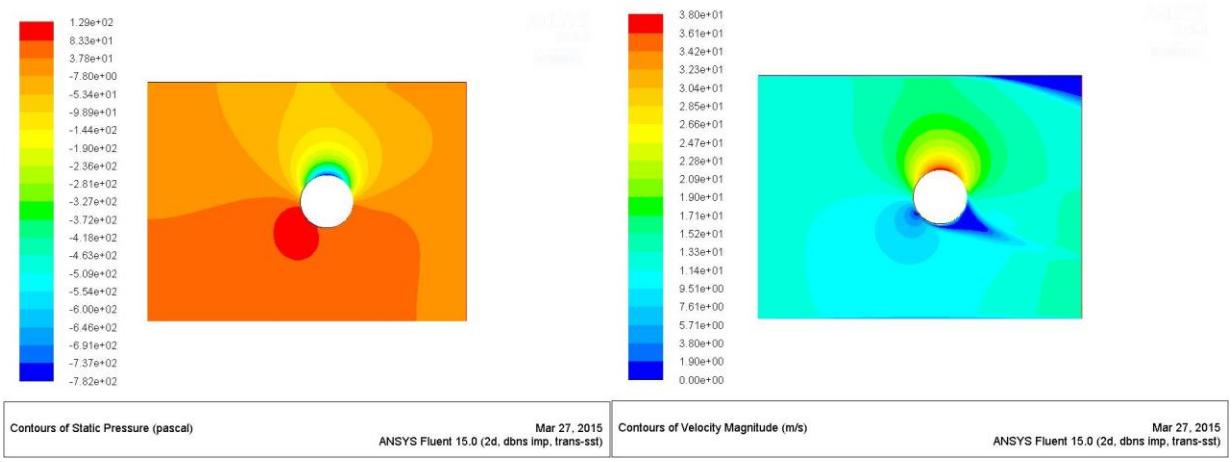

Position 2

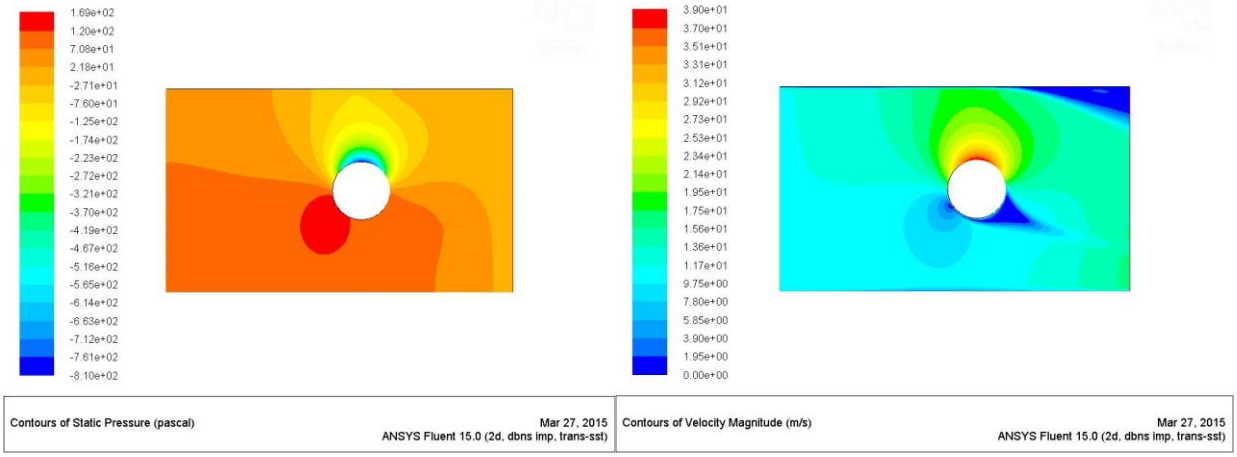

Position 3

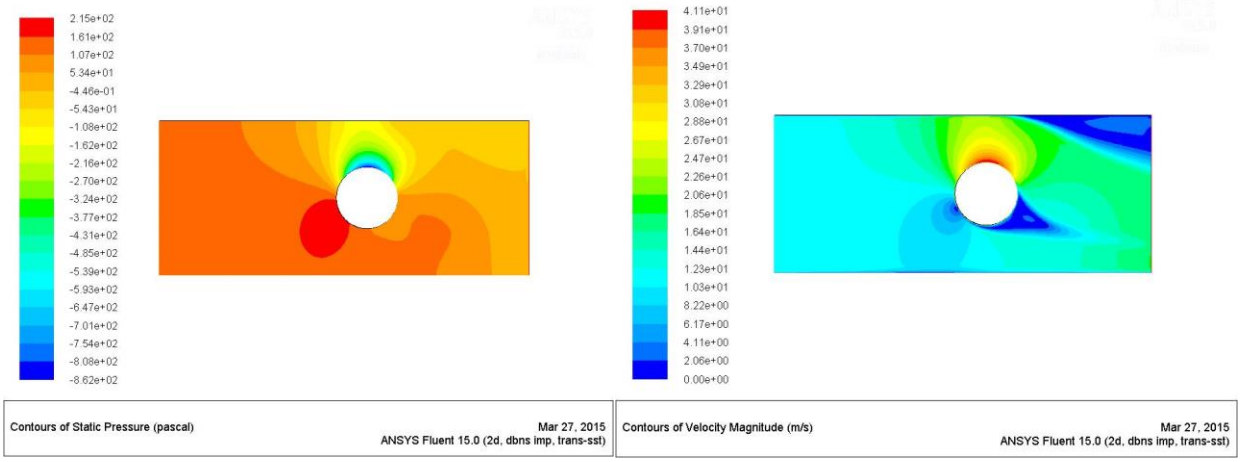

Position 4

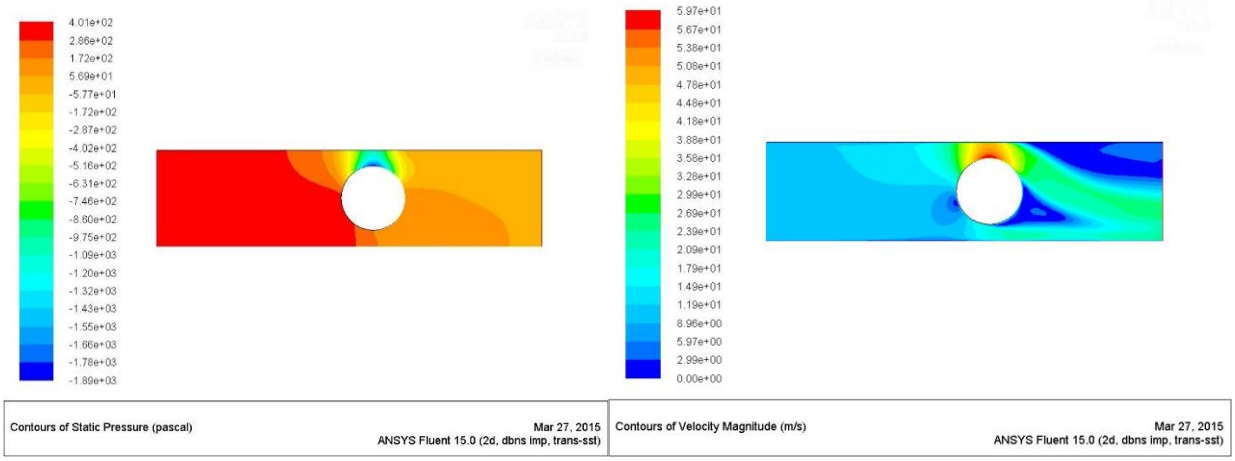

B.4 Final CFD 3D

Position 1

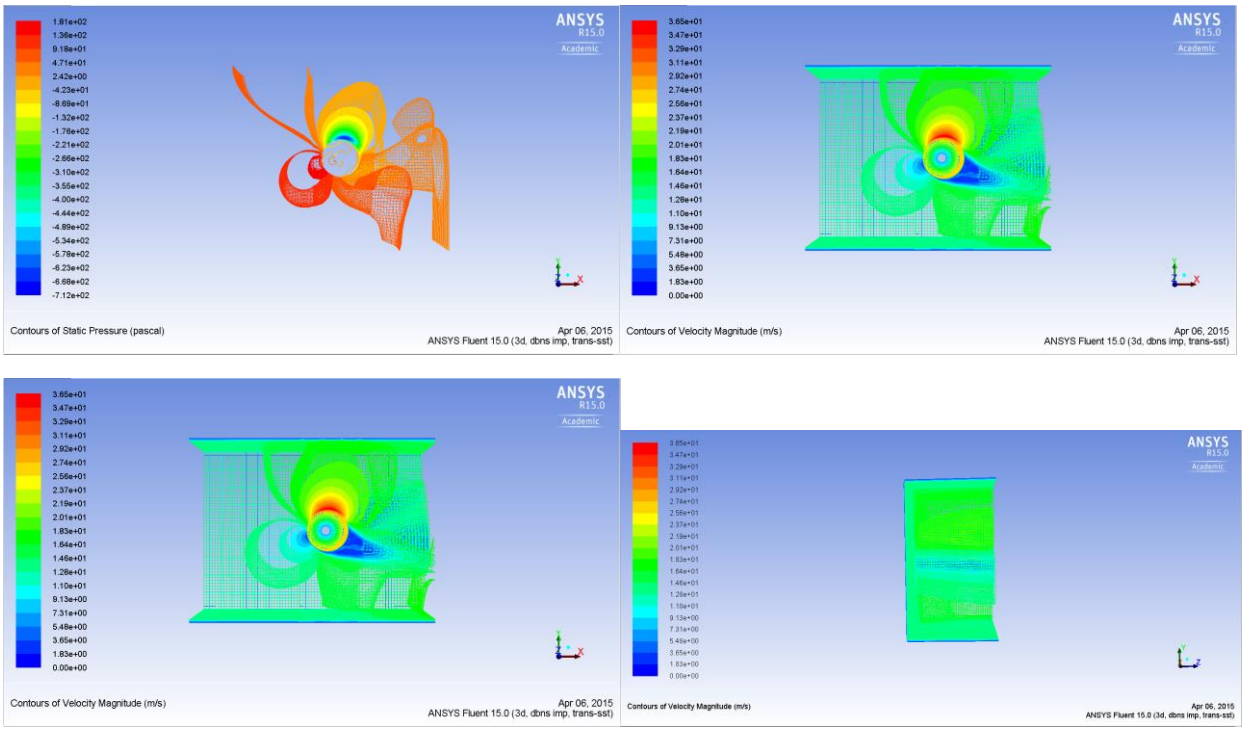

Position 2

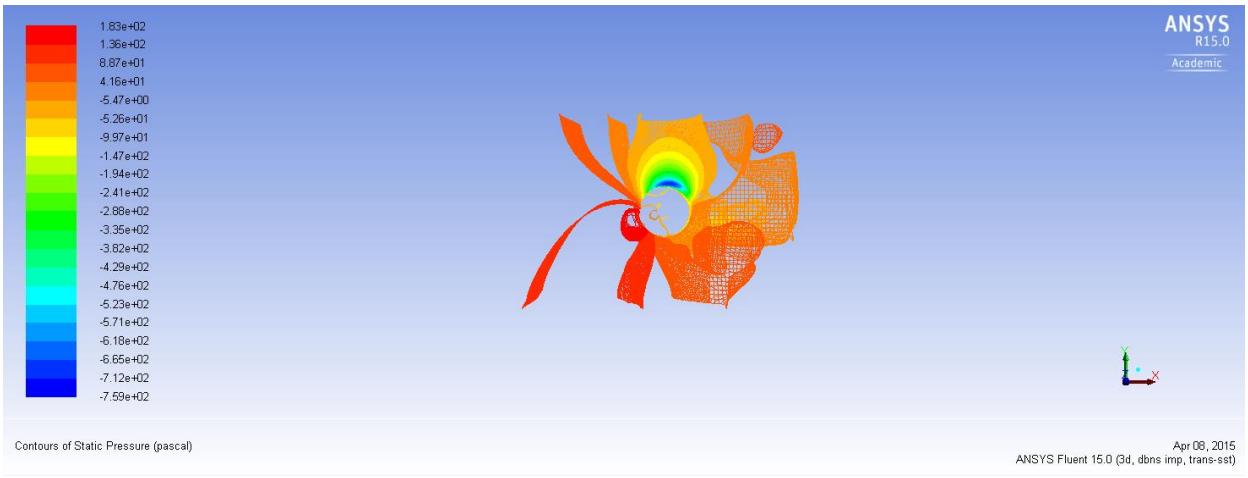
1.83e+02
1.36e+02
8.87e+01
4.16e+01
-5.47e+00
-5.26e+01
-9.97e+01
-1.47e+02
-1.94e+02
-2.41e+02
-2.88e+02
-3.35e+02
-3.82e+02
-4.29e+02
-4.76e+02
-5.23e+02
-5.71e+02
-6.18e+02
-6.65e+02
-7.12e+02
-7.59e+02
ANSYS
R15.0
Academic
Contours of Static Pressure (pascal)
Apr 08, 2015
ANSYS Fluent 15.0 (3d, dbns imp, trans-sst)

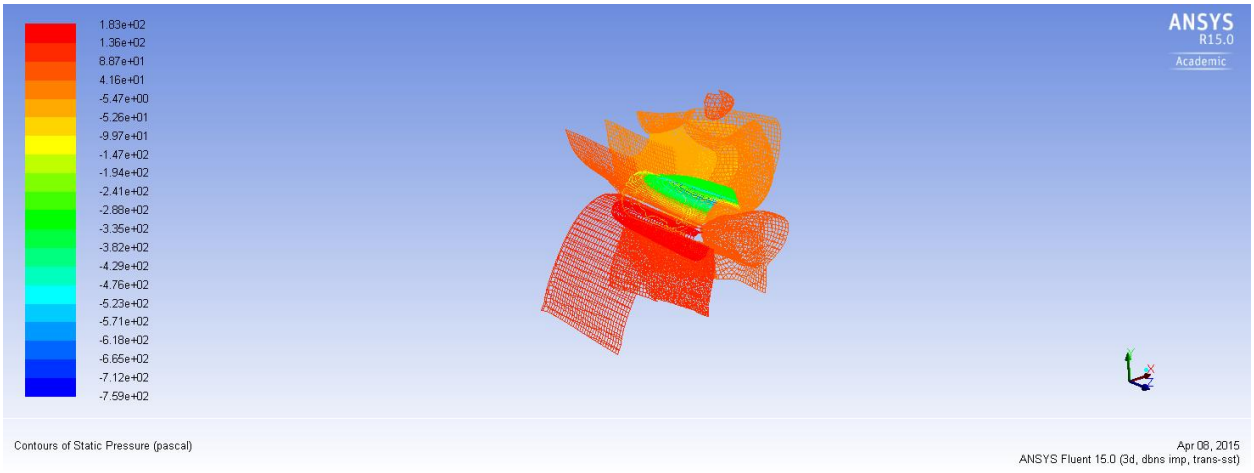
1.83e+02
1.36e+02
8.87e+01
4.16e+01
-5.47e+00
-5.26e+01
-9.97e+01
-1.47e+02
-1.94e+02
-2.41e+02
-2.88e+02
-3.35e+02
-3.82e+02
-4.29e+02
-4.76e+02
-5.23e+02
-5.71e+02
-6.18e+02
-6.65e+02
-7.12e+02
-7.59e+02
ANSYS
R15.0
Academic
Contours of Static Pressure (pascal)
Apr 08, 2015
ANSYS Fluent 15.0 (3d, dbns imp, trans-sst)

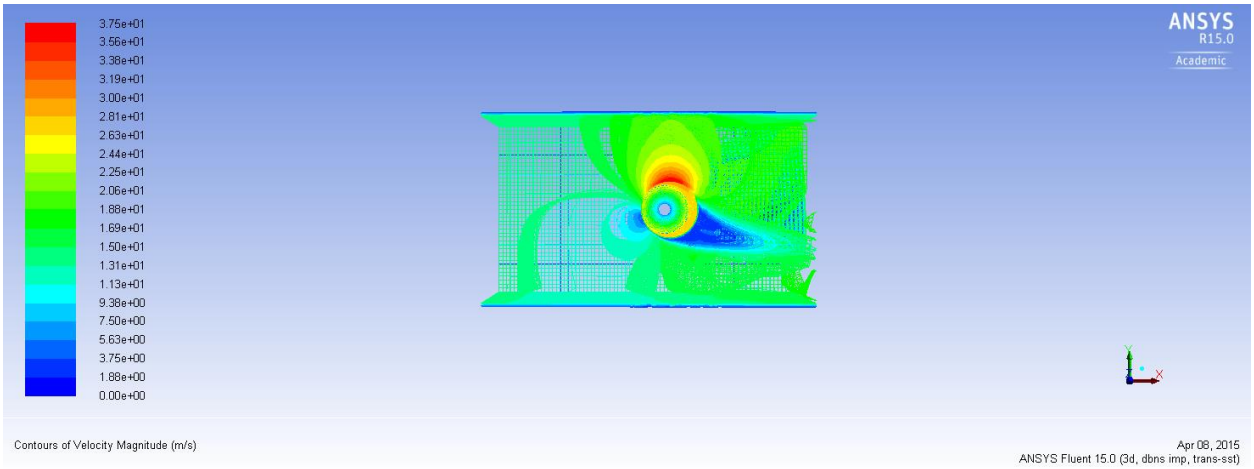
3.75e+01
3.56e+01
3.38e+01
3.19e+01
3.00e+01
2.81e+01
2.63e+01
2.44e+01
2.25e+01
2.06e+01
1.88e+01
1.69e+01
1.50e+01
1.31e+01
1.13e+01
9.38e+00
7.50e+00
5.63e+00
3.75e+00
1.88e+00
0.00e+00
ANSYS
R15.0
Academic
Contours of Velocity Magnitude (m/s)
Apr 08, 2015
ANSYS Fluent 15.0 (3d, dbns imp, trans-sst)

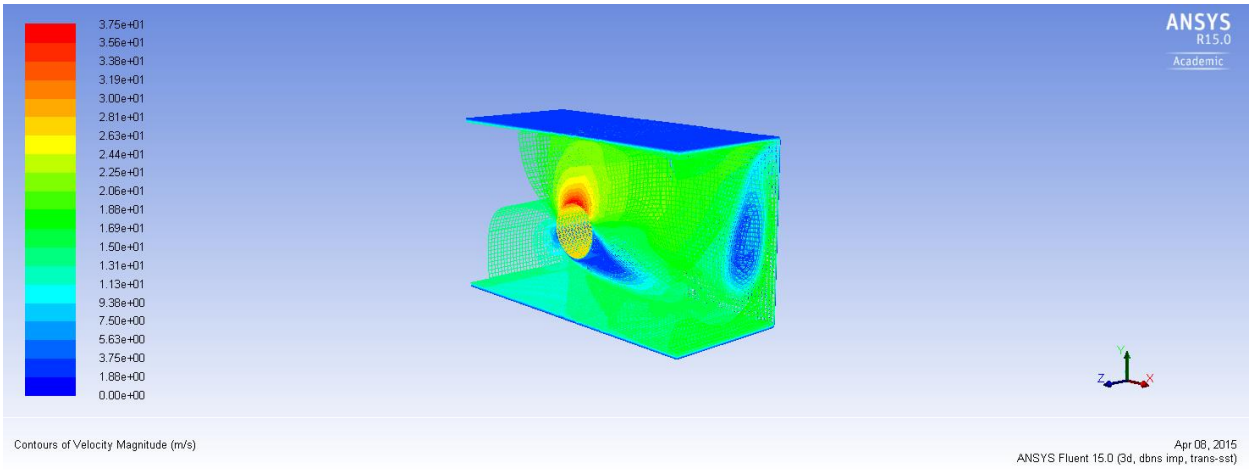
3.75e+01
3.56e+01
3.38e+01
3.19e+01
3.00e+01
2.81e+01
2.63e+01
2.44e+01
2.25e+01
2.06e+01
1.88e+01
1.69e+01
1.50e+01
1.31e+01
1.13e+01
9.38e+00
7.50e+00
5.63e+00
3.75e+00
1.88e+00
0.00e+00
ANSYS
R15.0
Academic
Contours of Velocity Magnitude (m/s)
Apr 08, 2015
ANSYS Fluent 15.0 (3d, dbns imp, trans-sst)

Position 3

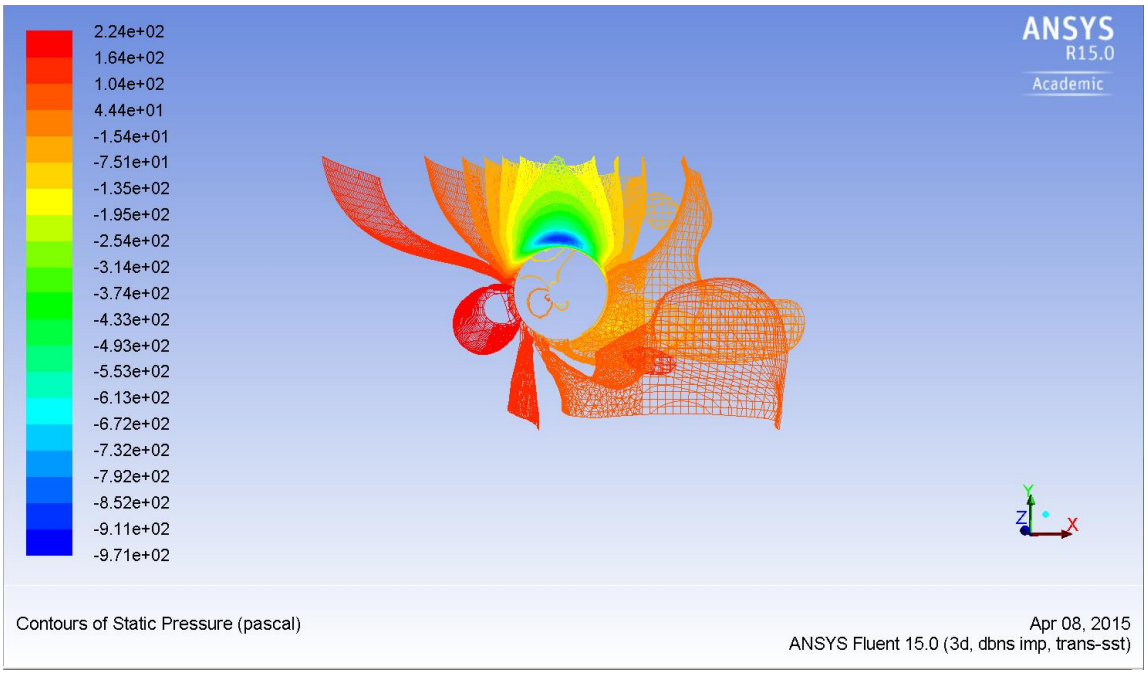
2.24e+02
1.64e+02
1.04e+02
4.44e+01
-1.54e+01
-7.51e+01
-1.35e+02
-1.95e+02
-2.54e+02
-3.14e+02
-3.74e+02
-4.33e+02
-4.93e+02
-5.53e+02
-6.13e+02
-6.72e+02
-7.32e+02
-7.92e+02
-8.52e+02
-9.11e+02
-9.71e+02
ANSYS
R15.0
Academic
Contours of Static Pressure (pascal)
Apr 08, 2015
ANSYS Fluent 15.0 (3d, dbns imp, trans-sst)

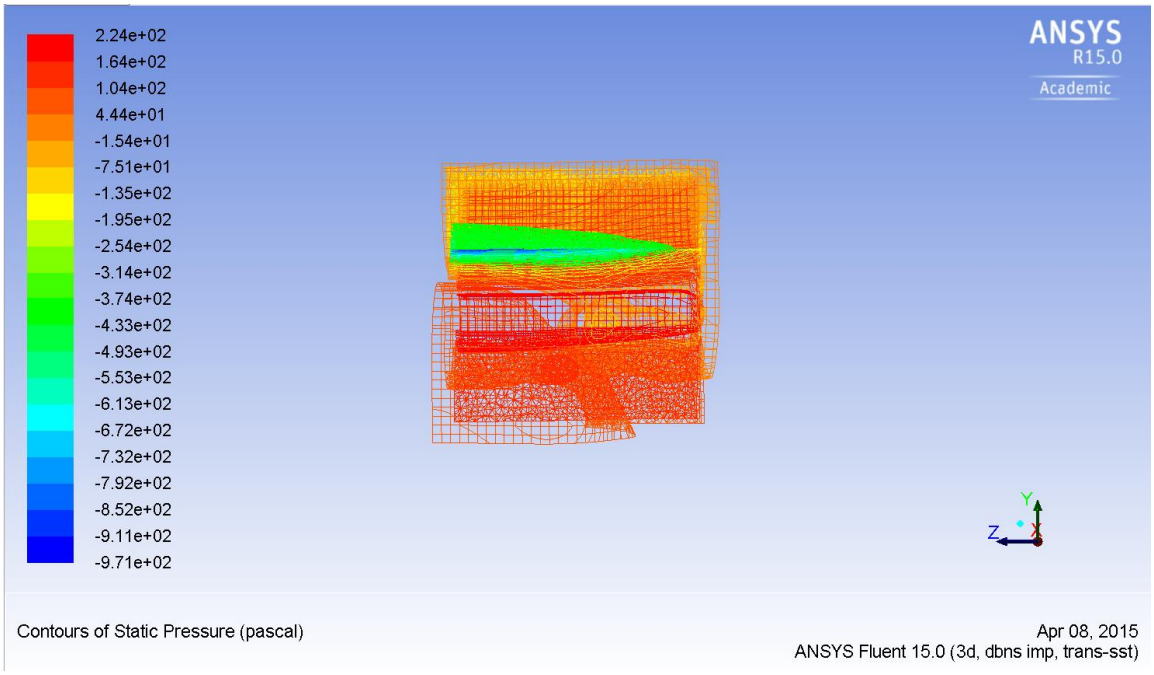
2.24e+02
1.64e+02
1.04e+02
4.44e+01
-1.54e+01
-7.51e+01
-1.35e+02
-1.95e+02
-2.54e+02
-3.14e+02
-3.74e+02
-4.33e+02
-4.93e+02
-5.53e+02
-6.13e+02
-6.72e+02
-7.32e+02
-7.92e+02
-8.52e+02
-9.11e+02
-9.71e+02
ANSYS
R15.0
Academic
Y
Z
X
Contours of Static Pressure (pascal)
Apr 08, 2015
ANSYS Fluent 15.0 (3d, dbns imp, trans-sst)

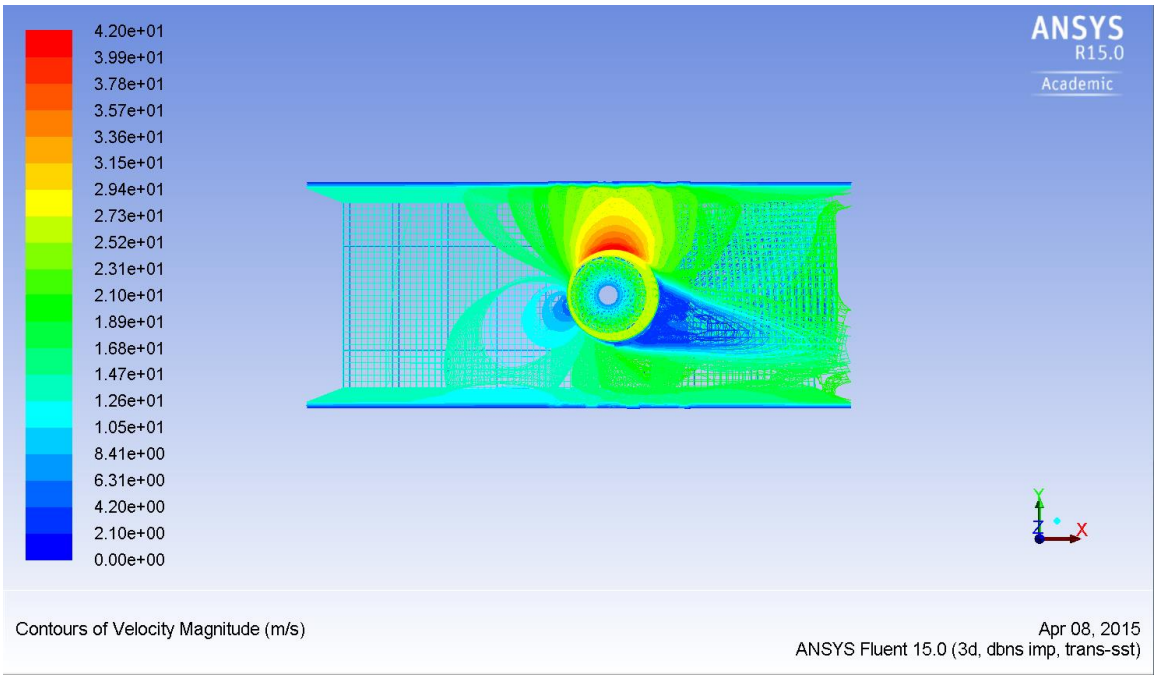
4.20e+01
3.99e+01
3.78e+01
3.57e+01
3.36e+01
3.15e+01
2.94e+01
2.73e+01
2.52e+01
2.31e+01
2.10e+01
1.89e+01
1.68e+01
1.47e+01
1.26e+01
1.05e+01
8.41e+00
6.31e+00
4.20e+00
2.10e+00
0.00e+00
ANSYS
R15.0
Academic
Y
Z
X
Contours of Velocity Magnitude (m/s)
Apr 08, 2015
ANSYS Fluent 15.0 (3d, dbns imp, trans-sst)

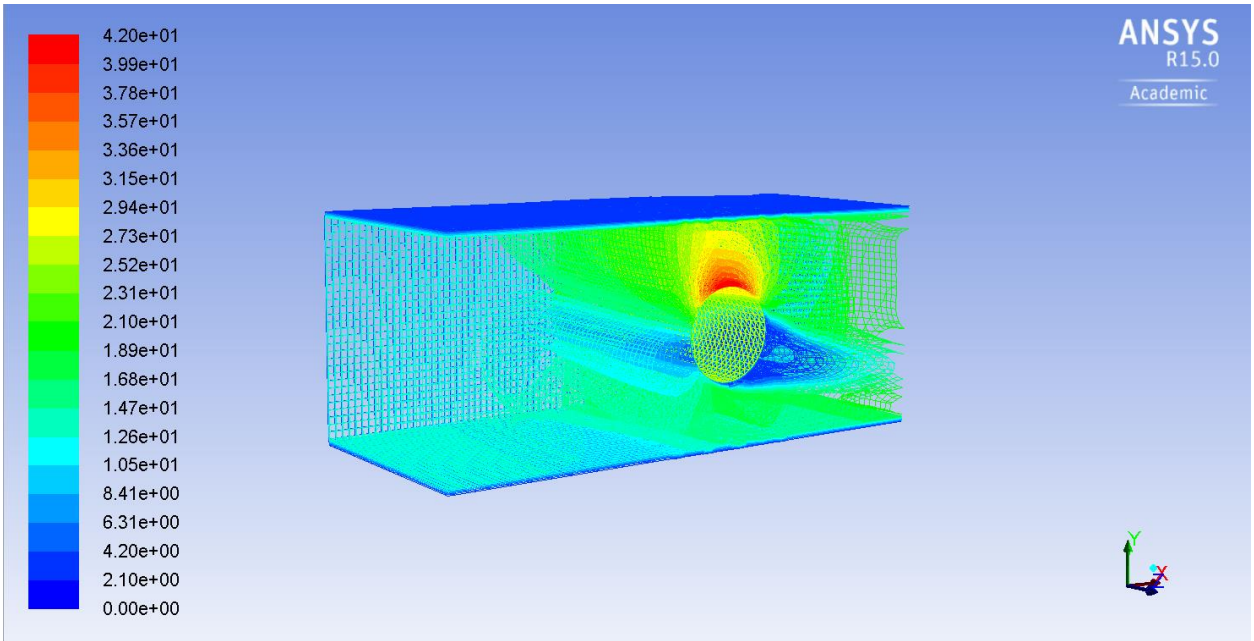
4.20e+01
3.99e+01
3.78e+01
3.57e+01
3.36e+01
3.15e+01
2.94e+01
2.73e+01
2.52e+01
2.31e+01
2.10e+01
1.89e+01
1.68e+01
1.47e+01
1.26e+01
1.05e+01
8.41e+00
6.31e+00
4.20e+00
2.10e+00
0.00e+00
ANSYS
R15.0
Academic
Y
X
Z
Contours of Velocity Magnitude (m/s)
Apr 08, 2015
ANSYS Fluent 15.0 (3d, dbns imp, trans-sst)

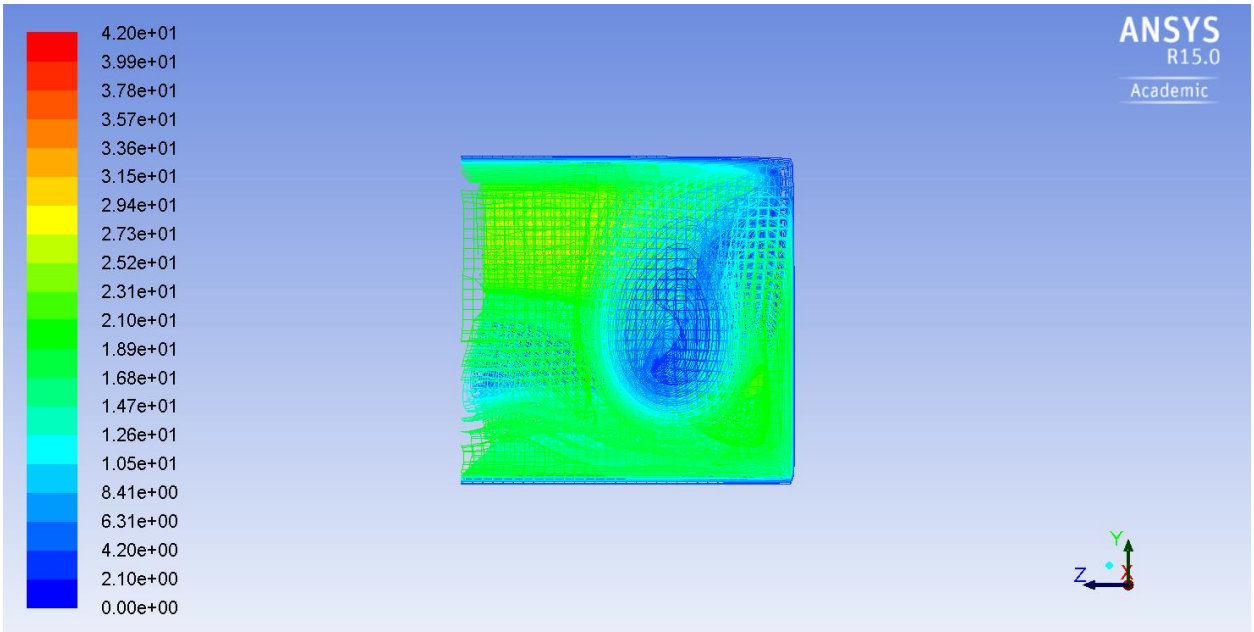
4.20e+01
3.99e+01
3.78e+01
3.57e+01
3.36e+01
3.15e+01
2.94e+01
2.73e+01
2.52e+01
2.31e+01
2.10e+01
1.89e+01
1.68e+01
1.47e+01
1.26e+01
1.05e+01
8.41e+00
6.31e+00
4.20e+00
2.10e+00
0.00e+00
ANSYS
R15.0
Academic
Y
Z
X
Contours of Velocity Magnitude (m/s)
Apr 08, 2015
ANSYS Fluent 15.0 (3d, dbns imp, trans-sst)

Position 4

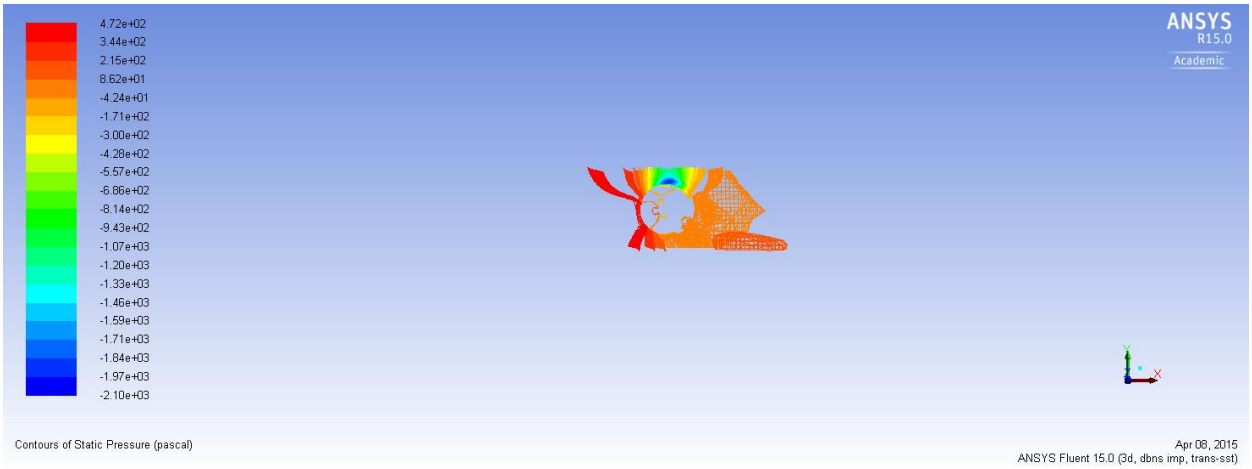
4.72e+02
3.44e+02
2.15e+02
8.62e+01
-4.24e+01
-1.71e+02
-3.00e+02
-4.28e+02
-5.57e+02
-6.86e+02
-8.14e+02
-9.43e+02
-1.07e+03
-1.20e+03
-1.33e+03
-1.46e+03
-1.59e+03
-1.71e+03
-1.84e+03
-1.97e+03
-2.10e+03
ANSYS
R15.0
Academic
Contours of Static Pressure (pascal)
Apr 08, 2015
ANSYS Fluent 15.0 (3d, dbns imp, trans-sst)

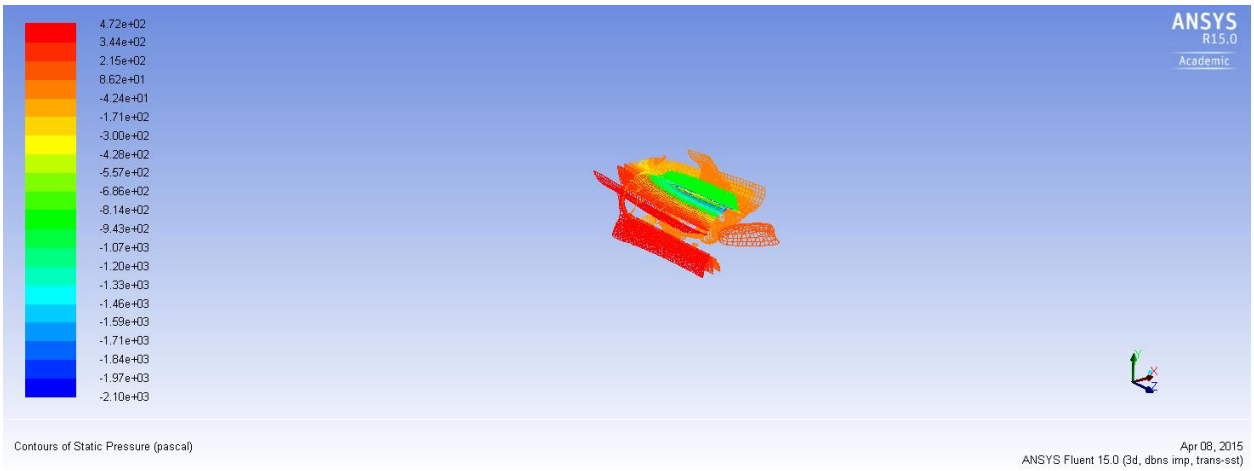
4.72e+02
3.44e+02
2.15e+02
8.62e+01
-4.24e+01
-1.71e+02
-3.00e+02
-4.28e+02
-5.57e+02
-6.86e+02
-8.14e+02
-9.43e+02
-1.07e+03
-1.20e+03
-1.33e+03
-1.46e+03
-1.59e+03
-1.71e+03
-1.84e+03
-1.97e+03
-2.10e+03
ANSYS
R15.0
Academic
Contours of Static Pressure (pascal)
Apr 08, 2015
ANSYS Fluent 15.0 (3d, dbns imp, trans-sst)

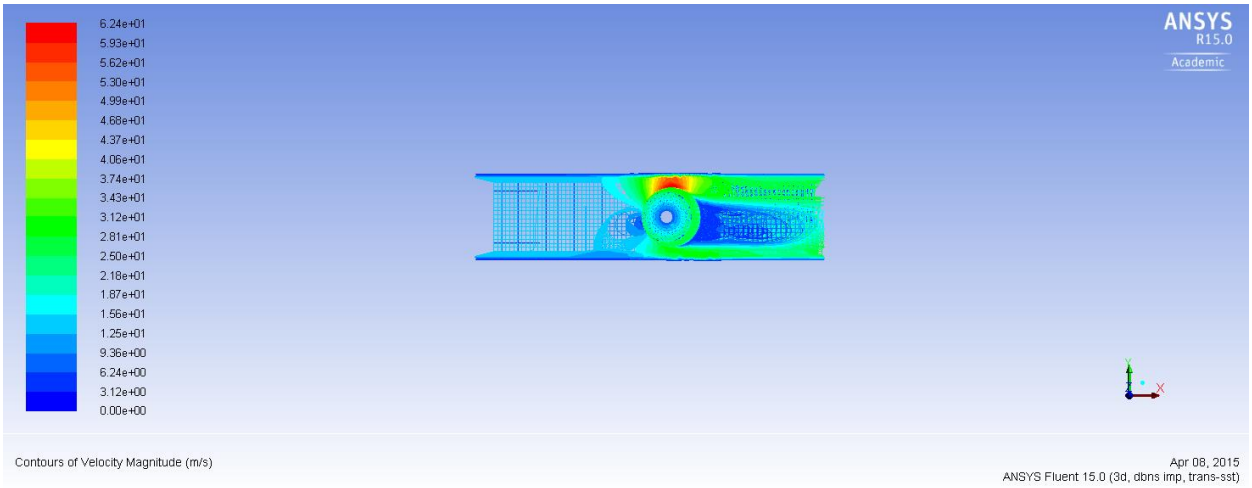
6.24e+01
5.93e+01
5.62e+01
5.30e+01
4.99e+01
4.68e+01
4.37e+01
4.06e+01
3.74e+01
3.43e+01
3.12e+01
2.81e+01
2.50e+01
2.18e+01
1.87e+01
1.56e+01
1.25e+01
9.36e+00
6.24e+00
3.12e+00
0.00e+00
ANSYS
R15.0
Academic
Contours of Velocity Magnitude (m/s)
Apr 08, 2015
ANSYS Fluent 15.0 (3d, dbns imp, trans-sst)

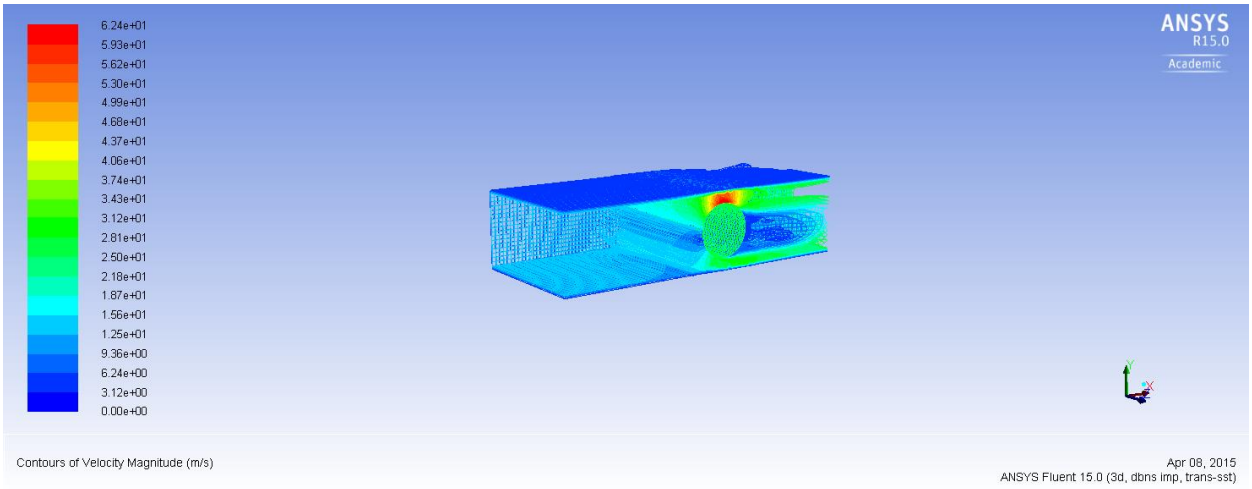
6.24e+01
5.93e+01
5.62e+01
5.30e+01
4.99e+01
4.68e+01
4.37e+01
4.06e+01
3.74e+01
3.43e+01
3.12e+01
2.81e+01
2.50e+01
2.18e+01
1.87e+01
1.56e+01
1.25e+01
9.36e+00
6.24e+00
3.12e+00
0.00e+00
ANSYS
R15.0
Academic
Contours of Velocity Magnitude (m/s)
Apr 08, 2015
ANSYS Fluent 15.0 (3d, dbns imp, trans-sst)

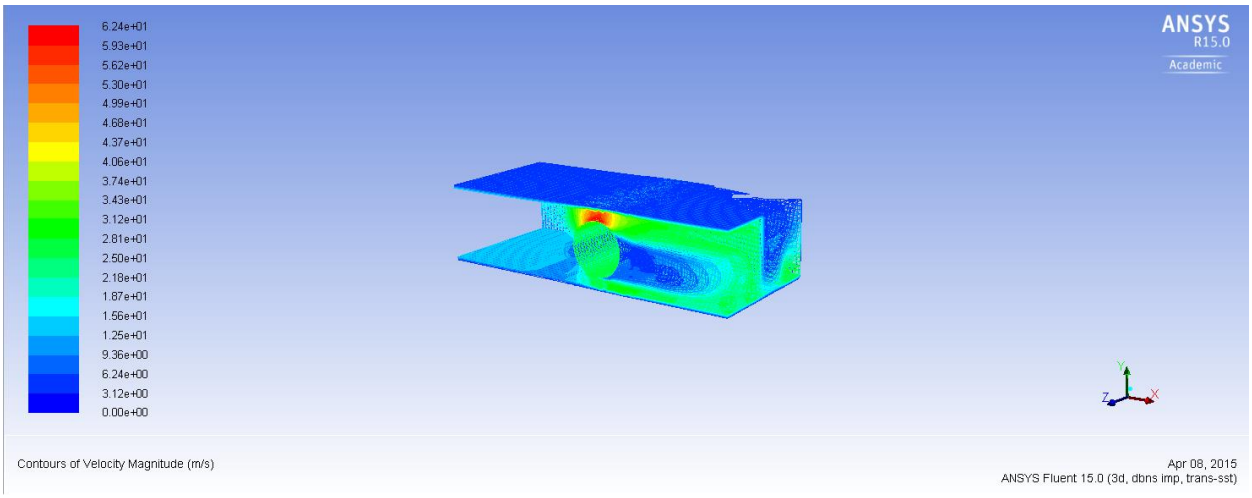
6.24e+01
5.93e+01
5.62e+01
5.30e+01
4.99e+01
4.68e+01
4.37e+01
4.06e+01
3.74e+01
3.43e+01
3.12e+01
2.81e+01
2.50e+01
2.18e+01
1.87e+01
1.56e+01
1.25e+01
9.36e+00
6.24e+00
3.12e+00
0.00e+00
ANSYS
R15.0
Academic
Contours of Velocity Magnitude (m/s)
Apr 08, 2015
ANSYS Fluent 15.0 (3d, dbns imp, trans-sst)

Appendix C: ANSYS Fluent Setup

Defaults	
Physics Preference	CFD
Solver Preference	Fluent
Relevance	0
Sizing	
Use Advanced Size Fun...	On: Curvature
Relevance Center	Coarse
Initial Size Seed	Active Assembly
Smoothing	Medium
Transition	Slow
Span Angle Center	Fine
Curvature Normal A...	Default (18.0 °)
Min Size	Default (3.6857e-004 m)
Max Face Size	Default (3.6857e-002 m)
Max Size	Default (7.3714e-002 m)
Growth Rate	Default (1.20)
Minimum Edge Length	3.175e-003 m
Inflation	
Use Automatic Inflation	None
Inflation Option	Smooth Transition
Transition Ratio	0.272
Maximum Layers	5
Growth Rate	1.2
Inflation Algorithm	Pre
View Advanced Options	No
Assembly Meshing	
Method	None
Patch Conforming Options	
Triangle Surface Mesher	Program Controlled
Patch Independent Options	
Topology Checking	Yes
Advanced	
Number of CPUs for Pa...	Program Controlled
Shape Checking	CFD
Element Midside Nodes	Dropped
Straight Sided Elements	
Number of Retries	0
Extra Retries For Assem...	Yes
Rigid Body Behavior	Dimensionally Reduced
Mesh Morphing	Disabled
Defeaturing	
Statistics	
Nodes	123913
Elements	283906

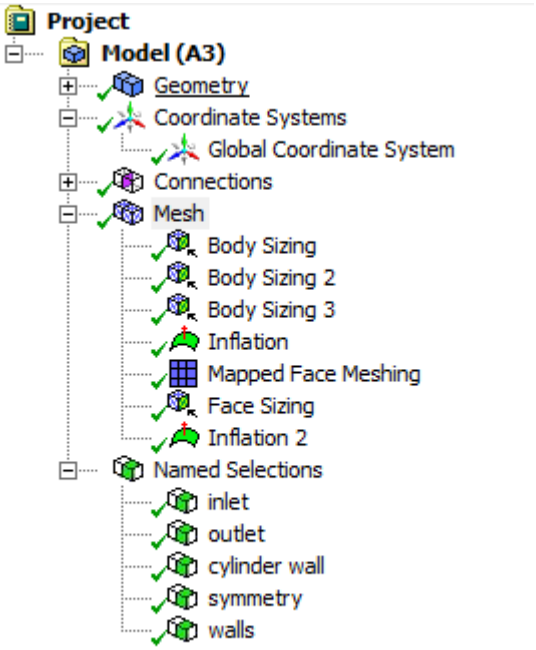

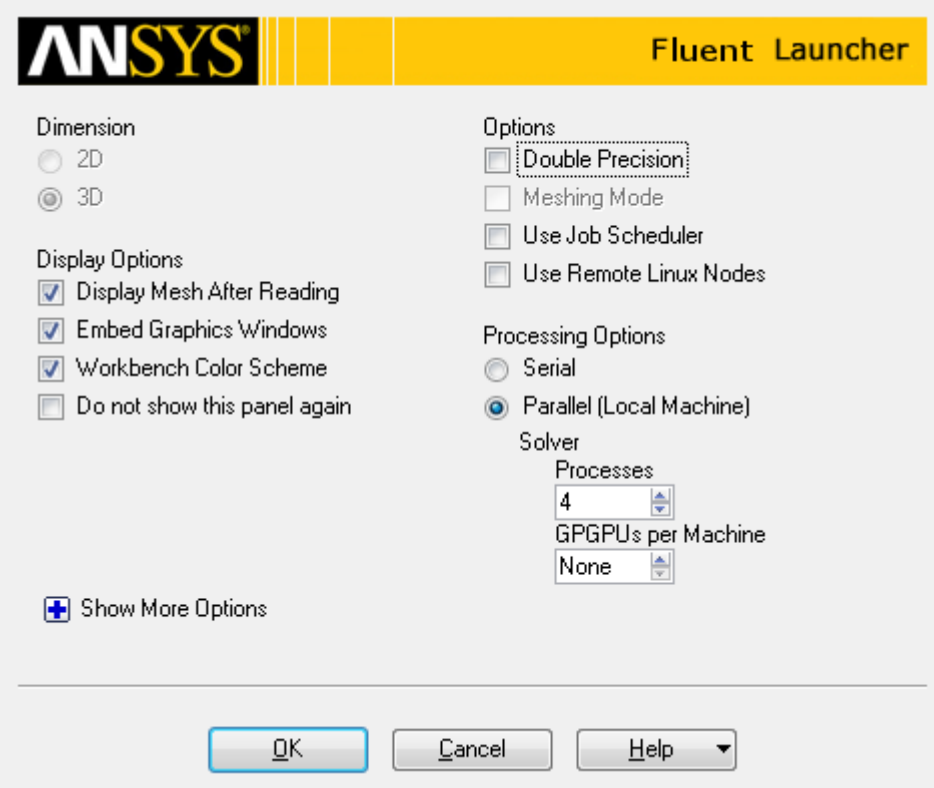
ANSYS
Fluent Launcher
Dimension
2D
3D
Display Options
Display Mesh After Reading
Embed Graphics Windows
Workbench Color Scheme
Do not show this panel again
Options
Double Precision
Meshing Mode
Use Job Scheduler
Use Remote Linux Nodes
Processing Options
Serial
Parallel (Local Machine)
Solver
Processes
4
GPGPUs per Machine
None
Show More Options
OK
Cancel
Help

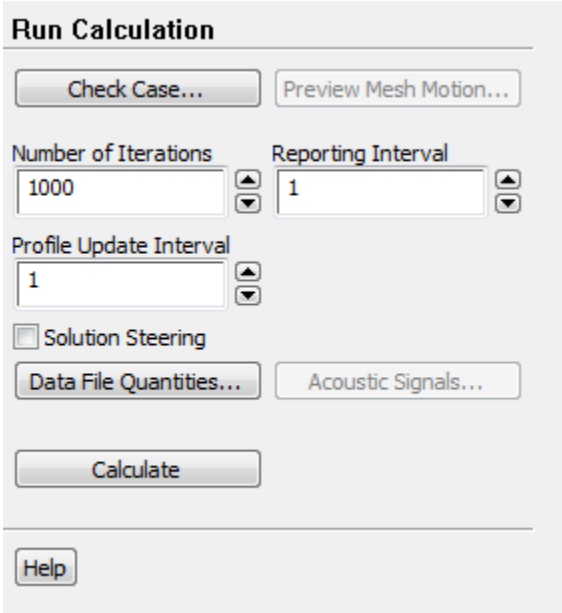
Run Calculation
Check Case...
Preview Mesh Motion...
Number of Iterations
1000
Reporting Interval
1
Profile Update Interval
1
Solution Steering
Data File Quantities...
Acoustic Signals...
Calculate
Help

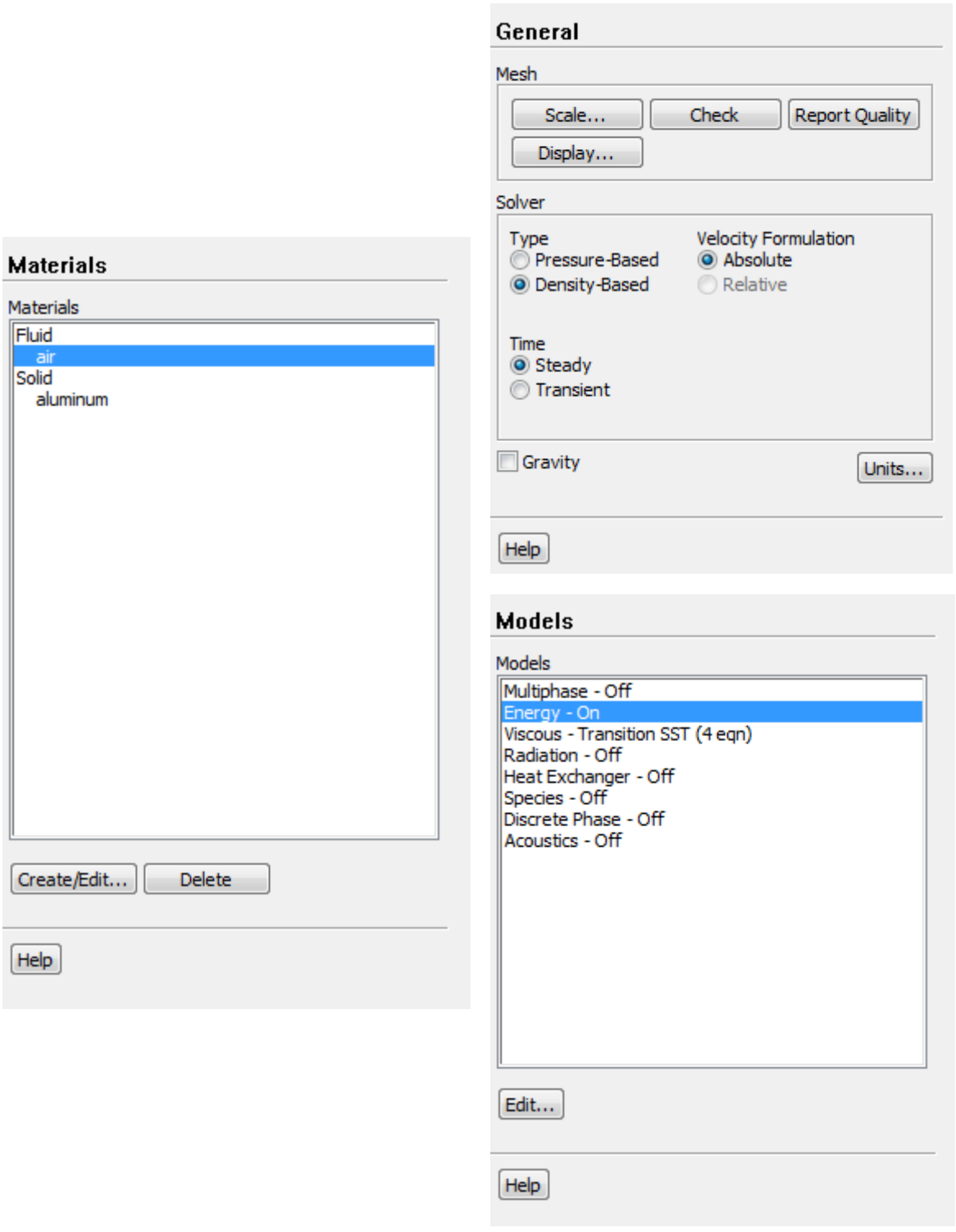
General
Mesh
Scale...
Check
Report Quality
Display...
Solver
Type
Pressure-Based
Density-Based
Velocity Formulation
Absolute
Relative
Time
Steady
Transient
Gravity
Units...
Help
Materials
Materials
Fluid
air
Solid
aluminum
Create/Edit...
Delete
Help
Models
Models
Multiphase - Off
Energy - On
Viscous - Transition SST (4 eqn)
Radiation - Off
Heat Exchanger - Off
Species - Off
Discrete Phase - Off
Acoustics - Off
Edit...
Help

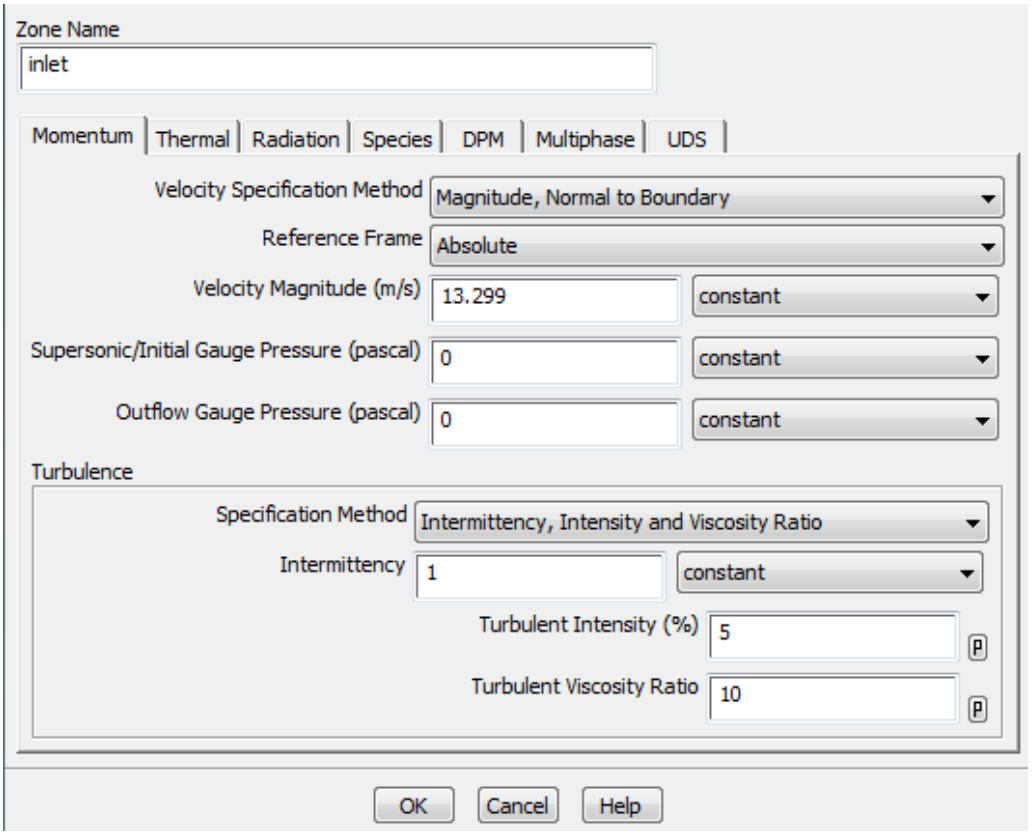
Zone Name
inlet
Momentum
Thermal
Radiation
Species
DPM
Multiphase
UDS
Velocity Specification Method
Magnitude, Normal to Boundary
Reference Frame
Absolute
Velocity Magnitude (m/s)
13.299
constant
Supersonic/Initial Gauge Pressure (pascal)
0
constant
Outflow Gauge Pressure (pascal)
0
constant
Turbulence
Specification Method
Intermittency, Intensity and Viscosity Ratio
Intermittency
1
constant
Turbulent Intensity (%)
5
Turbulent Viscosity Ratio
10
OK
Cancel
Help

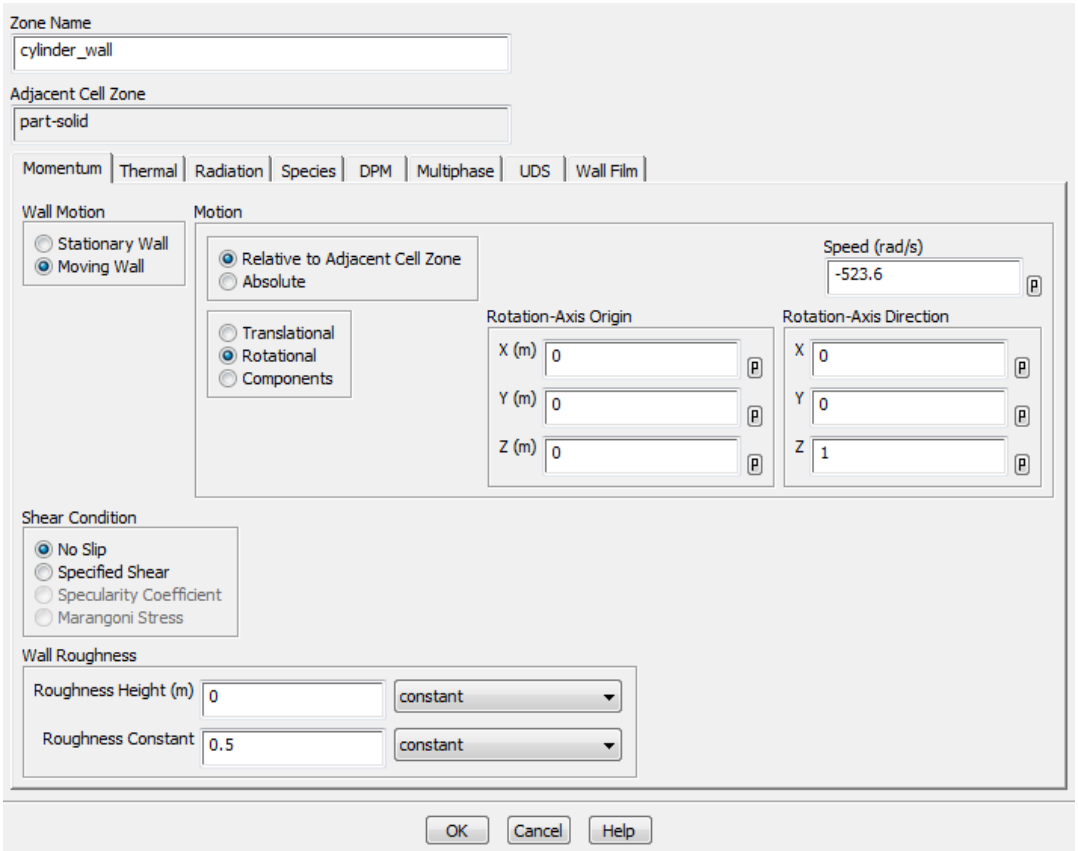
Zone Name
cylinder_wall
Adjacent Cell Zone
part-solid
Momentum
Thermal
Radiation
Species
DPM
Multiphase
UDS
Wall Film
Wall Motion
Stationary Wall
Moving Wall
Motion
Relative to Adjacent Cell Zone
Absolute
Speed (rad/s)
-523.6
Translational
Rotational
Components
Rotation-Axis Origin
X (m) 0
Y (m) 0
Z (m) 0
Rotation-Axis Direction
X 0
Y 0
Z 1
Shear Condition
No Slip
Specified Shear
Specularity Coefficient
Marangoni Stress
Wall Roughness
Roughness Height (m) 0
constant
Roughness Constant 0.5
constant
OK
Cancel
Help

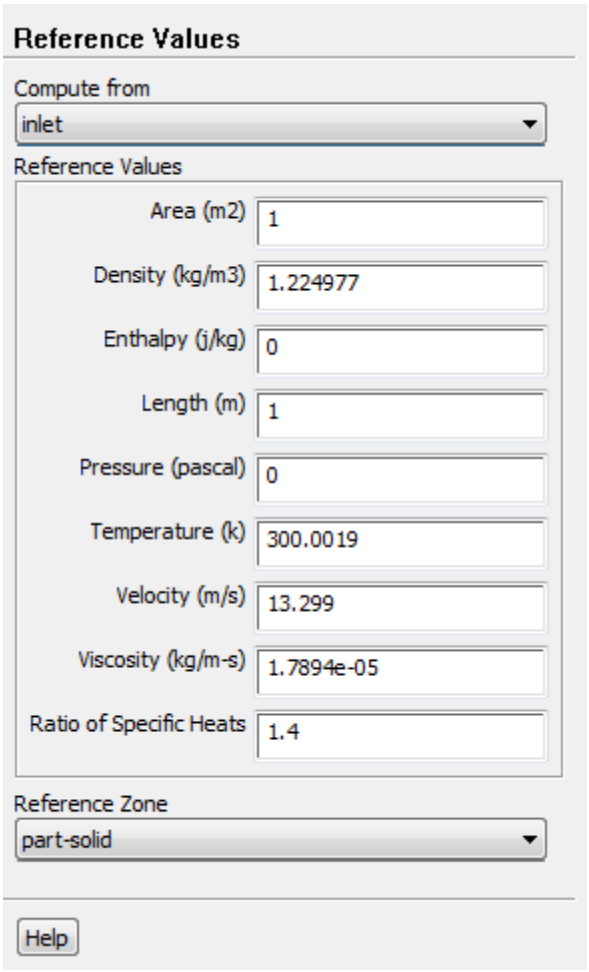
Reference Values
Compute from
inlet
Reference Values
Area (m2)
1
Density (kg/m3)
1.224977
Enthalpy (j/kg)
0
Length (m)
1
Pressure (pascal)
0
Temperature (k)
300.0019
Velocity (m/s)
13.299
Viscosity (kg/m-s)
1.7894e-05
Ratio of Specific Heats
1.4
Reference Zone
part-solid
Help

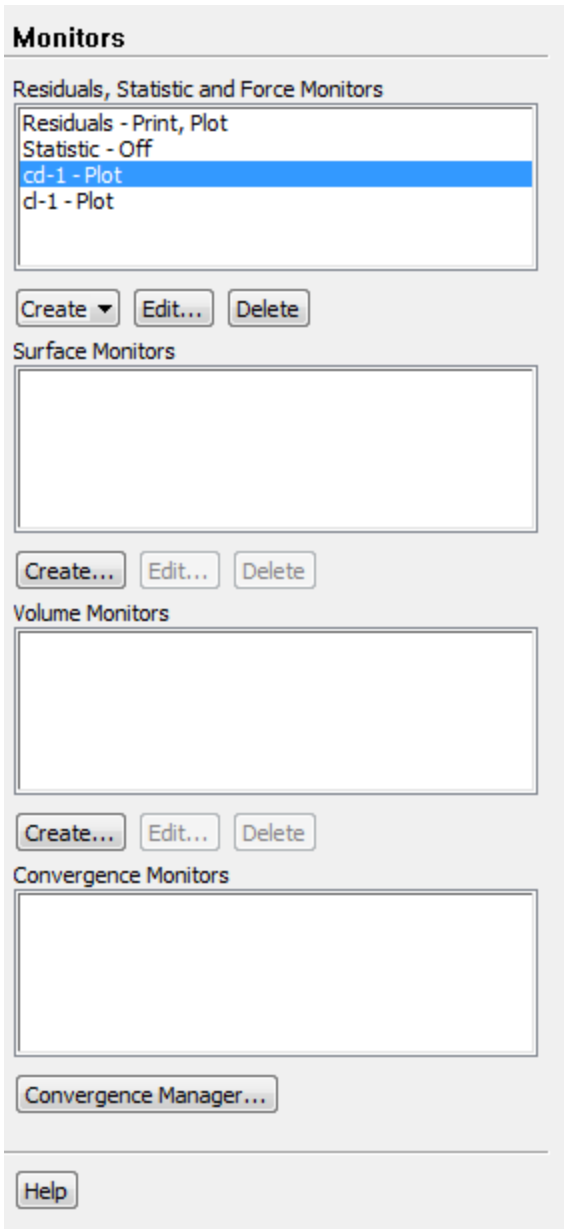
Monitors
Residuals, Statistic and Force Monitors
Residuals - Print, Plot
Statistic - Off
cd-1 - Plot
cl-1 - Plot
Create
Edit...
Delete
Surface Monitors
Create...
Edit...
Delete
Volume Monitors
Create...
Edit...
Delete
Convergence Monitors
Convergence Manager...
Help

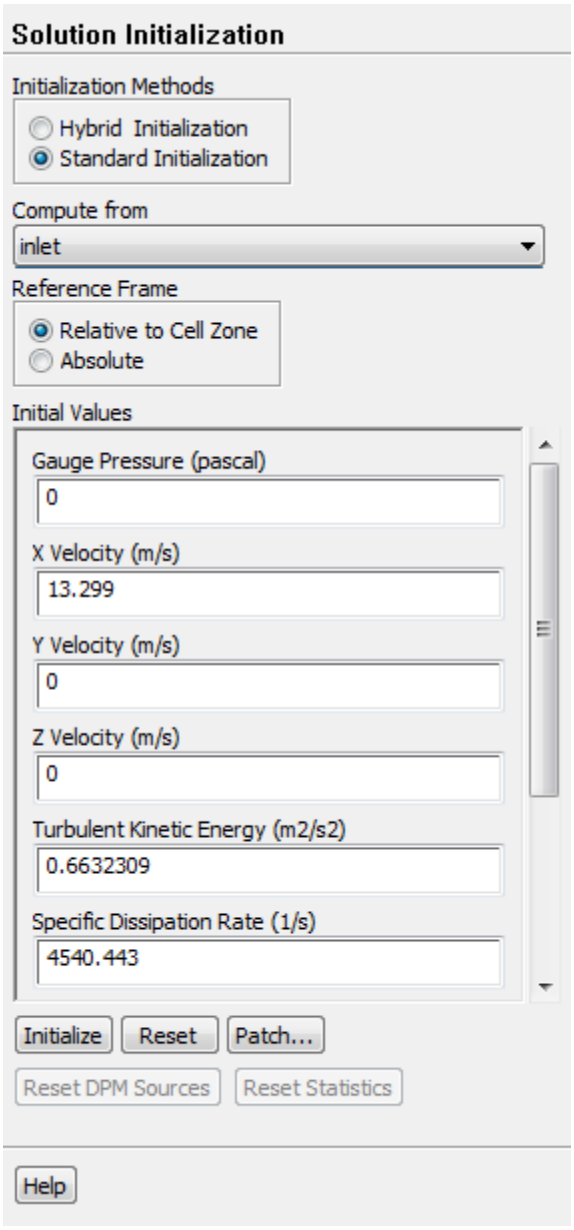
Solution Initialization
Initialization Methods
Hybrid Initialization
Standard Initialization
Compute from
inlet
Reference Frame
Relative to Cell Zone
Absolute
Initial Values
Gauge Pressure (pascal)
0
X Velocity (m/s)
13.299
Y Velocity (m/s)
0
Z Velocity (m/s)
0
Turbulent Kinetic Energy (m2/s2)
0.6632309
Specific Dissipation Rate (1/s)
4540.443
Initialize
Reset
Patch...
Reset DPM Sources
Reset Statistics
Help

Appendix D: Lift vs. Air Speed and Cylinder RPM

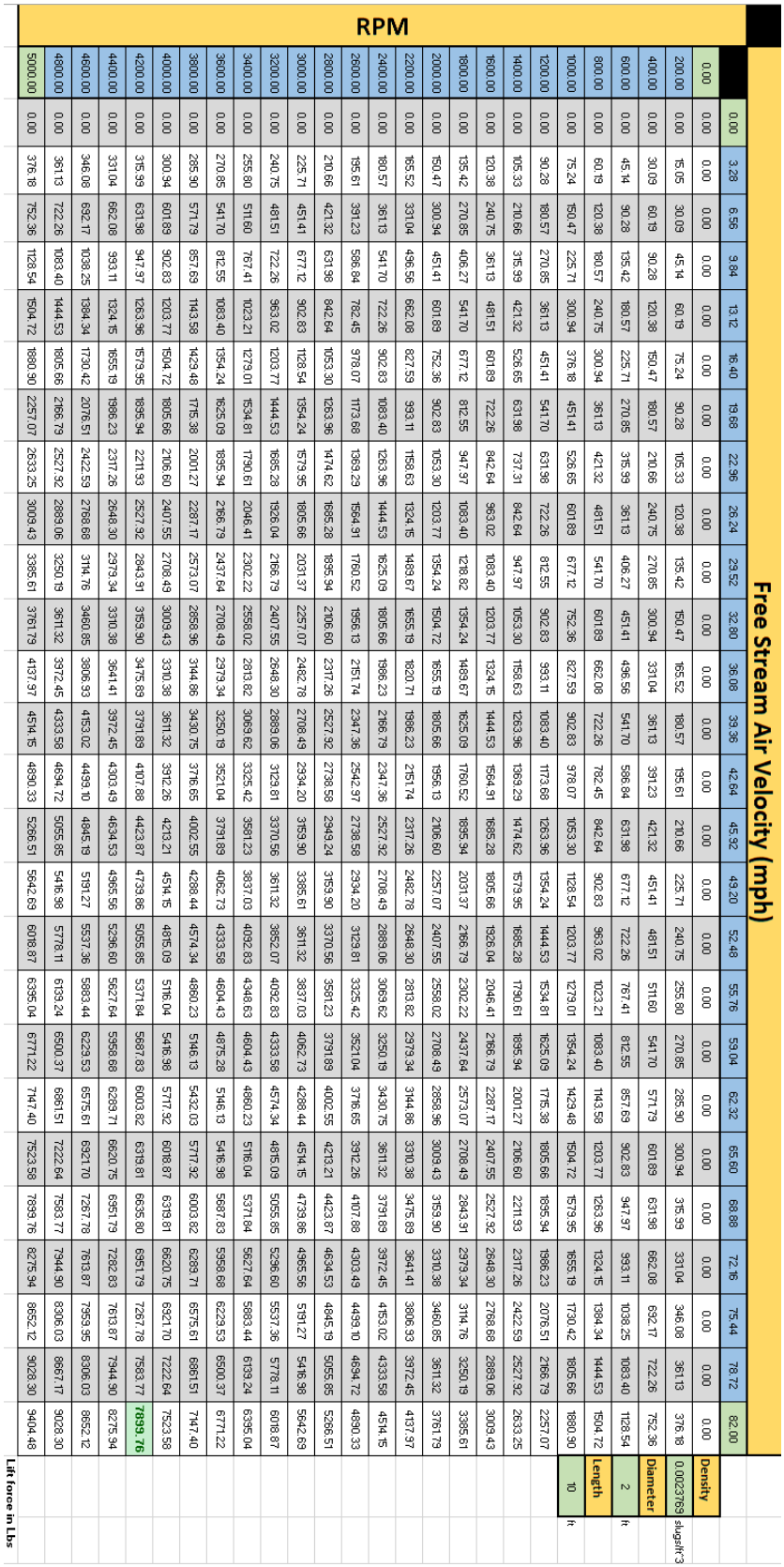

RPM \ Free Stream Air Velocity (mph)	0.00	3.28	6.56	9.84	13.12	16.40	19.68	22.96	26.24	29.52	32.80	36.08	39.36	42.64	45.92	49.20	52.48	55.76	59.04	62.32	65.60	68.88	72.16	75.44	78.72	82.00
0.00	0.00	0.00	0.00	0.00	0.00	0.00	0.00	0.00	0.00	0.00	0.00	0.00	0.00	0.00	0.00	0.00	0.00	0.00	0.00	0.00	0.00	0.00	0.00	0.00	0.00	0.00
200.00	0.00	15.05	30.09	45.14	60.19	75.24	90.28	105.33	120.38	135.42	150.47	165.52	180.57	195.61	210.66	225.71	240.75	255.80	270.85	285.90	300.94	315.99	331.04	346.08	361.13	376.18
400.00	0.00	30.09	60.19	90.28	120.38	150.47	180.57	210.66	240.75	270.85	300.94	331.04	361.13	391.23	421.32	451.41	481.51	511.60	541.70	571.79	601.89	631.98	662.08	692.17	722.26	752.36
600.00	0.00	45.14	90.28	135.42	180.57	225.71	270.85	315.99	361.13	406.27	451.41	496.56	541.70	586.84	631.98	677.12	722.26	767.41	812.55	857.69	902.83	947.97	993.11	1038.25	1083.40	1128.54
800.00	0.00	60.19	120.38	180.57	240.75	300.94	361.13	421.32	481.51	541.70	601.89	662.08	722.26	782.45	842.64	902.83	963.02	1023.21	1083.40	1143.59	1203.77	1263.96	1324.15	1384.34	1444.53	1504.72
1000.00	0.00	75.24	150.47	225.71	300.94	376.18	451.41	526.65	601.89	677.12	752.36	827.59	902.83	978.07	1053.30	1128.54	1203.77	1279.01	1354.24	1429.48	1504.72	1579.95	1655.19	1730.42	1805.66	1880.90
1200.00	0.00	90.28	180.57	270.85	361.13	451.41	541.70	631.98	722.26	812.55	902.83	993.11	1083.40	1173.68	1263.96	1354.24	1444.53	1534.81	1625.09	1715.38	1805.66	1895.94	1986.23	2076.51	2166.79	2257.07
1400.00	0.00	105.33	210.66	315.99	421.32	526.65	631.98	737.31	842.64	947.97	1053.30	1158.63	1263.96	1369.29	1474.62	1579.95	1685.28	1790.61	1895.94	2001.27	2106.60	2211.93	2317.26	2422.59	2527.92	2633.25
1600.00	0.00	120.38	240.75	361.13	481.51	601.89	722.26	842.64	963.02	1083.40	1203.77	1324.15	1444.53	1564.91	1685.28	1805.66	1926.04	2046.41	2166.79	2287.17	2407.55	2527.92	2648.30	2768.68	2889.06	3009.43
1800.00	0.00	135.42	270.85	406.27	541.70	677.12	812.55	947.97	1083.40	1218.82	1354.24	1489.67	1625.09	1760.52	1895.94	2031.37	2166.79	2302.22	2437.64	2573.07	2708.49	2843.91	2979.34	3114.76	3250.19	3385.61
2000.00	0.00	150.47	300.94	451.41	601.89	752.36	902.83	1053.30	1203.77	1354.24	1504.72	1655.19	1805.66	1956.13	2106.60	2257.07	2407.55	2558.02	2708.49	2858.96	3009.43	3159.90	3310.38	3460.85	3611.32	3761.79
2200.00	0.00	165.52	331.04	496.56	662.08	827.59	993.11	1158.63	1324.15	1489.67	1655.19	1820.71	1986.23	2151.74	2317.26	2482.78	2648.30	2813.82	2979.34	3144.86	3310.38	3475.89	3641.41	3806.93	3972.45	4137.97
2400.00	0.00	180.57	361.13	541.70	722.26	902.83	1083.40	1263.96	1444.53	1625.09	1805.66	1986.23	2166.79	2347.36	2527.92	2708.49	2889.06	3069.62	3250.19	3430.75	3611.32	3791.89	3972.45	4153.02	4333.58	4514.15
2600.00	0.00	195.61	391.23	586.84	782.45	978.07	1173.68	1369.29	1564.91	1760.52	1956.13	2151.74	2347.36	2542.97	2738.58	2934.20	3129.81	3325.42	3521.04	3716.65	3912.26	4107.88	4303.49	4499.10	4694.72	4890.33
2800.00	0.00	210.66	421.32	631.98	842.64	1053.30	1263.96	1474.62	1685.28	1895.94	2106.60	2317.26	2527.92	2738.58	2949.24	3159.90	3370.56	3581.23	3791.89	4002.55	4213.21	4423.87	4634.53	4845.19	5055.85	5266.51
3000.00	0.00	225.71	451.41	677.12	902.83	1128.54	1354.24	1579.95	1805.66	2031.37	2257.07	2482.78	2708.49	2934.20	3159.90	3385.61	3611.32	3837.03	4062.73	4288.44	4514.15	4739.86	4965.56	5191.27	5416.98	5642.69
3200.00	0.00	240.75	481.51	722.26	963.02	1203.77	1444.53	1685.28	1926.04	2166.79	2407.55	2648.30	2889.06	3129.81	3370.56	3611.32	3852.07	4092.83	4333.58	4574.34	4815.09	5055.85	5296.60	5537.36	5778.11	6018.87
3400.00	0.00	255.80	511.60	767.41	1023.21	1279.01	1534.81	1790.61	2046.41	2302.22	2558.02	2813.82	3069.62	3325.42	3581.23	3837.03	4092.83	4348.63	4604.43	4860.23	5116.04	5371.84	5627.64	5883.44	6139.24	6395.04
3600.00	0.00	270.85	541.70	812.55	1083.40	1354.24	1625.09	1895.94	2166.79	2437.64	2708.49	2979.34	3250.19	3521.04	3791.89	4062.73	4333.58	4604.43	4875.28	5146.13	5416.98	5687.83	5958.68	6229.53	6500.37	6771.22
3800.00	0.00	285.90	571.79	857.69	1143.59	1429.48	1715.38	2001.27	2287.17	2573.07	2858.96	3144.86	3430.75	3716.65	4002.55	4288.44	4574.34	4860.23	5146.13	5432.03	5717.92	6003.82	6289.71	6575.61	6861.51	7147.40
4000.00	0.00	300.94	601.89	902.83	1203.77	1504.72	1805.66	2106.60	2407.55	2708.49	3009.43	3310.38	3611.32	3912.26	4213.21	4514.15	4815.09	5116.04	5416.98	5717.92	6018.87	6319.81	6620.75	6921.70	7222.64	7523.58
4200.00	0.00	315.99	631.98	947.97	1263.96	1579.95	1895.94	2211.93	2527.92	2843.91	3159.90	3475.89	3791.89	4107.88	4423.87	4739.86	5055.85	5371.84	5687.83	6003.82	6319.81	6635.80	6951.79	7267.78	7583.77	**7899.76**
4400.00	0.00	331.04	662.08	993.11	1324.15	1655.19	1986.23	2317.26	2648.30	2979.34	3310.38	3641.41	3972.45	4303.49	4634.53	4965.56	5296.60	5627.64	5958.68	6289.71	6620.75	6951.79	7282.83	7613.87	7944.90	8275.94
4600.00	0.00	346.08	692.17	1038.25	1384.34	1730.42	2076.51	2422.59	2768.68	3114.76	3460.85	3806.93	4153.02	4499.10	4845.19	5191.27	5537.36	5883.44	6229.53	6575.61	6921.70	7267.78	7613.87	7959.95	8306.03	8652.12
4800.00	0.00	361.13	722.26	1083.40	1444.53	1805.66	2166.79	2527.92	2889.06	3250.19	3611.32	3972.45	4333.58	4694.72	5055.85	5416.98	5778.11	6139.24	6500.37	6861.51	7222.64	7583.77	7944.90	8306.03	8667.17	9028.30
5000.00	0.00	376.18	752.36	1128.54	1504.72	1880.90	2257.07	2633.25	3009.43	3385.61	3761.79	4137.97	4514.15	4890.33	5266.51	5642.69	6018.87	6395.04	6771.22	7147.40	7523.58	7899.76	8275.94	8652.12	9028.30	9404.48

Density	
0.0023769	slugs/ft^3
Diameter	
2	ft
Length	
10	ft

Lift force in Lbs

Appendix F: Derivation of Kutta-Joukowski Lift Theorem

Derivation

Please note that most the following figures and derivations were taken from The Fundamentals of Aerodynamics by John D. Anderson. This is an excellent textbook on aerodynamic theory, and should be referenced for a more in depth analysis on the concepts described in this report.

Lift on a cylinder is derived from the superimposition of elementary incompressible flows. By doing this a complex incompressible flow can be synthesized. For Magnus lift four elementary flows are required:

- Uniform Flow
- Source/Sink Flow
- Doublet Flow
- Vortex Flow

Each of these flows can be represented by three major components, velocity potential, the stream function, and circulation.

Notes:
The del operator, **∇**, is just a differential operator denoted as such in three dimensional Cartesian (X, Y, Z) in standard basis $\{\overrightarrow{e_x}, \overrightarrow{e_y}, \overrightarrow{e_z}\}$. $$\nabla = \left(\frac{\partial}{\partial x}, \frac{\partial}{\partial y}, \frac{\partial}{\partial z}\right) = \left\{\overrightarrow{e_x}\frac{\partial}{\partial x} + \overrightarrow{e_y}\frac{\partial}{\partial y} + \overrightarrow{e_z}\frac{\partial}{\partial z}\right\}$$
Incompressibility: $$\nabla \cdot V = 0$$ **Irrotationality**: $$\nabla \times V = 0$$
Denoting **ϕ** as **velocity potential** which is the scalar quantity whose negative gradient equals the velocity in the case of irrotational flow of a fluid. Using the del operator as shown before we see that $V = \nabla\phi$ or $$u = \frac{\partial\phi}{\partial x} \quad v = \frac{\partial\phi}{\partial y} \quad w = \frac{\partial\phi}{\partial z}$$ Where u is velocity in x, v is velocity in the y and w is velocity in the z.
The potential is not the only scalar field which a vector field can be expressed in terms of. Velocity can also be expressed in terms of a stream function. The **stream function** differs from potential by being described to satisfy continuity instead of irrotationality. The stream function is denoted by **ψ**. $$\frac{dy}{dx} = \frac{v}{u}$$

And

$$u = \frac{\partial \psi}{\partial y} \ and \ v = -\frac{\partial \psi}{\partial x}$$

In fluid dynamics, circulation is the line integral around a closed curve of the velocity field. Circulation is normally denoted **Γ**.

$$\Gamma = \iint_S (\nabla \text{ x } V) \cdot ds \Rightarrow -\oint_c V \cdot ds$$

F.1 Uniform Flow

Consider a uniform flow with velocity V_∞ oriented in the positive x direction, as shown in Figure123123. The flow is both incompressible ($\nabla \cdot V = 0$) and irrotational ($\nabla \text{ x } V = 0$). Hence, a velocity potential for uniform flow can be obtained such that ($\nabla \phi = V$)

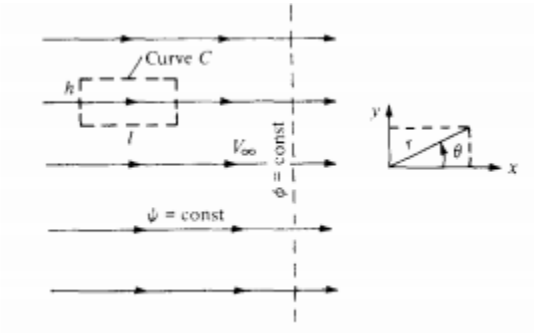

Figure 56: Uniform Flow

Interpreting **Error! Reference source not found.** we get

$$\frac{\partial \phi}{\partial x} = u = V_\infty \ and \ \frac{\partial \phi}{\partial y} = v = 0$$

Integrating $\frac{\partial \phi}{\partial x}$ (This will be the only example I show full integration)

$$\int \partial \phi = \int V_\infty \partial x$$

Thus,

$$\phi = V_\infty x + f(y)$$

Taking the derivative with respect to y

$$\frac{\partial \phi}{\partial y} = f'(y) = v = 0$$

We can conclude from

$$f'(y) = 0$$

That f(y) is a constant thus

$$\phi = V_\infty x + constant$$

However the actual value of ϕ is not significant, it is its derivative to obtain the velocities that is most important, thus the constant can be dropped with no consequences resulting in

$$\phi = V_\infty x$$

Looking at the stream function,

$$\frac{\partial \psi}{\partial y} = u = V_\infty \; and \; \frac{\partial \psi}{\partial x} = -v = 0$$

Similarly it the stream function reduces to

$$\psi = V_\infty y$$

This makes sense since with uniform flow; the streamline is constant in the x direction. Now notice that with uniform flow ψ and ϕ are constant in mutually perpendicular axis.

As a reference, the velocity potential and stream function can be expressed in polar coordinates. Note that x=rcosθ and y=rsinθ, hence

$$\phi = V_\infty r \cos\theta \;\; and \; \psi = V_\infty r \sin\theta$$

Now looking at circulation for uniform flow. Since this is irrotational we know that Γ will be zero. However let's prove it.

$$\Gamma = -\oint_c V \cdot ds$$

And from the figure we get

$$\oint_c V \cdot ds = -V_\infty l - 0(h) + V_\infty l + 0(h) = 0$$

thus

$$\Gamma = 0$$

F.2 Source and Sink Flow

The second elementary flow is a source flow. Consider a two-dimensional, incompressible flow where all the streamlines are straight lines emanating from a central point, as shown in **Error! Reference source not found.**. Moreover, let the velocity along each of the streamlines vary inversely with distance from point 0. Such a flow is called a source flow. All the velocity components are radial, thus V_θ is zero. With source flow it is usually easier to use polar coordinates (Cylindrical Coordinates for three dimensions), hence the conversion for uniform flows. Again this is incompressible ($\nabla \cdot V = 0$) except at the origin and source flow is irrotational at every point ($\nabla \times V = 0$).

Similarly sink flow is a point source form of flow, however as the name suggest it acts as a sink with the flow coming in radial towards the point, the exact opposite as a source flow. So sink flow is simply the negative of source flow. This can also be seen in **Error! Reference source not found.**.

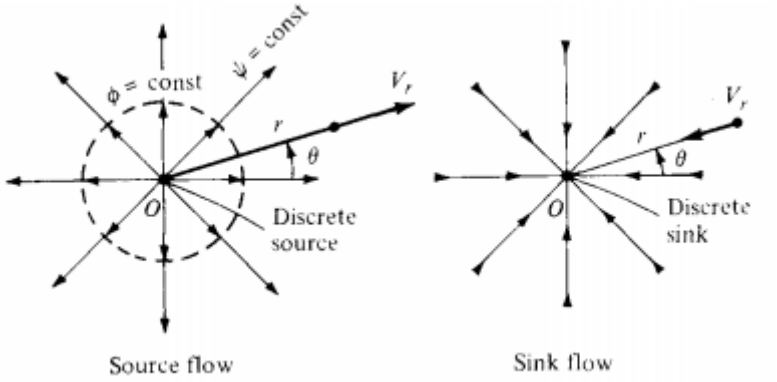

Figure 57: Source and Sink Flow

The volumetric flowrate from a line source (an extruded circle aka cylinder) per unit length is $\frac{\dot{v}}{l}$ ($\dot{v} = \frac{\dot{m}}{\rho}$). A new variable will be introduced for simplicity that will represent this volume flow rate, Λ. Λ defines the source strength. A positive value represents a source and a negative value represents a sink.

$$\Lambda = \frac{\dot{v}}{l} = 2\pi r V_r$$

Solving for the radial velocity,

$$V_r = \frac{\Lambda}{2\pi r}$$

Finding velocity potential (Polar Coordinates)

$$\frac{\partial \phi}{\partial r} = V_r = \frac{\Lambda}{2\pi r} \; and \frac{1}{r}\frac{\partial \phi}{\partial \theta} = V_\theta = 0$$

Using the same method as uniform flow

$$\phi = \frac{\Lambda}{2\pi}\ln(\mathrm{r})$$

Similarly

$$\frac{1}{r}\frac{\partial \psi}{\partial \theta} = V_r = \frac{\Lambda}{2\pi r} \; and - \frac{\partial \psi}{\partial r} v = 0$$

$$\psi = \frac{\Lambda}{2\pi}\theta$$

Again, evaluating circulation is easy since $\nabla \mathrm{x}\, V = 0$ (irrotational)

$$\Gamma = -\oiint_S (\nabla \mathrm{x}\, V) \cdot ds = 0$$

F.3 Doublet Flow

Doublet flow is the case where a source and a sink are merged together at a singular point that lead to a singularity called a doublet. Consider a source and a sink of equal and opposite magnitude of Λ, separated at a distance of l. The stream function at any point P would be

$$\psi = -\frac{\Lambda}{2\pi}\Delta\theta = \frac{\Lambda}{2\pi}(\theta_1 - \theta_2)$$

Where $\Delta\theta = (\theta_2 - \theta_1)$, P and l can be seen derived from **Error! Reference source not found.**. L is approaching 0.

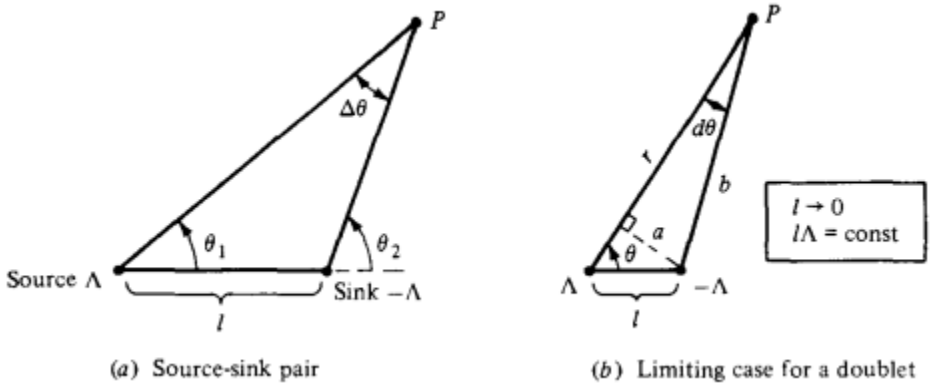

Figure 58: Forming a Solid Boundary Using Sources and Sinks

By letting the distance l approach zero while the absolute magnitudes of the strengths of the source and sink increase in such as fashion that $l\Lambda$ remains constant. The strength of this doublet will be defined as $\kappa \equiv l\Lambda$.

Since l is now approaching 0 a limit must be taken to obtain the stream function of the doublet.

$$\lim_{l\to 0}\left(-\frac{\Lambda}{2\pi}\mathrm{d}\theta\right)\ (\kappa = constant)$$

Where the limit of $\mathrm{d}\theta$ will be approaching zero. (Note that the source strength Λ approaches an infinite value in the limit.) r and b denote the distances to point P from the source and sink, respectively. The line perpendicular from the source of the sink is denoted as a. For an infinitesimal dθ, the geometry becomes:

$$a = l\sin\theta\,, b = r - l\cos\theta\,, \mathrm{d}\theta = \frac{a}{b}$$

Thus

$$\mathrm{d}\theta = \frac{a}{b} = \frac{l\sin\theta\,,}{r - l\cos\theta}$$

substituting

$$\lim_{l\to 0}\left(-\frac{\Lambda}{2\pi}\frac{l\sin\theta\,,}{r - l\cos\theta}\right) = \lim_{l\to 0}\left(-\frac{\kappa}{2\pi}\frac{\sin\theta\,,}{r - l\cos\theta}\right)\ (\kappa = constant)$$

$$\psi = -\frac{\kappa}{2\pi r}\frac{\sin\theta}{r}$$

The same procedure is done with the velocity potential as one would obtain

$$\phi = \frac{\kappa}{2\pi r}\frac{\cos\theta}{r}$$

With these three elementary flows we can model several fluid models, such as flow over a cylinder, which is needed to model the Magnus effect. The only thing is that with all these there is no circulation, and what causes lift in a cylinder is due to this circulation. So similarly to a symmetric airfoil at zero angle of attack, no lift is generated; thus the importance of the final elementary flow, vortex flow.

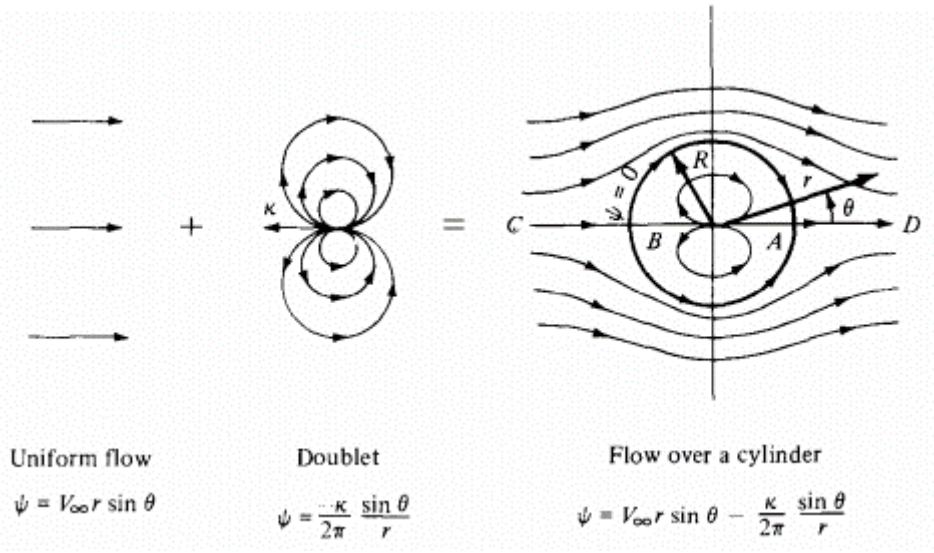

Figure 59: Uniform Flow+Doublet Flow=Flow Over A Cylinder

F.4 Vortex Flow

Vortex is the first of the elementary flows that will have some sort of circulation corresponded with it. Consider a flow where all the streamlines are concentric circles about a given point, as shown in **Error! Reference source not found.** below. Moreover, let the velocity along any given circular streamline be constant, but let it vary from one streamline to another inversely with distance from the common center. Such a flow is called a vortex flow.

Looking at this flow it looks like there is rotation, but in reality vortex flow is still irrotational at every point except at the origin and is incompressible everywhere. What is unique is all the flow is in the theta direction and can be represented as:

$$V_\theta = \frac{Constant}{radius} = \frac{C}{r} \; and \; V_r = 0$$

To evaluate the constant C, take the circulation around a given circular streamline of radius r:

$$\Gamma = -\oint_c V \cdot ds = -V_\theta(2\pi r)$$

Solving:

$$V_\theta = -\frac{\Gamma}{2\pi r}, c = \frac{-\Gamma}{2\pi}$$

Finding velocity potential (Polar Coordinates)

$$\frac{\partial \phi}{\partial r} = V_r = 0 \; and \frac{1}{r}\frac{\partial \phi}{\partial \theta} = V_\theta = -\frac{\Gamma}{2\pi r}$$

Using the same method as uniform flow

$$\phi = -\frac{\Gamma}{2\pi r}\theta$$

Similarly

$$\frac{1}{r}\frac{\partial \psi}{\partial \theta} = V_r = 0 \; and -\frac{\partial \psi}{\partial r} = V_\theta = -\frac{\Gamma}{2\pi r}$$

$$\psi = \frac{\Gamma}{2\pi}\ln(\mathrm{r})$$

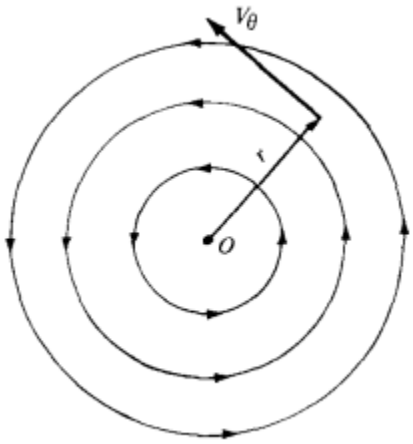

Figure 60: Vortex Flow

F.5 Summary

Error! Reference source not found. sums up what has been done so far:

Table 6: Summary of Velocity Equations for Various Types of Flow

Type of Flow	Velocity	ϕ	ψ
Uniform Flow in X	$u = V_\infty$	$V_\infty x$=$V_\infty r\cos\theta$	$V_\infty y = V_\infty r\sin\theta$
Source	$V_r = \frac{\Lambda}{2\pi r}$	$\frac{\Lambda}{2\pi}\ln(\mathrm{r})$	$\frac{\Lambda}{2\pi}\theta$

Vortex	$V_\theta = -\frac{\Gamma}{2\pi r}$	$-\frac{\Gamma}{2\pi r}\theta$	$\frac{\Gamma}{2\pi}\ln(r)$
Doublet	$V_r = -\frac{\kappa}{2\pi r}\frac{\cos\theta}{r^2}$ $V_\theta = -\frac{\kappa}{2\pi r}\frac{\sin\theta}{r^2}$	$\frac{\kappa}{2\pi r}\frac{\cos\theta}{r}$	$-\frac{\kappa}{2\pi r}\frac{\sin\theta}{r}$

Lifting Flow over a Cylinder

As shown before, to model a non-lifting cylinder one needs uniform flow and doublet flow, but by adding circulation we can now obtain lift. This can be seen in **Error! Reference source not found.**.

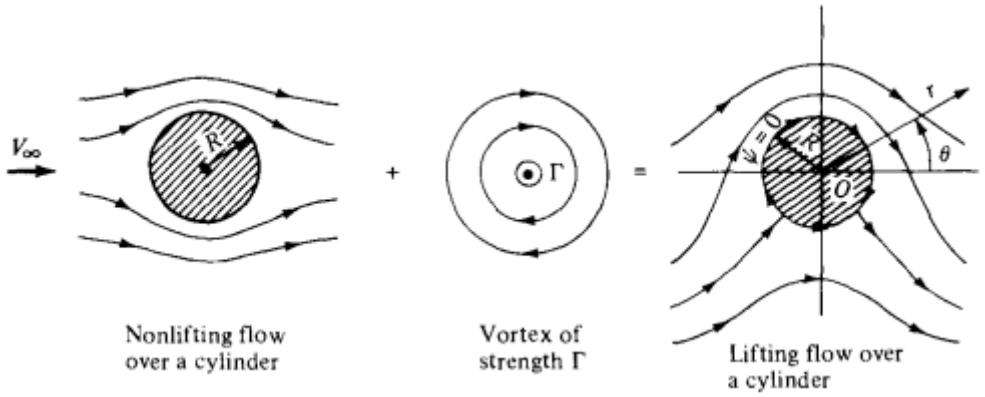

Figure 61: Non-lifting Flow Over a Cylinder+Vortex Flow=Magnus Lift

The resulting summed stream function comes from the addition of

$$\psi = V_\infty r\sin\theta + \frac{\Gamma}{2\pi}\ln(r) + -\frac{\kappa}{2\pi r}\frac{\sin\theta}{r}$$

Set r=r/R and (radius ratio) simplifying

$$\psi = V_\infty r\sin\theta\left(1-\frac{R^2}{r^2}\right) + \frac{\Gamma}{2\pi}\ln\left(\frac{r}{R}\right)$$

Solving for the polar velocities:

$$V_r = V_\infty\cos\theta\left(1-\frac{R^2}{r^2}\right)\ and\ V_\theta = -V_\infty\sin\theta\left(1+\frac{R^2}{r^2}\right) - \frac{\Gamma}{2\pi r}$$

Using these two it is possible to solve for many things, such as stagnation point etc. **Error! Reference source not found.** shows stagnation points with respect to changing vortex strength

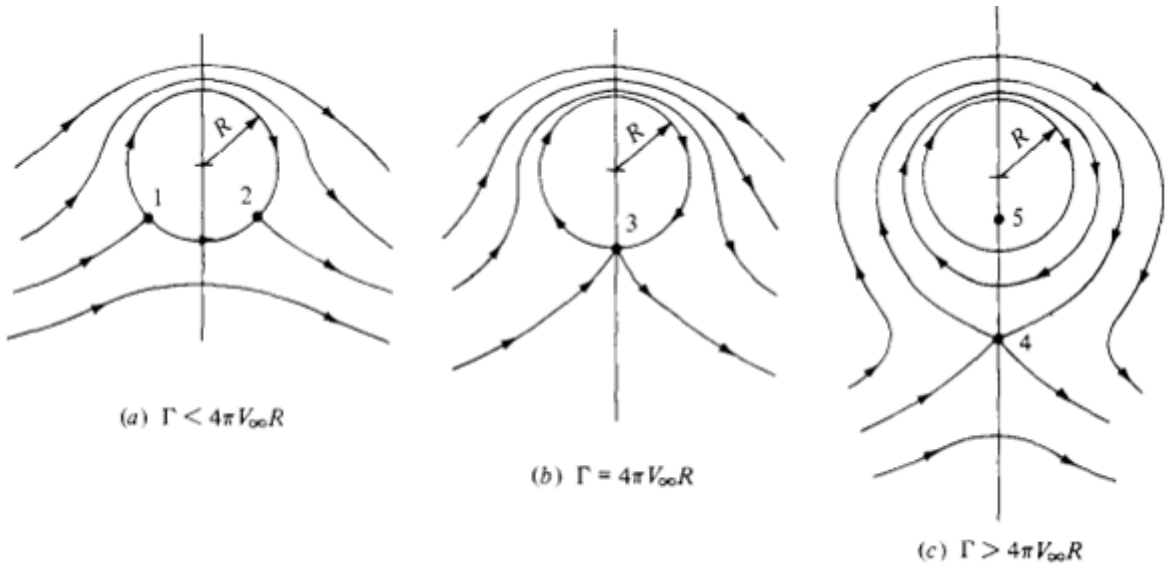

Figure 62: Vortex Strength and Stagnation Point

To obtain the lift it is necessary to calculate the coefficient of pressure along the cylinder, but to do that we need to obtain the velocity at the edge of the cylinder. (R=r)

$$V = V_\theta = -2V_\infty \sin\theta \ - \frac{\Gamma}{2\pi R}$$

The incompressible coefficient can shown as

$$C_p = 1 - \left(\frac{V}{V_\infty}\right)^2 = 1 - \left(-2\sin\theta \ - \frac{\Gamma}{2\pi R V_\infty}\right)$$

Note that this is inviscid thus we would obtain a coefficient of drag of zero, so let's see what the coefficient of lift would be.

In this case the coefficient of lift is equal to the normal coefficient which is:

$$c_l = c_n = \frac{1}{c}\int_0^c C_{p,l}dx - \frac{1}{c}\int_0^c C_{p,u}dx$$

Converting to polar coordinates

$$x = R\cos\theta \ \ dx = -R\sin\theta \, d\theta$$

Substituting

$$c_l = c_n = -\frac{1}{2}\int_\pi^{2\pi} C_{p,l}\sin\theta \, d\theta + \frac{1}{2}\int_\pi^0 C_{p,u}\sin\theta \, d\theta$$

Here the expression for $C_{p,u}$ and $C_{p,l}$ have the same analytic expression, thus:

$$c_l = -\frac{1}{2}\int_0^{2\pi} C_p \sin\theta \, d\theta$$

Substituting

$$c_l = -\frac{1}{2}\int_0^{2\pi} \left[1 - \left(-2\sin\theta \; - \frac{\Gamma}{2\pi R V_\infty}\right)\right] \sin\theta \, d\theta$$

$$c_l = \frac{\Gamma}{R V_\infty}$$

Lift is equal to

$$L' = q_\infty S c_l = \frac{1}{2}\rho_\infty {V_\infty}^2 S c_l = \frac{1}{2}\rho_\infty {V_\infty}^2 (2R)\frac{\Gamma}{R V_\infty}$$

And finally

$$L' = \rho_\infty V_\infty \Gamma$$

It is called the Kutta-Joukowski theorem, named after the German mathematician M. Wilheim Kutta (1867-1944) and the Russian physicist Nikolai E. Joukowski (1847-1921), who independently obtained it during the first decade of this century. It is simple, but powerful.

Appendix G: Hand Notes and Calculations

Please, do not disturb these computers.

ANSYS tests currently running.

3/26/15

Thanks.

Turn on energy/heating

Sizing -

4.5e-003

element size - 3e-003

'Hard'

Patch conforming meth

Method: 'tetrahedrons'

inflating 'First layer thickness

2e-005

max layers, 10

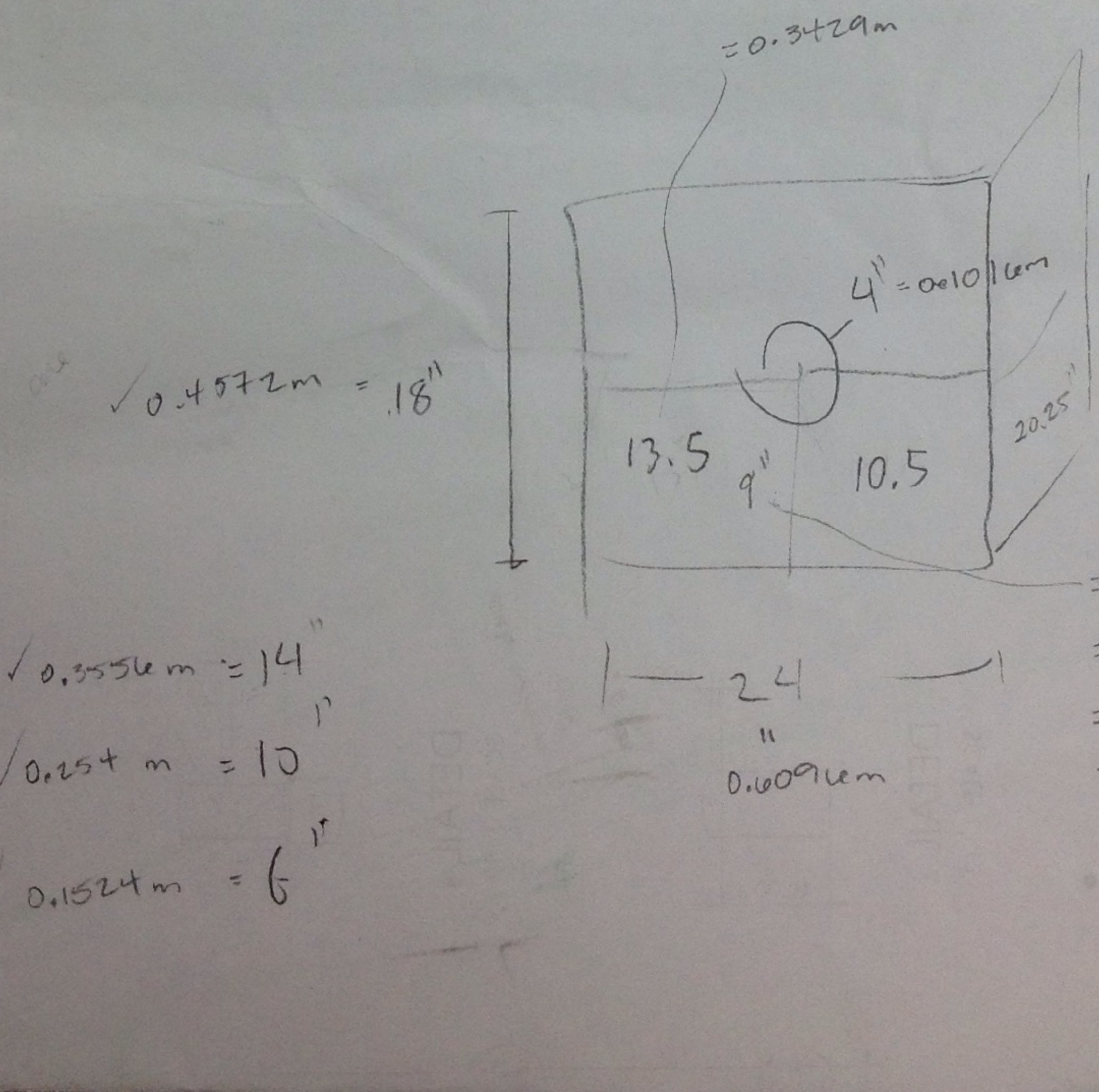

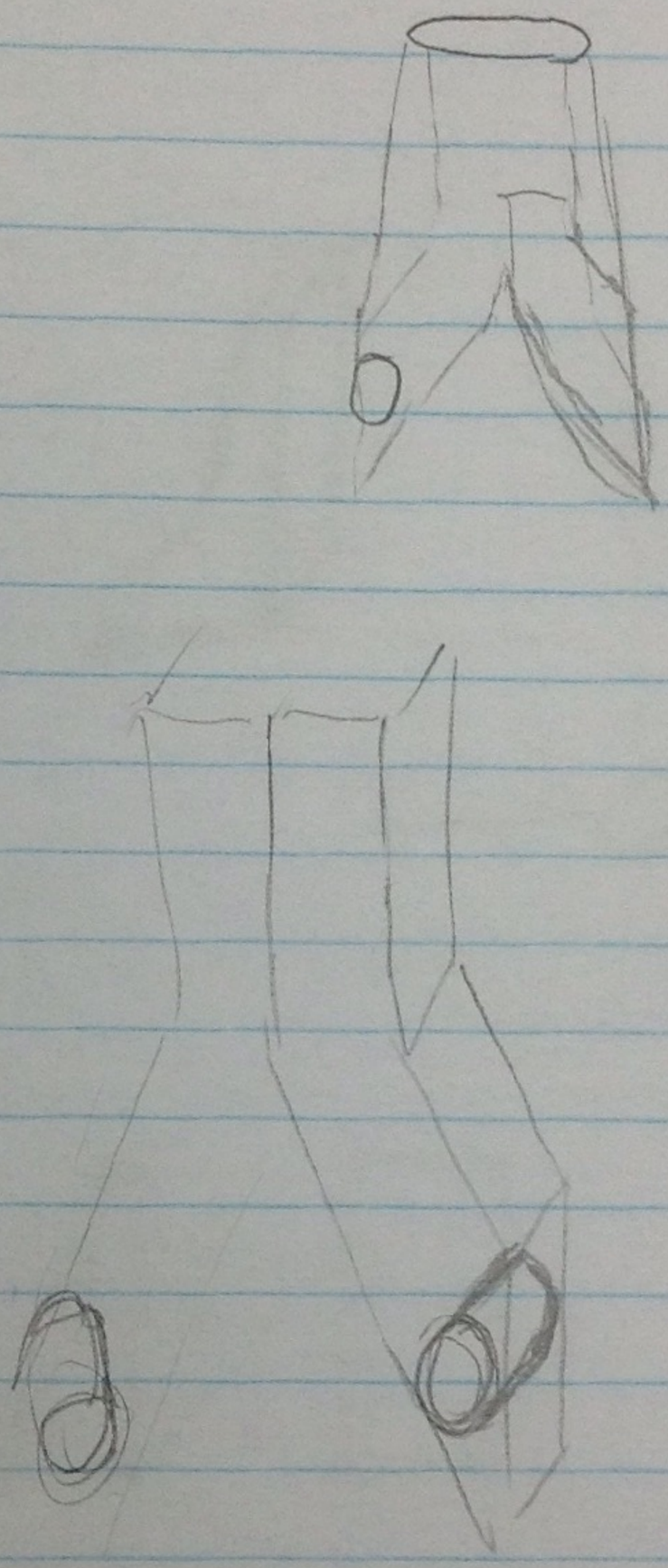

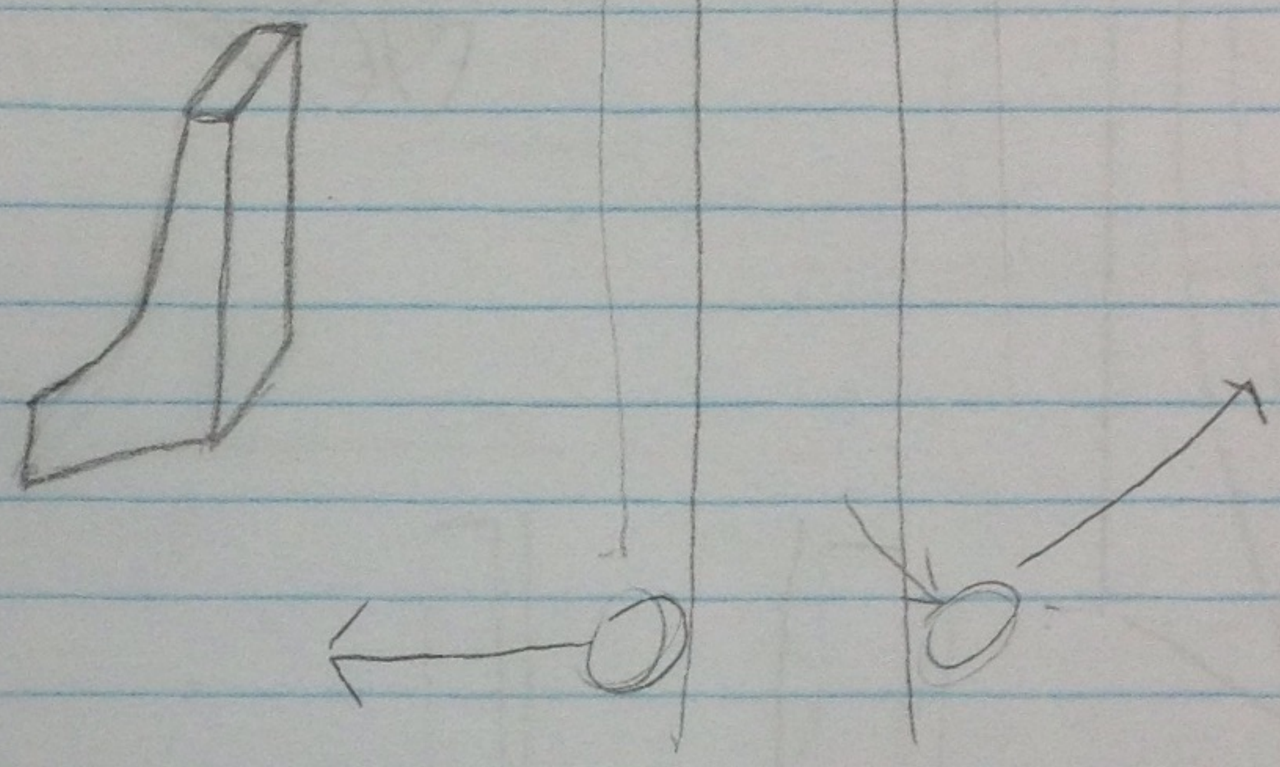
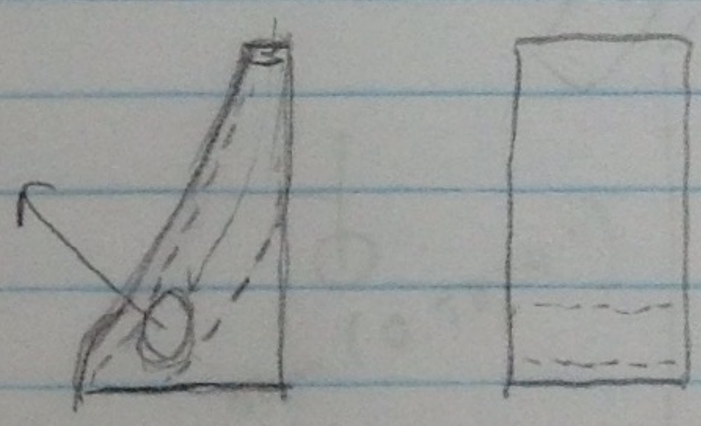
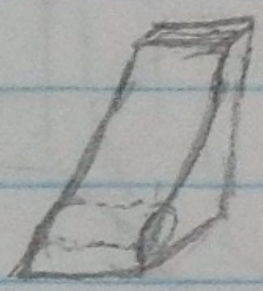

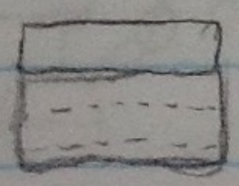
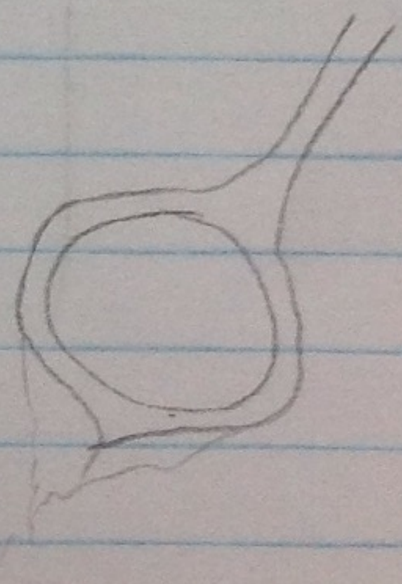

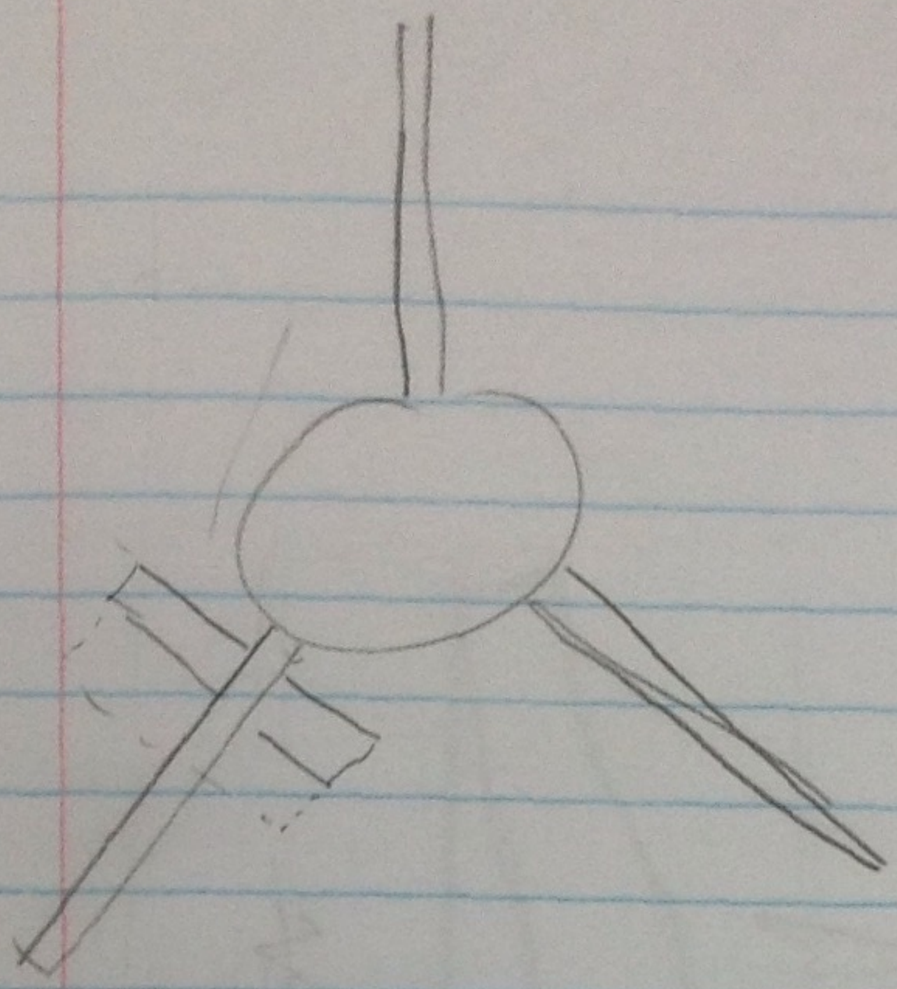

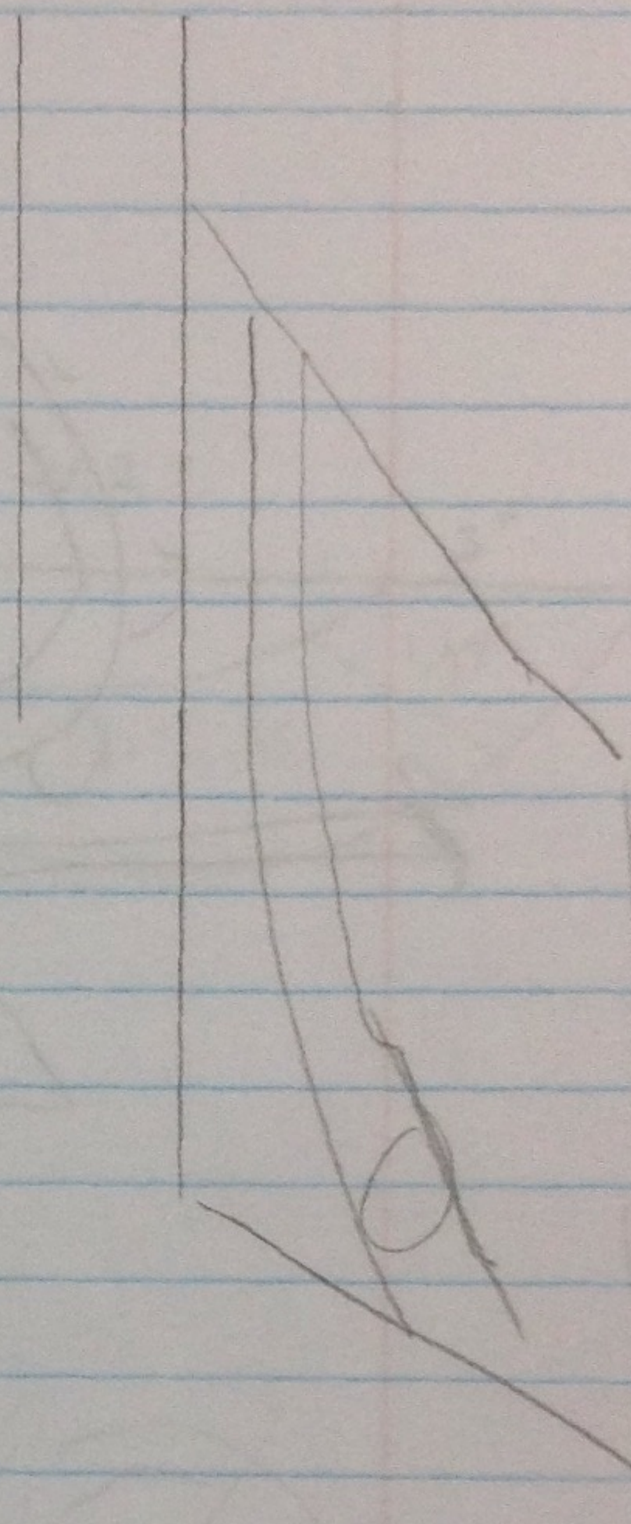

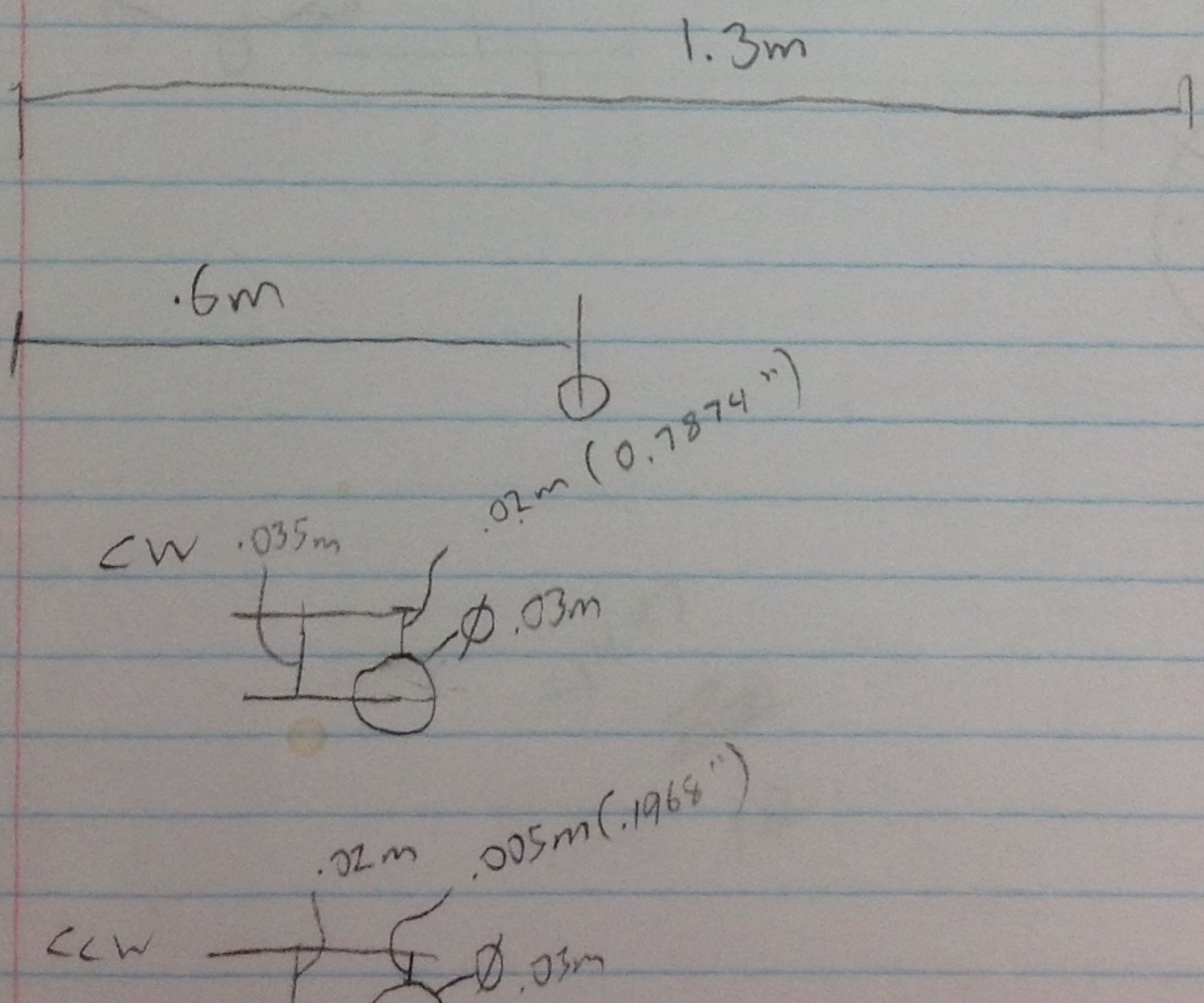
1.3m
.6m
.02m (0.7874")
CW .035m
.02m
Ø .03m
.02m
.005m (.1968")
CCW
Ø .03m

2/13/15

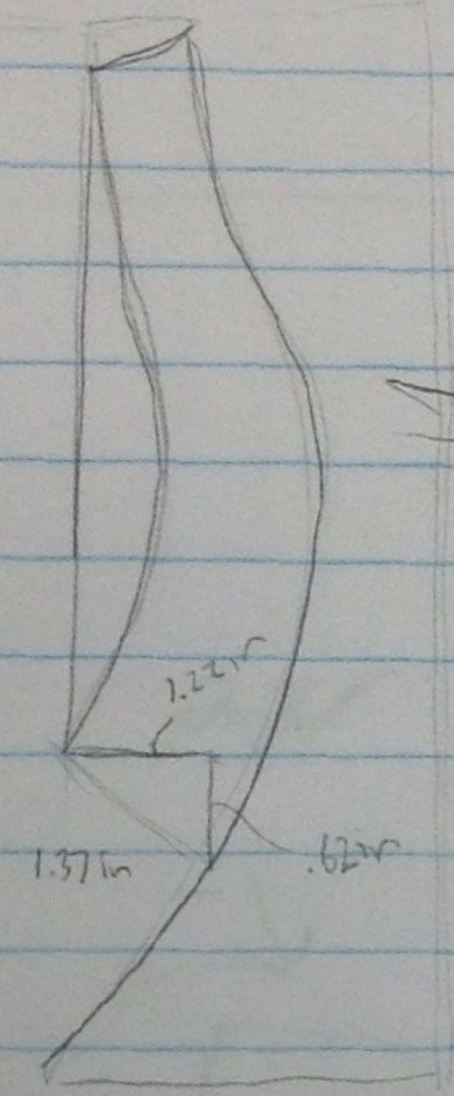

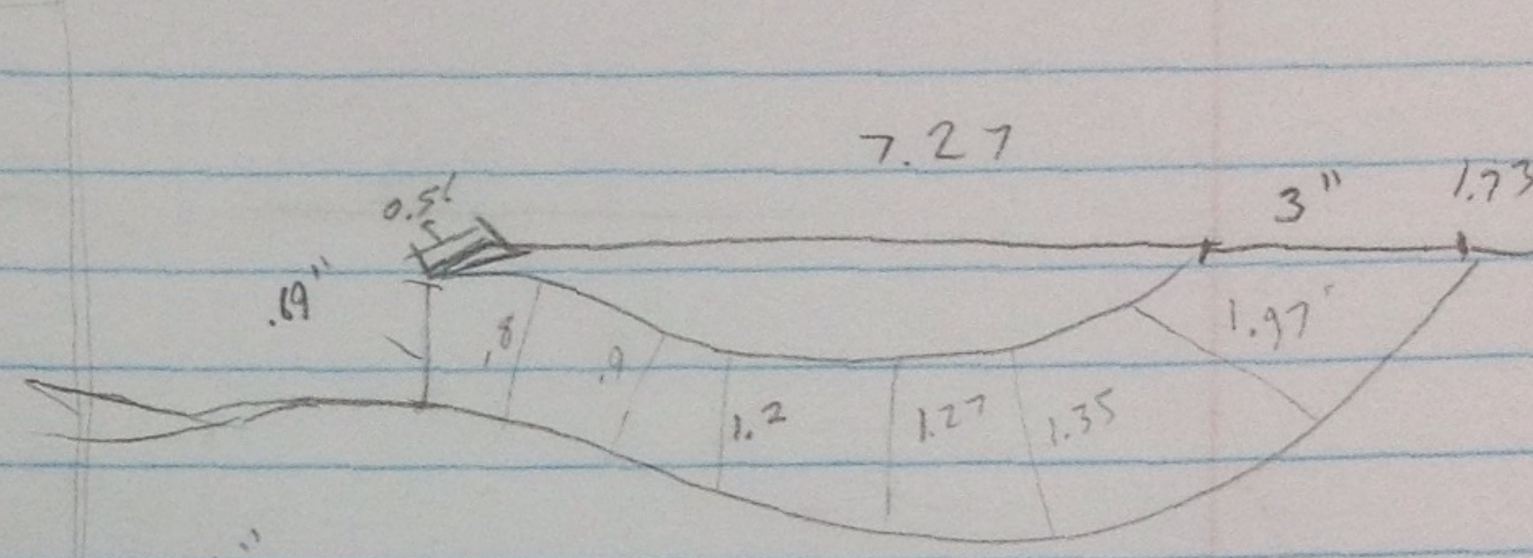

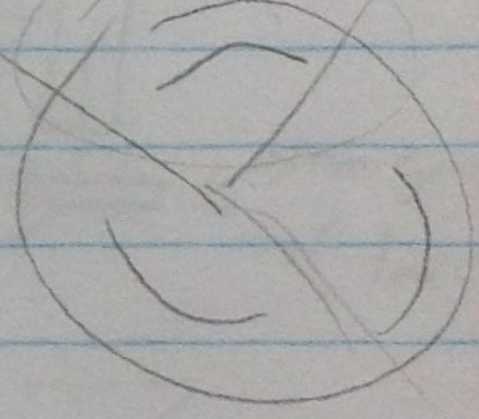

$\frac{1.47}{B \cdot h^2}$

1.62

2/13/15

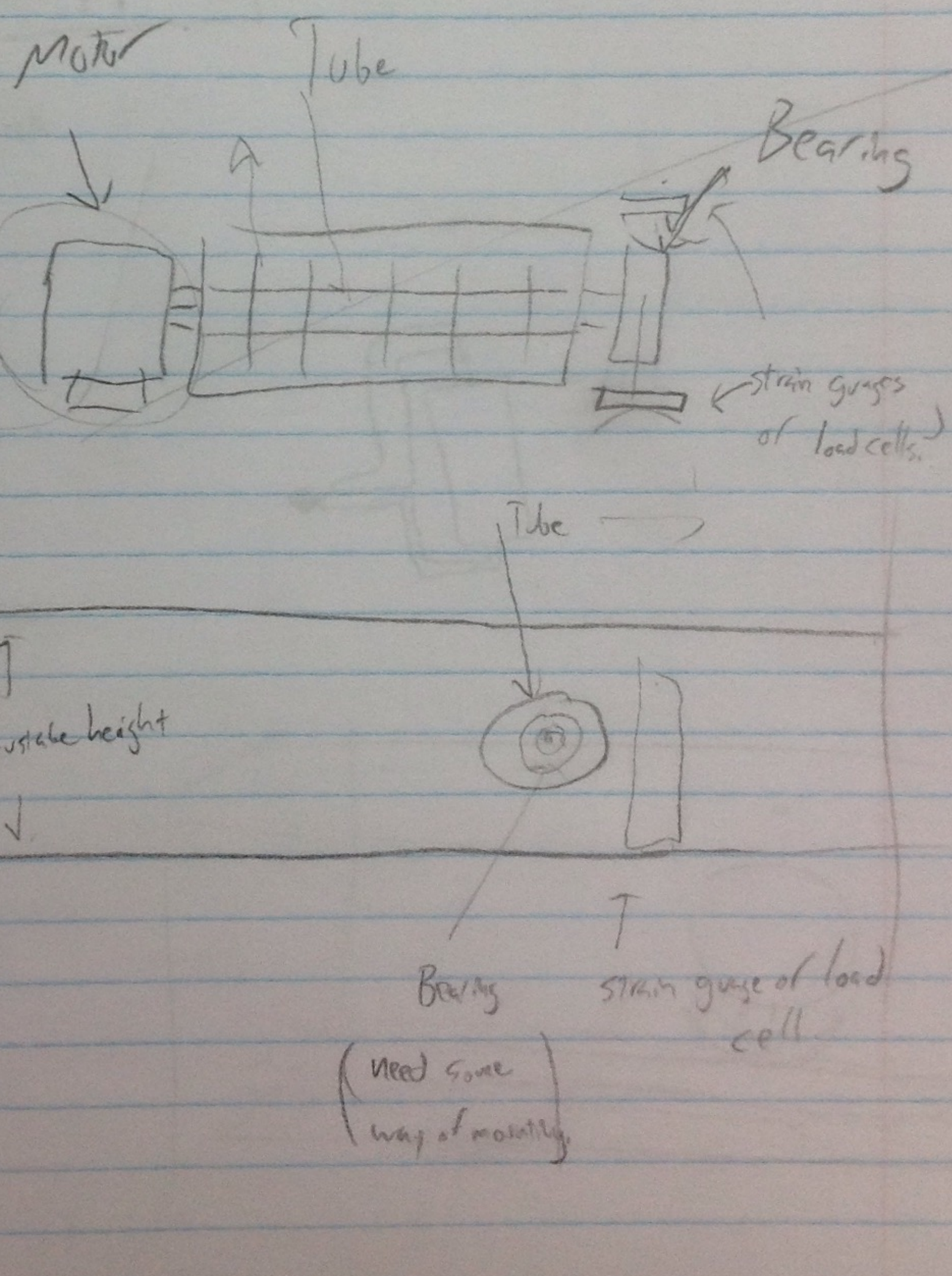
Motor
Tube
Bearings
strain gauges of load cells
Tube
adjustable height
Bearing
strain gage of load cell
(need some way of moving)

2/13/15

Ideas for adjusting height?

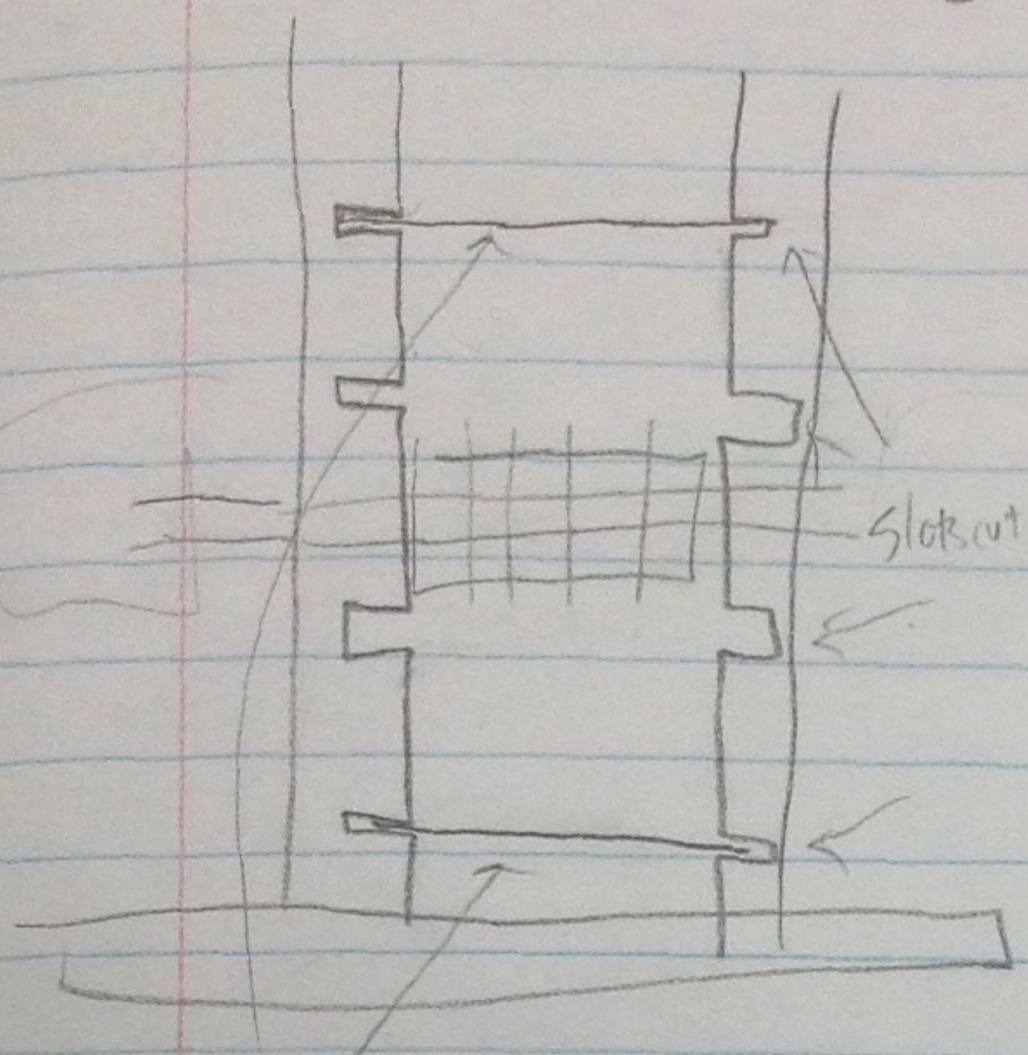

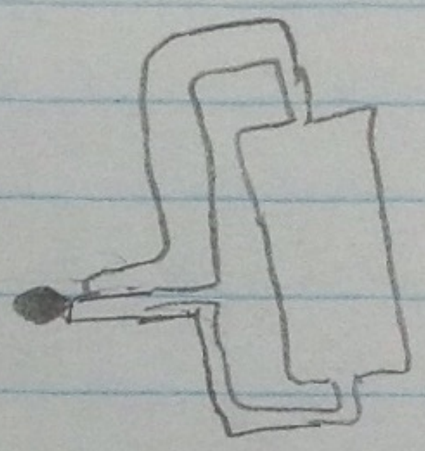

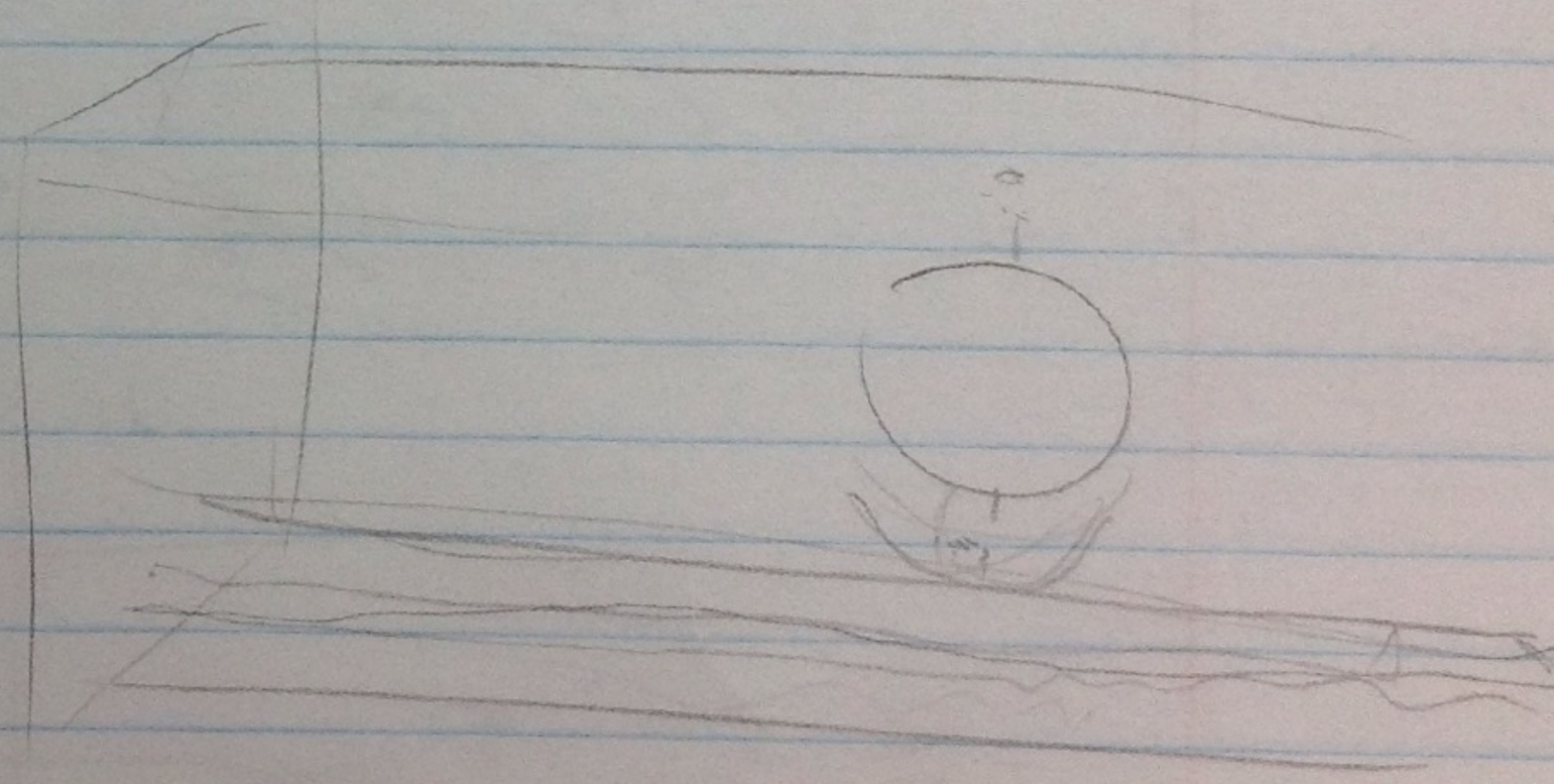

2/16/15

PVC cylinder

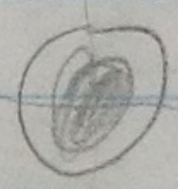

3" schedule 40

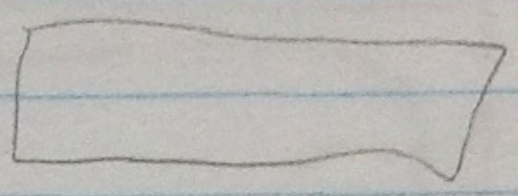

ABS End Cap

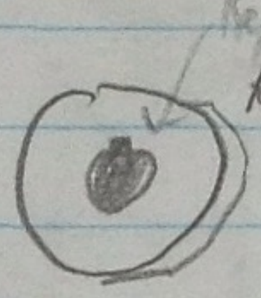

Keyslot for 1/8" or 1/4" rod

Assembly:

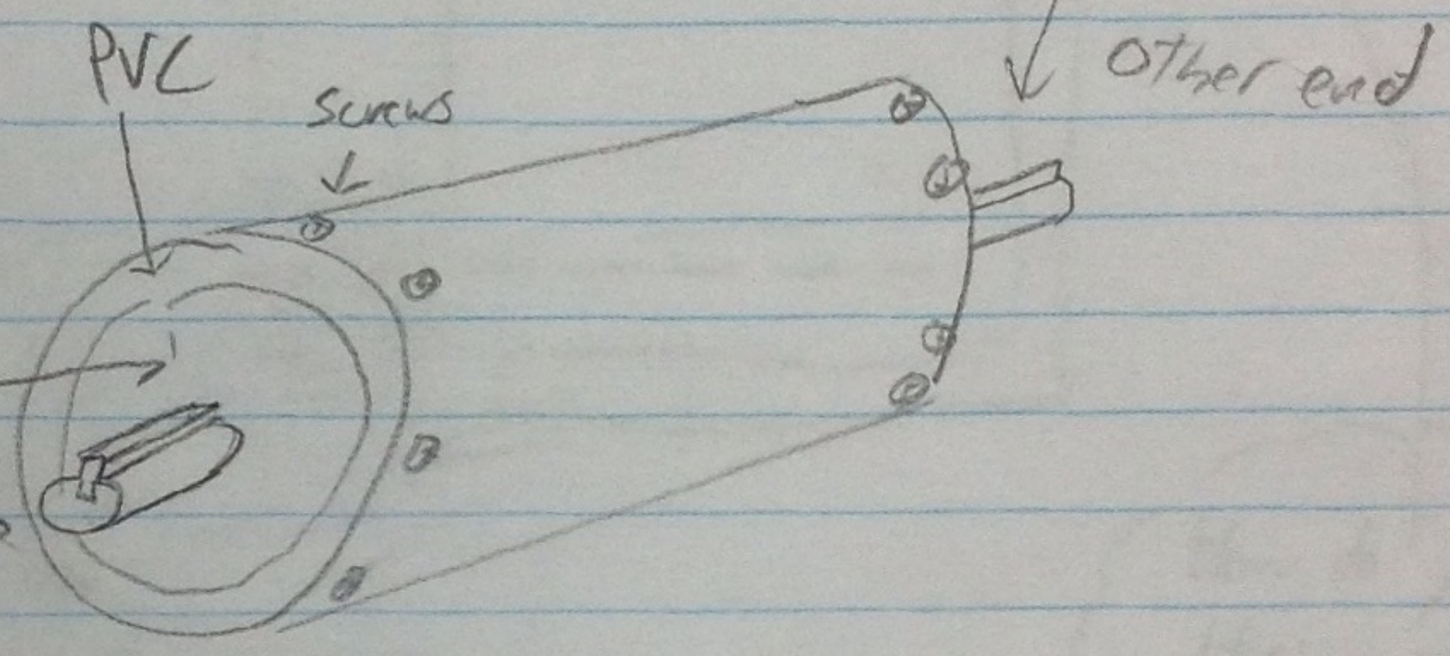

Attach motor to slotted rod

From transducer

Connecting arm:

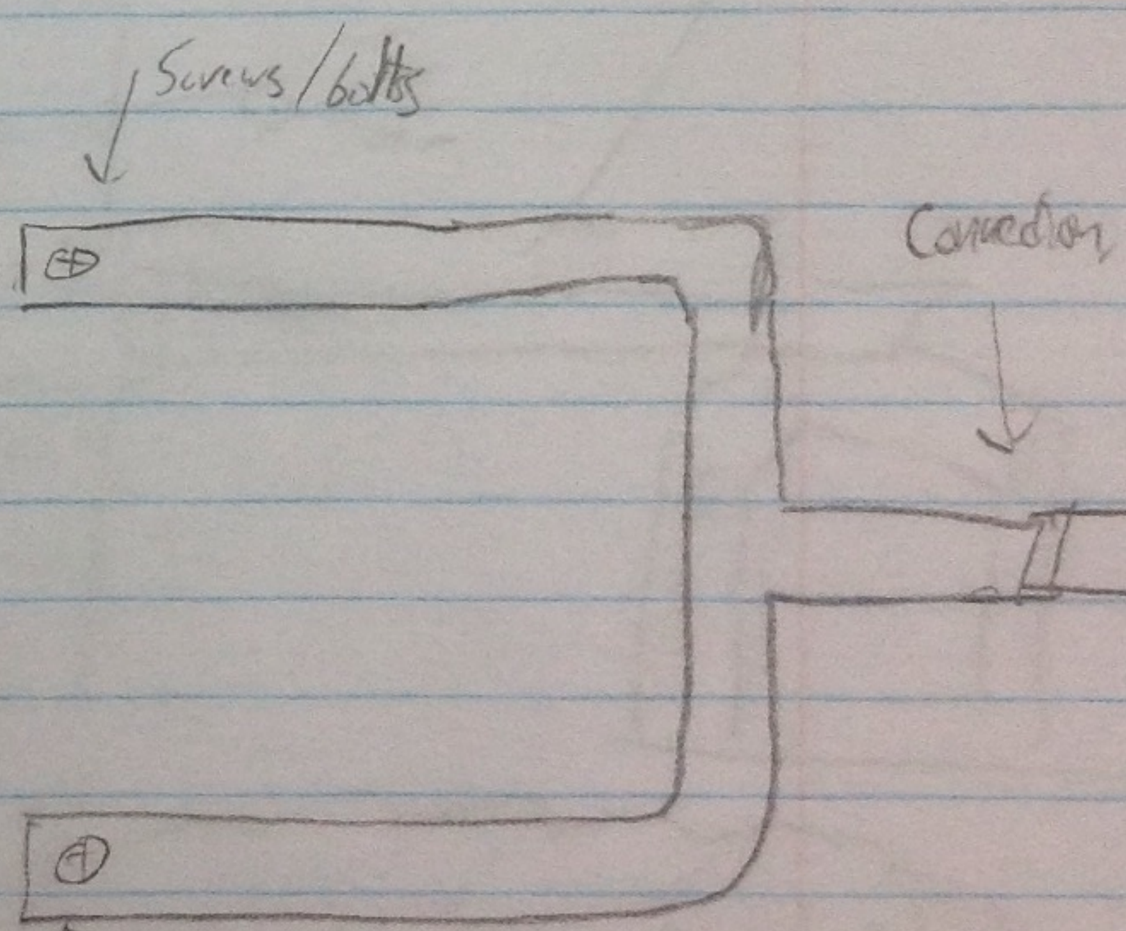

Slot for fixture w/cylinder...

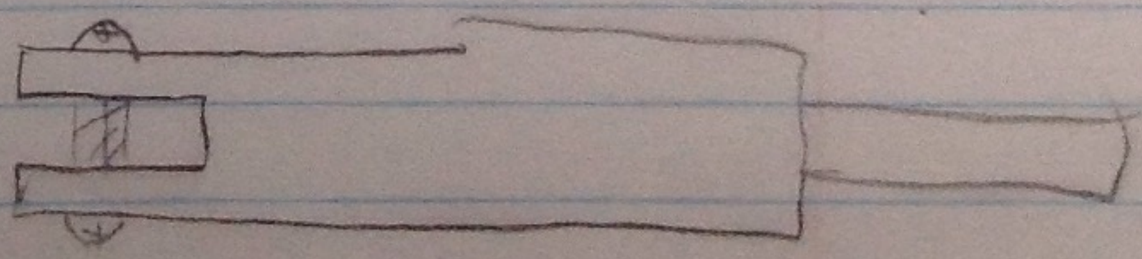

Side view

2/16/15

Assembly??

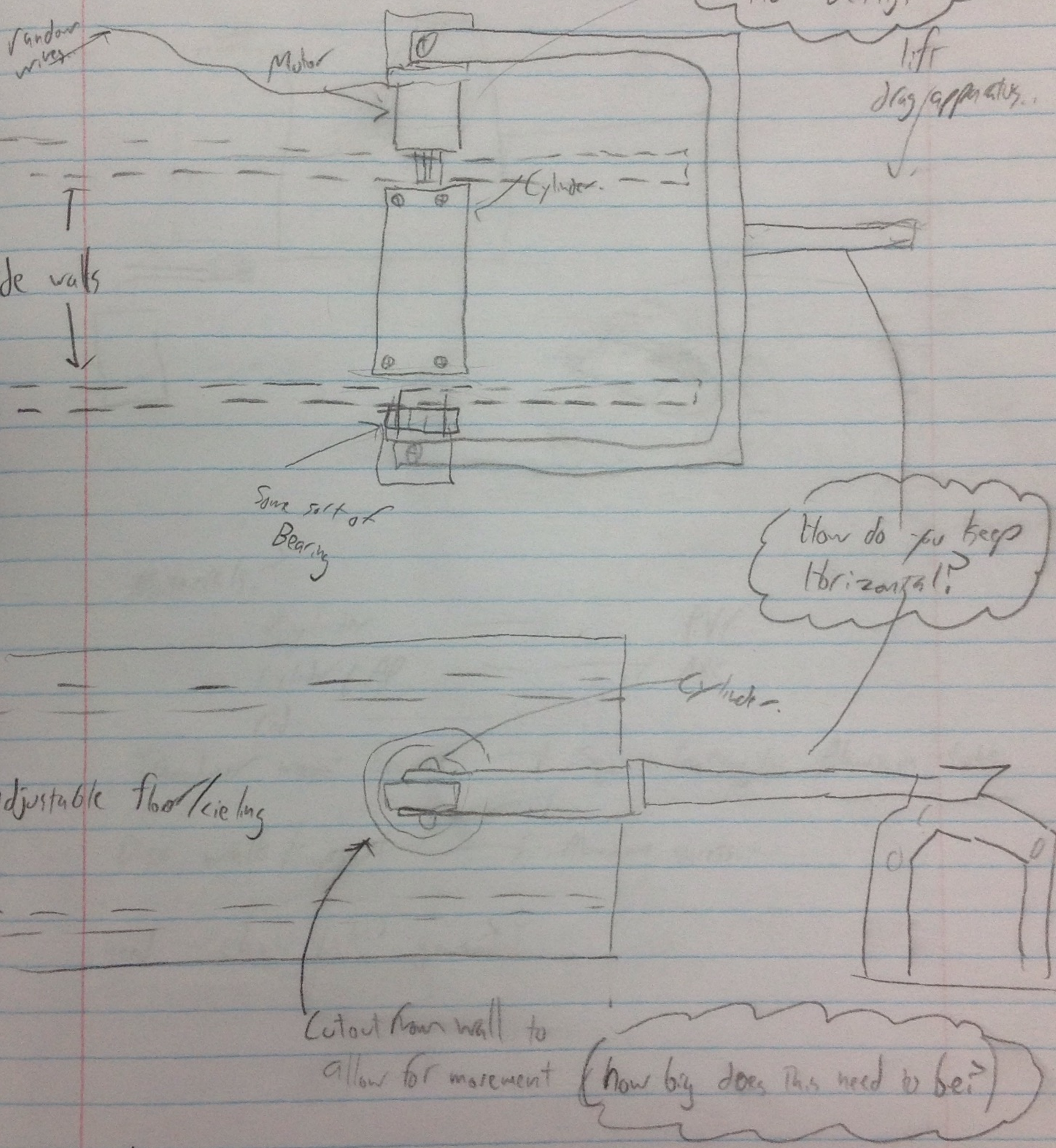

256 Limit

2/16/15

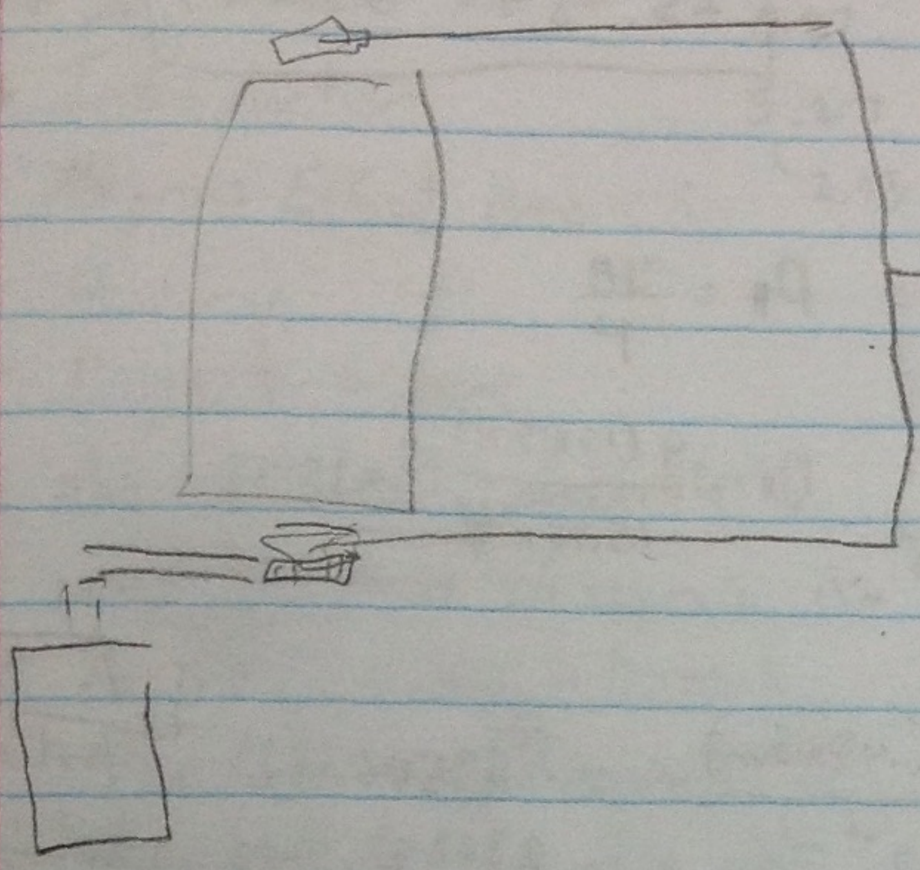

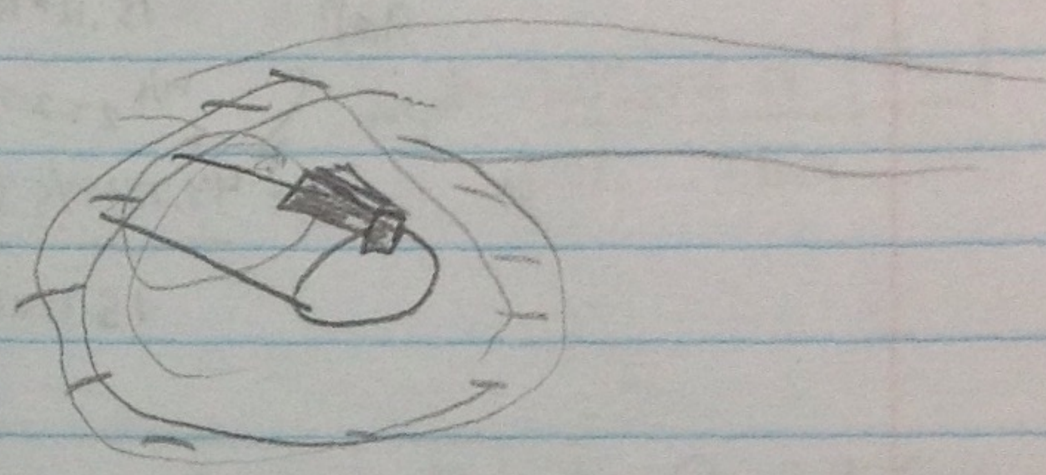

Materials:

Cylinder → PVC

Cylinder CAP → ABS

rod

Transducer mount, beams → Square/rectangular Aluminum tube

Duct walls/support → Aluminum sheets...

need - chain link? gears?

.0889 m

10741.59 RPM

100 m/s

44.704 m/s

which is impossible

25 to 40 diameters for turbulent flow to develop

.508

$$Re = \frac{VD_H}{\nu} \qquad D_H = \frac{4A}{P}$$

$$D_H = \frac{4(15.8 \times 15.7)}{15.75 \times 4} = 15.75$$

$$Re = \frac{44.704\ m/s\ (.40005\ m)}{15.11 \times 10^{-6}\ m^2/s} = 1183576.122 \therefore \text{turbulent}$$

$$= 238282.5943 \therefore \text{turbulent}$$

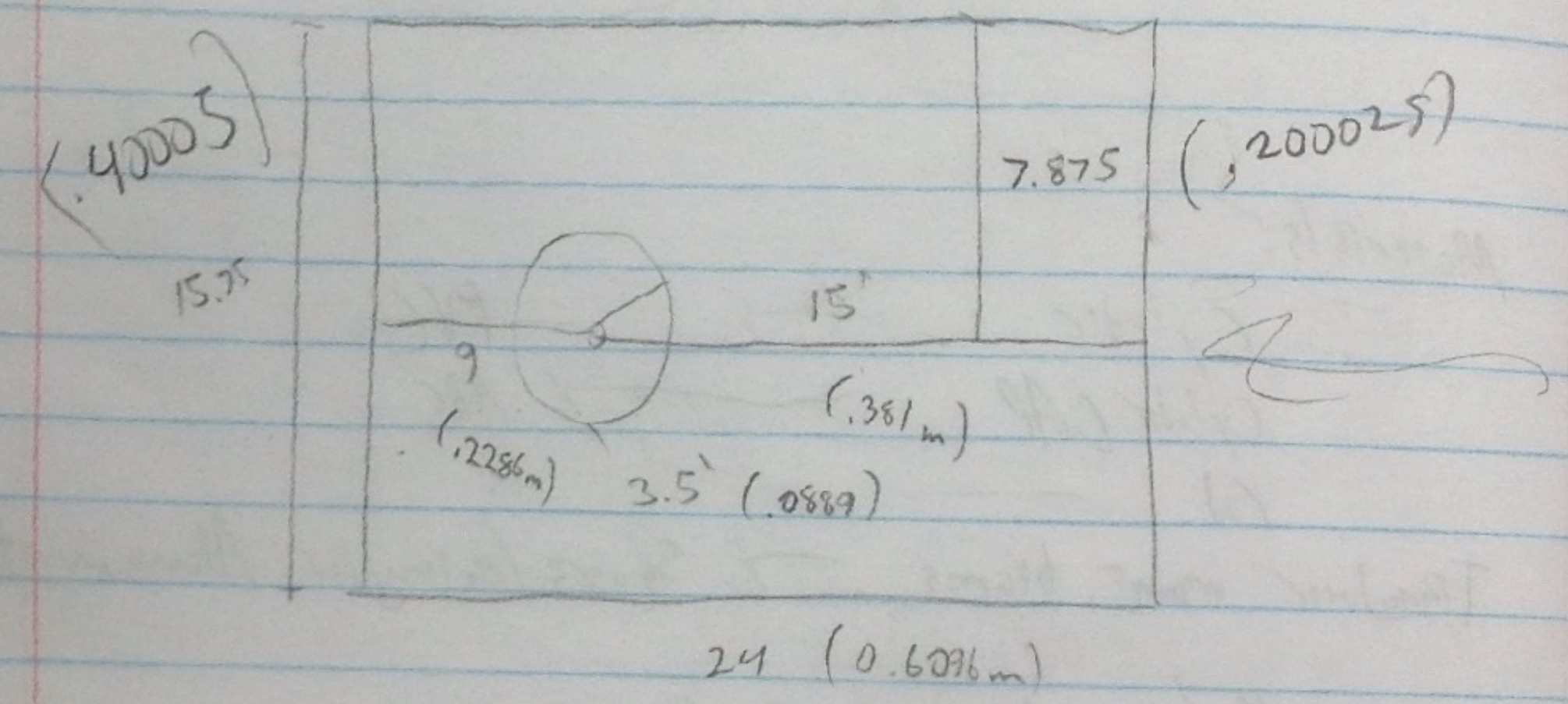

7.875

9m/s to RPM

$$V = C \cdot RPM = \pi D \cdot RPM$$

$$18\ m/s = \pi\ (.0889) \times X$$

202.5 Rad/s

Height: 2.35"
width: 3.17"

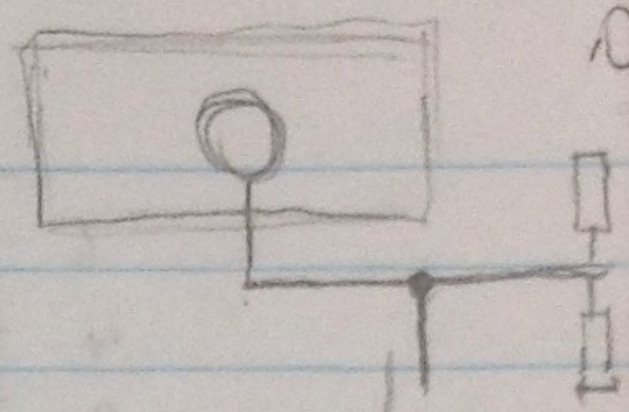

Presentation outline

0.27
3.27
2.93

- Introduction
- Magnus Effect Basics
- History
- Project Scope
- Applications: possible
- Test fixture designs
- Ansys Simulations
- Testing → wind tunnel
- Rocket design tie in

$mph = \frac{1mi}{hr} \left| \frac{5280}{1mi} \right| \frac{ft}{} \left| \frac{1hr}{3600} \right.$

$L = \rho G V$ (lbs/ft)

$\rho = .074887$ lb/ft^3

length = 15.5in or 1.3 Feet

$G = 2\pi b V_r$

$\left(\frac{}{.29166 ft}\right) \quad \frac{2\pi b s}{.29166 ft}$

$Ft \left(\frac{rad}{sec} Ft \frac{rev}{sec} \right)$

5000 RPM $\frac{rev}{min} \left(\frac{1min}{60sec} \right)$

83.333 rev/sec → 5000 RPM

$\frac{1 rev}{sec} \cdot ft$

$G = 2\pi \left(\frac{.29166 ft}{2}\right) \cdot \left(2\pi \left(\frac{.29166}{2}\right)(83.333)\right) = 69.9133$

$G = 279.8533$

25 meters/sec (55.9234 mph)

$L = .074887 (279.8533)(82.021)$

69.96333

.0023769 slug/ft^3

$L = .0023769 (69.9633)(82.021) = 13.6397$ lb/ft

$\left(13.6397 lb \right) \left(\frac{L ft}{sec} \right)$

$\times 1.3 ft = 17.73166$ lb

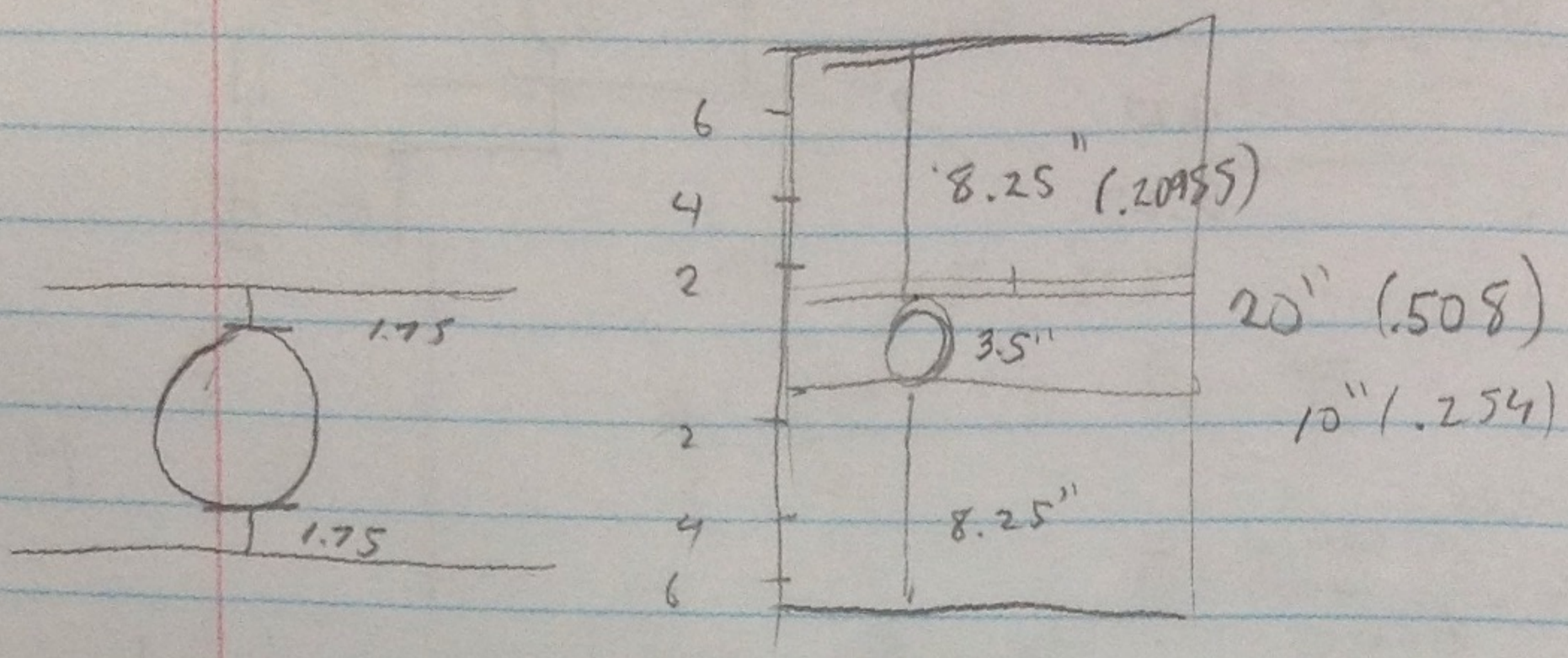

ratio of diameter to overall height

$Full = \frac{20}{3.5} = 5.714$ $\quad 15.5 = 0.3937$

Full	8.25
3/4	6
1/2	3.75
1/4	1.5

2.25"

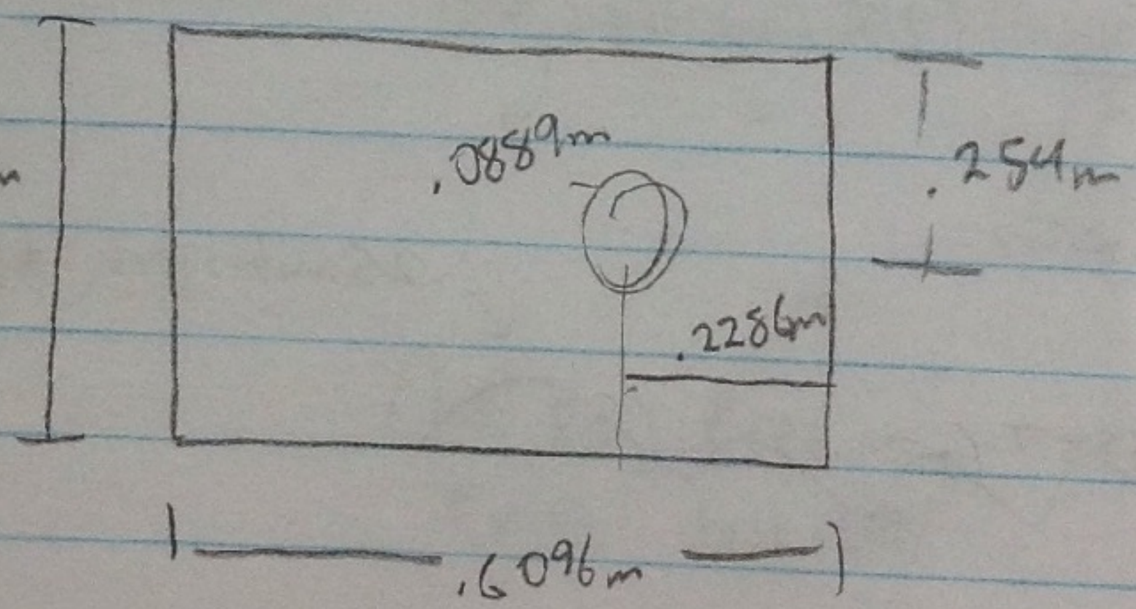

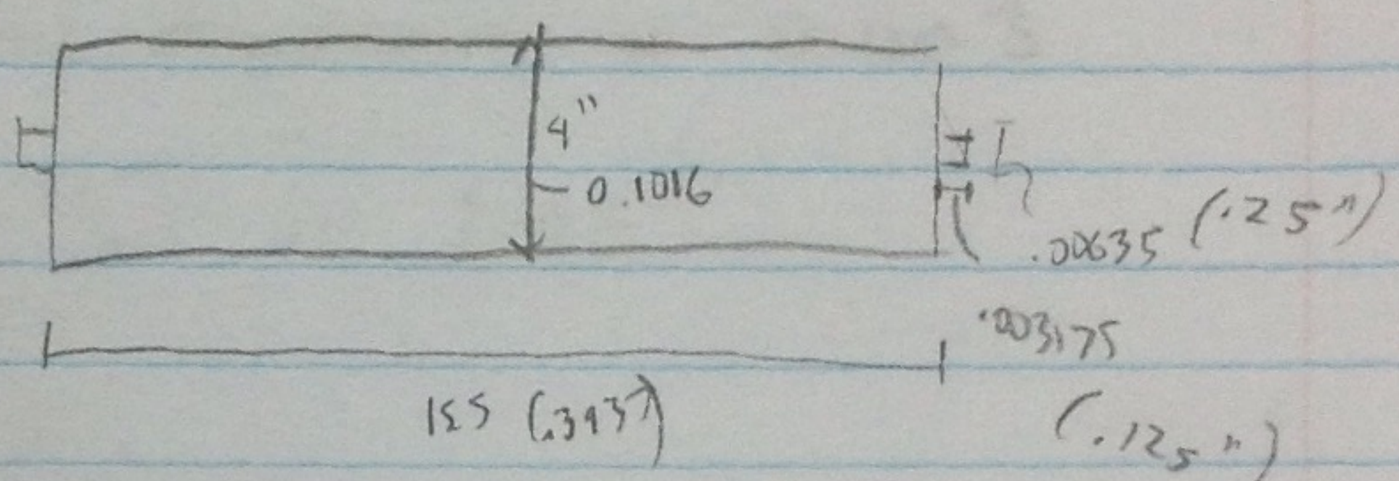

15.5 (.25)

15.75

.125

Meshing

- From Mesh, Insert Sizing. {Box} Select Cyl.

- Insert, Method, Box Select all.

- Insert inflation, Scoping outer Boundary
Boundary is your cyl.
Inflation - total thickness = 0.003
10 layers
Growth rate 1.1 or 1.05

Mesh option

Sizing
Relevance Center - Fine
Smoothing - high
Inflation

Generate

$$Pa = \frac{N}{m^2} = \frac{kg\,\not{m}}{s^2 m \not{z}} = \frac{kg}{s^2 m}$$

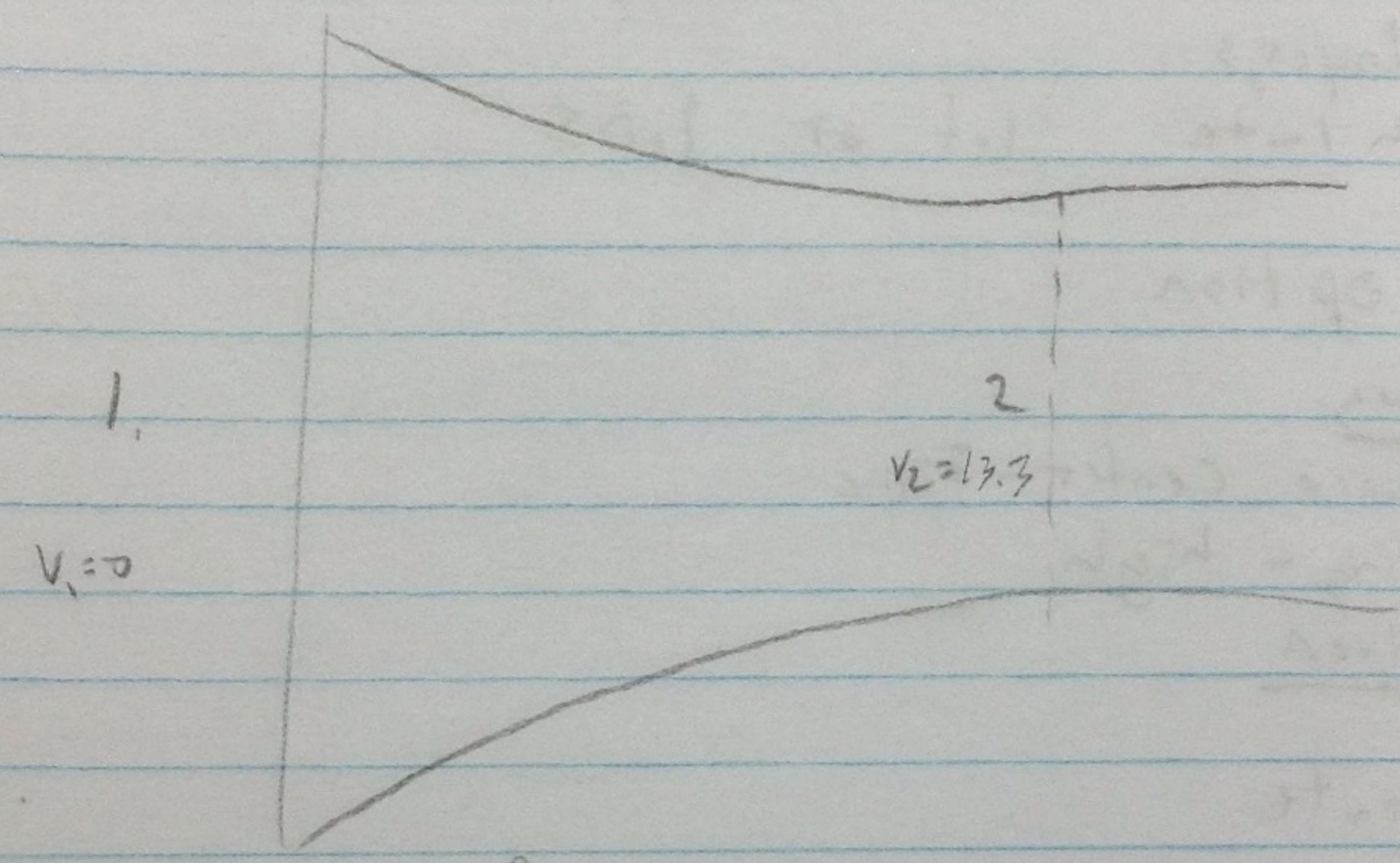

$$\frac{P_1}{\rho} + \frac{V_1^2}{2} + g z_1 = \frac{P_2}{\rho_2} + \frac{V_2^2}{2} + g z_1$$

$P_1 = 0$, $V_1^2 \to 0$, $z_1 \to 0$

$$P_2 = -\frac{(13.3)^2}{2}(\rho_2)$$

$1.204\ kg/m^3$

$m^2/s^2 \left(\frac{kg}{m^3}\right)$

$N \qquad \frac{kg}{s^2 m}$

↙ 202,5 rad/sec

1933 RPM → 18 m/s

← 13.3m/s air velocity (≈ 30 miles/hour)

[rad/s]	motor	wind speed
-523.6°/s	5000 RPM	
	46.54 m/s	23.27 m/s => 52 mph
261.8°/s	2500 RPM	
	23.27 m/s	11.64 m/s => 26.079 mph
104.72°/s	1000 RPM	
	9.309 m/s	4.6545 m/s => 10.411 mph

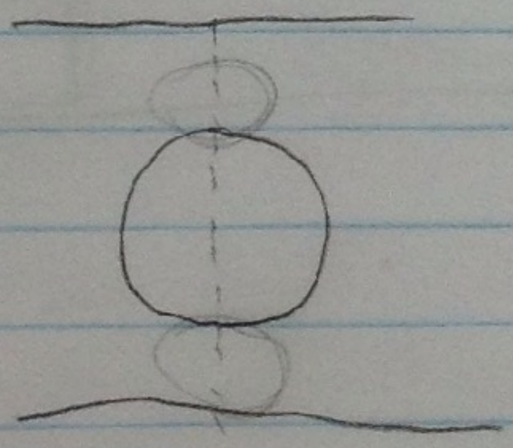

Position	1	2	3	4
Top	T		T	
Bottom	B	B		B

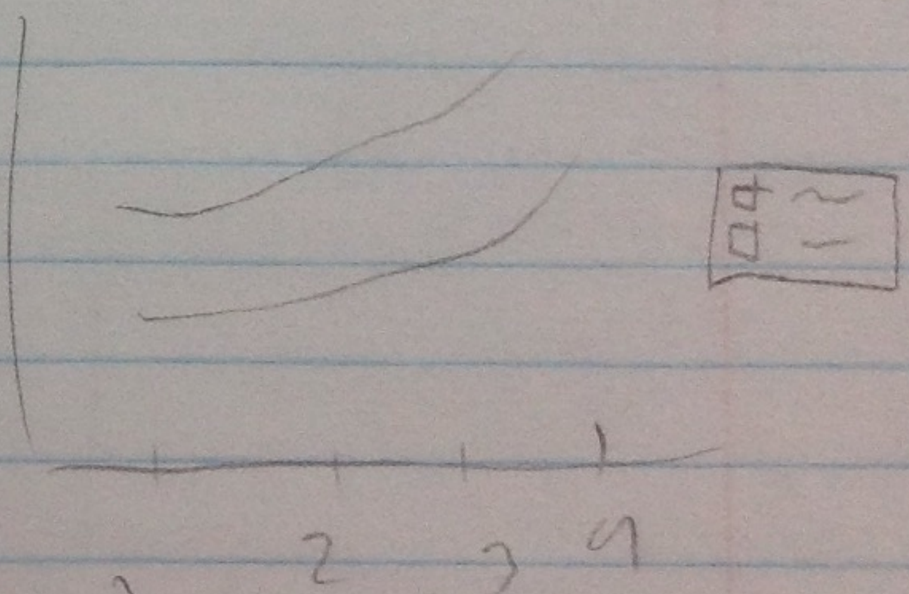

	1	2	3	4
Top	3.11×10^1	3.12×10^1	3.29×10^1	3.64×10^1
Bottom	1.57×10^1	1.57×10^1	1.97×10^1	2.00×10^1
	1.71×10^1	1.72×10^1	1.81×10^1	1.62×10^1

Top	59.4	60.4	63.8	68.3
Bottom	29.1	30.2	31.9	27.3
	26.7	27.2	28.7	23.9

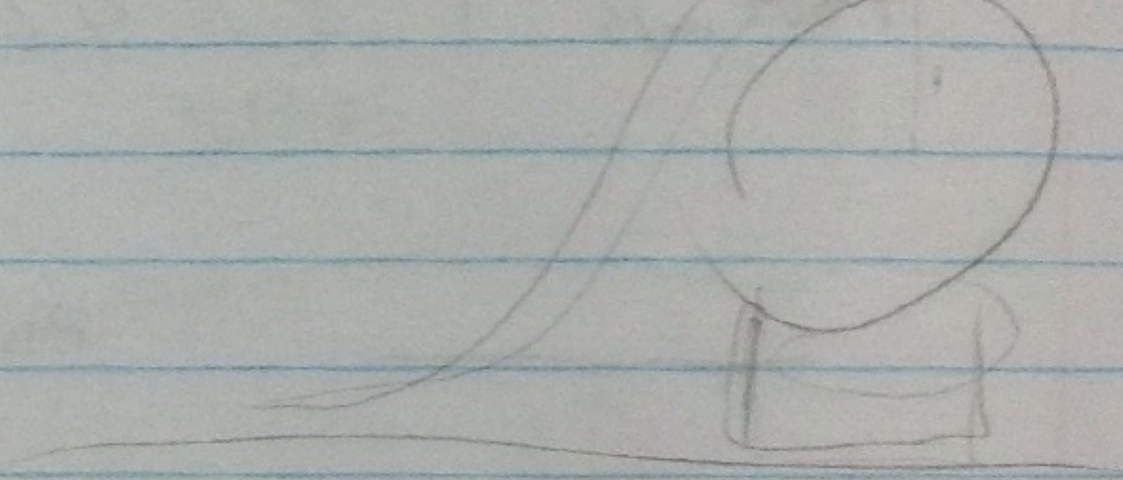

Tri all 4

Tri 2 4

Meshing

Geometry Face sizing Box select cylinder

Element size 1e-002

Automatic method Box select cylinder

Inflation

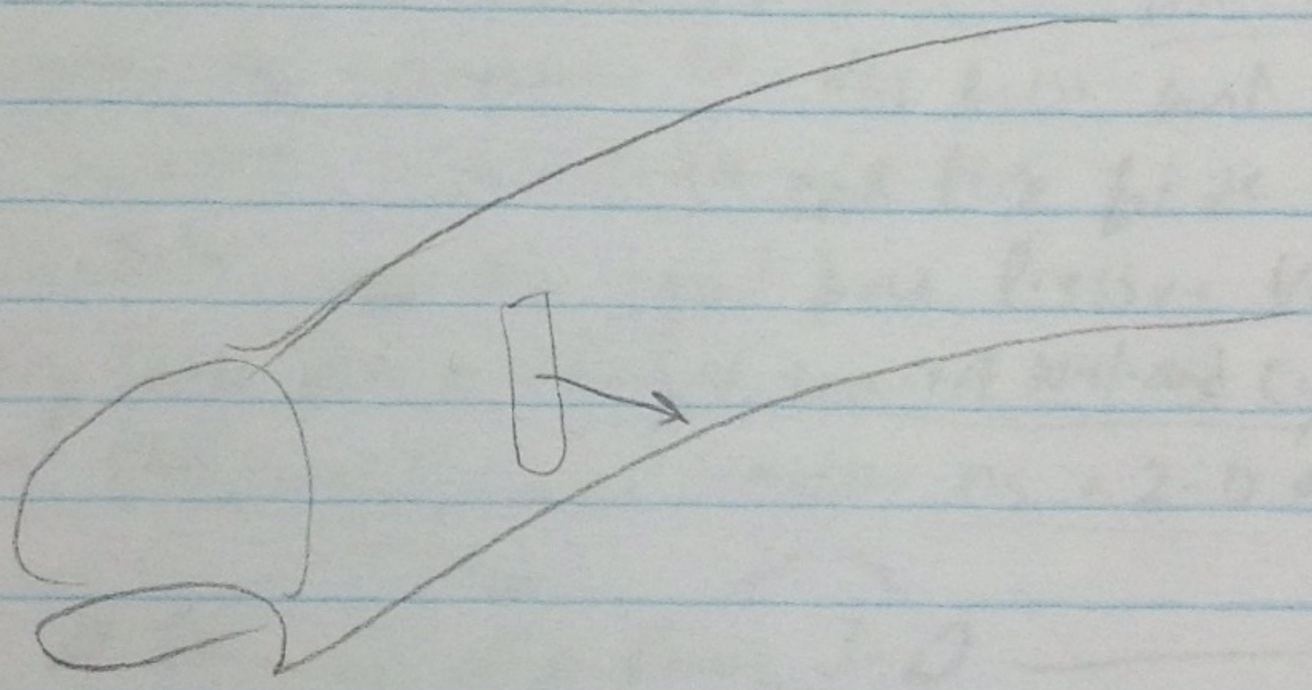

Air foil.
Assuming the Kutta condition is satisfied (air leaves the trailing edge smoothly)

Magnus Effect
given uniform flow toward cylinder

Slide (16) before (15), (16) But for 60 seconds turn on

3-Dimensional effects that must be accounted for. The effect of Mach with velocity ratio and End Plate Size are shown. See a correlation of Vel Ratio and Lift as well as increase Lift with the End Plate Size.
Fortran Model however my Closed duct Pressure Vorted Shedding is very small due to small little gap between Wall and Cylinder
Thus this three-D can be simulated as a 2-D cylinder
2-D Source or, 2-D Flush, 3-D

* Ekert Con E-Ship 1

* Boundary Anomaly

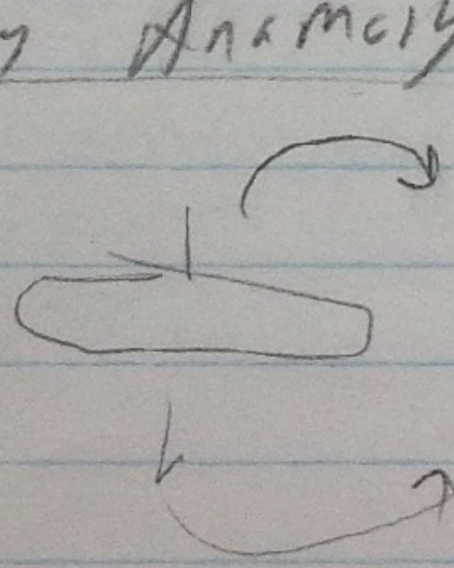

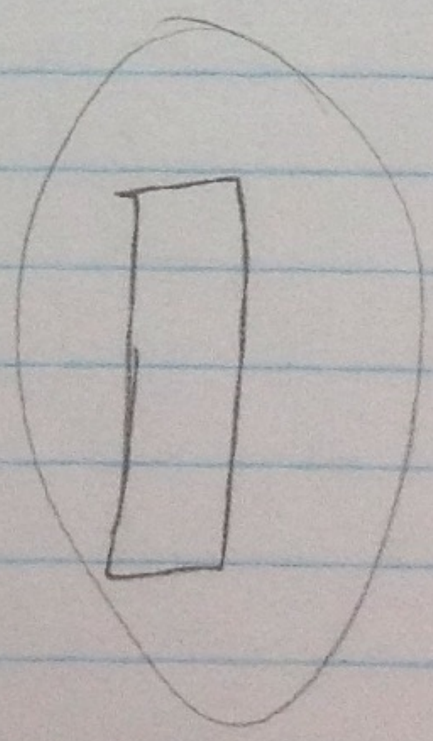

A30
A30 74

215

1	15.75	(.40005)
2	13.00	(.3302)
3	10.25	(.26035)
4	7.5	(.1905)
5	6	(.1524)

1.324N 13.4076N

1.324 N 13.412N

.130175 (1.0036) 15.280 42N

.09525 (2.m~) 18.43N 8.866N

.0762 4.25N 22.59N

11

Standard gauge = 4ft 8½in $\quad V = \frac{Egr}{G}$

$V = \sqrt{\frac{0.5 \cdot 30.3 \frac{ft}{s} \cdot r}{4.78 ft}}$

$44^2 = 566 ft = 172 m$

65700kg

$V = 80 mph = 36 m/s$

$a_r = \frac{V^2}{r} = \frac{36^2}{172} = 7.83 \frac{m}{s^2}$.

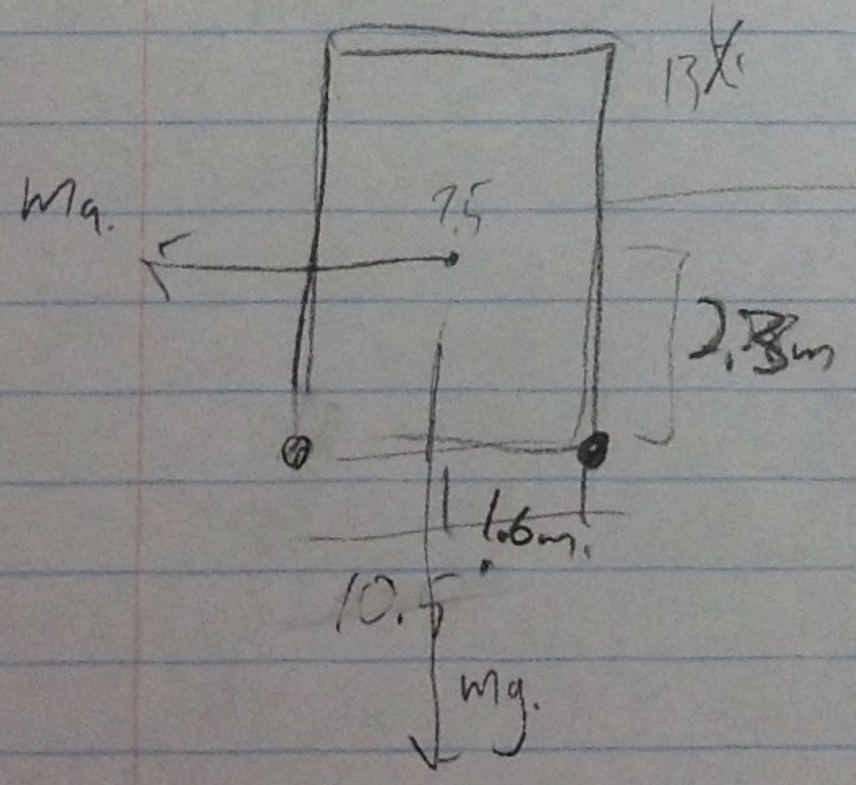

$T_c = m \cdot a \cdot r_{cgh}$
$= 65700 \cdot 7.83 \cdot 2.3 = 1183191 Nm$

$T_g = m \cdot g \cdot r_{cg}$
$= 65700 \cdot 9.8 \cdot 1.6 = 1030176 N \cdot m$

$\approx 153015 N \cdot m$ difference.